Best
Available
Copy

AD-A015 653

SOVIET MATERIAL ON INTERNAL WAVE EFFECTS, NUMBER 4, SEPTEMBER 1975

Stuart G. Hibben, et al

Informatics, Incorporated

Prepared for:

Defense Advanced Research Projects Agency
Defense Supply Service

September 1975

DISTRIBUTED BY:

NTIS

National Technical Information Service
U. S. DEPARTMENT OF COMMERCE

Informatics inc

293099

AD A015653

DDC
RECEIVED
OCT 6 1977
DISCLOSURE
A

Reproduced by
NATIONAL TECHNICAL
INFORMATION SERVICE
US Department of Commerce
Springfield, VA. 22151

UNCLASSIFIED

SECURITY CLASSIFICATION OF THIS PAGE (When Data Entered)

REPORT DOCUMENTATION PAGE		READ INSTRUCTIONS BEFORE COMPLETING FORM
1. REPORT NUMBER	2. GOVT ACCESSION NO.	3. RECIPIENT'S CATALOG NUMBER
4. TITLE (and Subtitle) Soviet Material on Internal Wave Effects No. 4, September, 1975		5. TYPE OF REPORT & PERIOD COVERED Scientific . . . Interim 6. PERFORMING ORG. REPORT NUMBER
7. AUTHOR(s) Stuart G. Hibben, John Konrilo, B. L. Shresta, M. Ness		8. CONTRACT OR GRANT NUMBER(s) MDA-903-76C-0099
9. PERFORMING ORGANIZATION NAME AND ADDRESS Informatics Inc. 6000 Executive Boulevard Rockville, Maryland 20852		10. PROGRAM ELEMENT, PROJECT, TASK AREA & WORK UNIT NUMBERS DARPA Order No. 3097 Program Code No. P6L10, P6D10, P6E20, P6G10
11. CONTROLLING OFFICE NAME AND ADDRESS Defense Advance Research Projects Agency/TAO 1400 Wilson Boulevard Arlington, Virginia 22209		12. REPORT DATE September, 1975 13. NUMBER OF PAGES 147
14. MONITORING AGENCY NAME & ADDRESS (if different from Controlling Office) Defense Supply Service - Washington Room 1D245, Pentagon Washington, D.C. 20310		15. SECURITY CLASS. (of this report) UNCLASSIFIED 15a. DECLASSIFICATION/DOWNGRADING SCHEDULE

16. DISTRIBUTION STATEMENT (of this Report)

Approved for public release; distribution unlimited.

17. DISTRIBUTION STATEMENT (of the abstract entered in Block 20, if different from Report)

18. SUPPLEMENTARY NOTES

Scientific . . . Interim

19. KEY WORDS (Continue on reverse side if necessary and identify by block number)

Internal Waves
Capillary Waves
Surface Signature
Turbulent Flow
Ocean Microstructure

20. ABSTRACT (Continue on reverse side if necessary and identify by block number)

This is the fourth collection of abstracts of recent Soviet articles on generation and detection of internal waves. It is based on items listed in the fourth Bibliography of Soviet Material on Internal Waves, published June 6, 1975 and covering material received from January through May 1975.

The abstracts are divided into internal effects, and surface effects comprising active and passive measurement of wave states. An author index is appended.

DD FORM 1 JAN 73 1473 EDITION OF 1 NOV 65 IS OBSOLETE

UNCLASSIFIED

SECURITY CLASSIFICATION OF THIS PAGE (When Data Entered)

SOVIET MATERIAL ON INTERNAL WAVE EFFECTS

No. 4, September, 1975

Sponsored by

Defense Advanced
Research Projects Agency

DARPA Order No. 3097

DDC
RECEIVED
OCT 8 1975
A

DARPA Order No. 3097
Program Code No. P6L10, P6D10, P6E20, P6G10
Name of Contractor:
Informatics Inc.
Effective Date of Contract:
September 1, 1975
Contract Expiration Date:
November 30, 1975
Amount of Contract: $100,617

Contract No. MDA-903-76C-0099
Principal Investigator:
Stuart G. Hibben
Tel: (301) 770-3000
Program Manager:
Ruth Ness
Tel: (301) 770-3000
Short Title of Work:
"Internal Waves"

This research was supported by the Defense Advanced Research Projects Agency and was monitored by the Defense Supply Service - Washington, under Contract No. MDA-903-76C-0099. The publication of this report does not constitute approval by any government organization or Informatics Inc. of the inferences, findings, and conclusions contained herein. It is published solely for the exchange and stimulation of ideas.

Informatics Inc
Information Systems Company
6000 Executive Boulevard
Rockville, Maryland 20852
(301) 770-3000

Approved for public release; distribution unlimited

INTRODUCTION

This is the fourth collection of abstracts of recent Soviet articles on generation and detection of internal waves. It is based on items listed in the fourth Bibliography of Soviet Material on Internal Waves, published June 6, 1975 and covering material received from January through May 1975.

The abstracts are divided into internal effects, and surface effects comprising active and passive measurement of wave states. An author index is appended.

TABLE OF CONTENTS

I. Internal Effects

Reproduced from best available copy.

Ozmidov, R. V., V. S. Belyayev, M. M. Lyubimtsev, and V. T. Paka. Investigation of the variability of hydrophysical fields in an ocean test area. IN: Sb. Issled. izmenchivosti gidrofiz. poley v okeane. Moskva, Nauka, 1974, 3-31.

A study is described on the variability of hydrophysical fields in the ocean over a wide range of space and time scales, as reported by the Shirshov Institute of Oceanology of the USSR Academy of Sciences. The sequence of measurements is described and illustrated, using as an example one of the test areas of the 7th cruise of the R/V Dmitriy Mendeleyev in 1972 (Fig. 1)

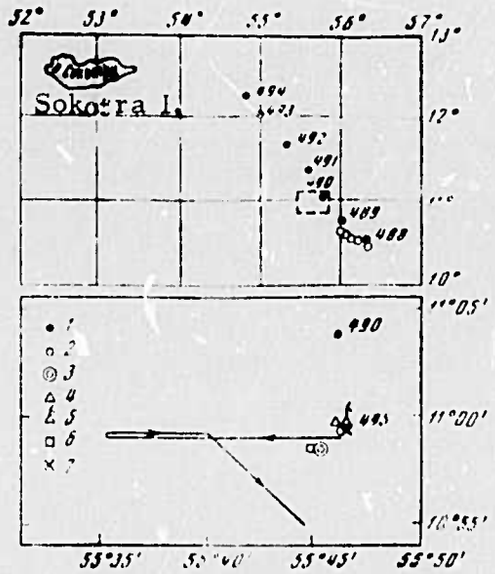

Fig. 1. Schematic of test area for measurement of oceanic turbulence and hydrological conditions, with hydrological stations labeled by numerals. Lower diagram is blowup of inset in upper map. Key for measurements:

1 - standard hydrological series bathythermography, sounding by Aist probe, and sounding of flow velocity by acoustic probe; 2 - sounding by Aist and acoustic probes; 3 - repeated soundings by Aist probe; 4 - flow velocity and photothermography at moored buoy; 5 - temperature from radio buoy; 6 - electrical conductivity by sigma probe; 7 - bathythermography; solid line is path of towed turbulimeter.

The measurements in a test area began with standard observations at hydrological stations (H.S.). The large-scale vertical structures of T, S, σ_t and flow velocity inferred from these measurements revealed that vertical density gradients are generated and maintained by the horizontal transport of water masses which acquired their physical characteristics before reaching the Somalia Current. In the vicinity of H.S. 490 (Fig. 1) there exists a weakly pronounced high-gradient layer and two almost opposite currents. In order to obtain more detailed information on flow velocity structure near H.S. 490, a moored buoy with BPV current meters and a recently developed acoustic probe was used. The probe detects Doppler shift of acoustic signals scattered at density inhomogeneities in a flow. More detailed information and space-time vertical structure of T, S, and σ_t was obtained by an Aist probe. These measurements were supplemented by temperature observations at the radio buoy, which revealed temperature fluctuations with periods of 3.5 hour and 5-10 min, and energy concentration at h = 140 m and $k = 10^{-3}\,cm^{-1}$.

The most detailed structure of hydrophysical fields were inferred from measurements of $\bar{u}$, u', $\bar{T}$, T', $\bar{\xi}$ and ξ' by towed sensor chains including thermistors, capacitance-type transducers and Stolypin-type hot-wire anemometers. The results of these measurements are illustrated in Figs. 2-6.

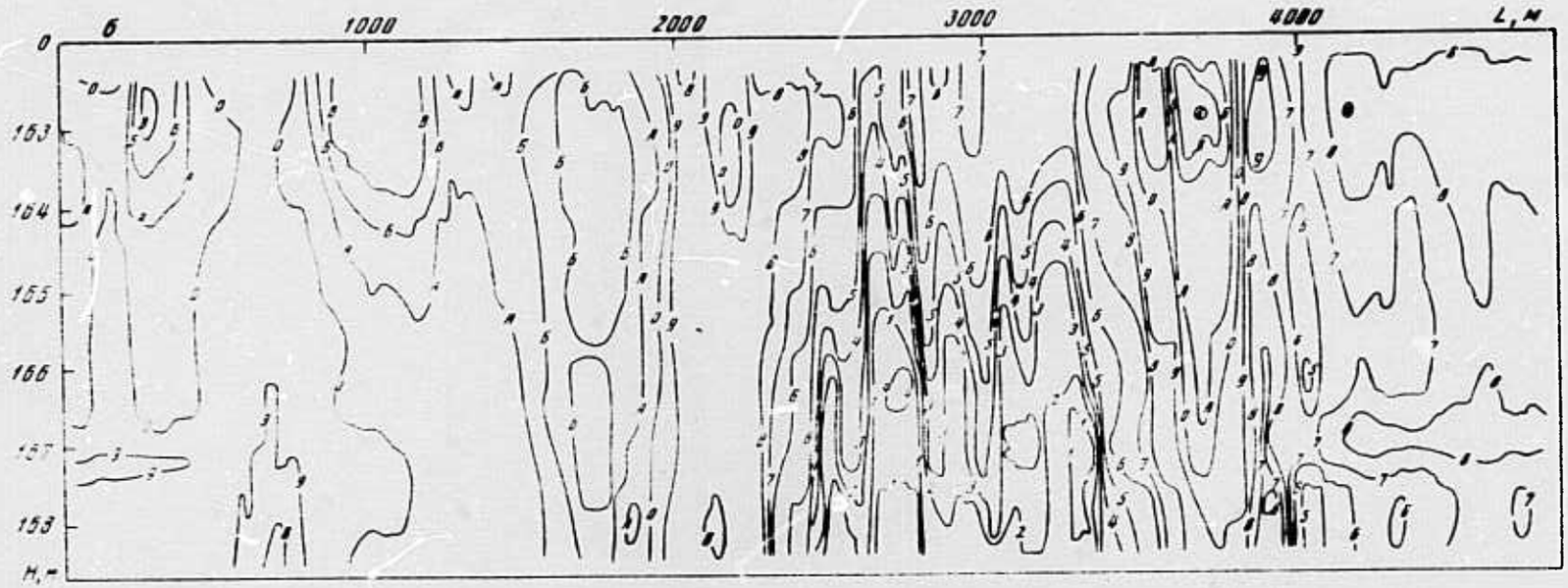

Fig. 2. Two-dimensional structure of temperature from measurements by towed sensor chains.

1 - 18.2°C; 2 - 18.3; 3 - 18.4; 4 - 18.5; 5 - 18.6; 6 - 18.7; 9 - 18.8; 8 - 18.9; 9 - 19.0; O - 19.1; A - 19.2; - 19.3; B - 19.4.

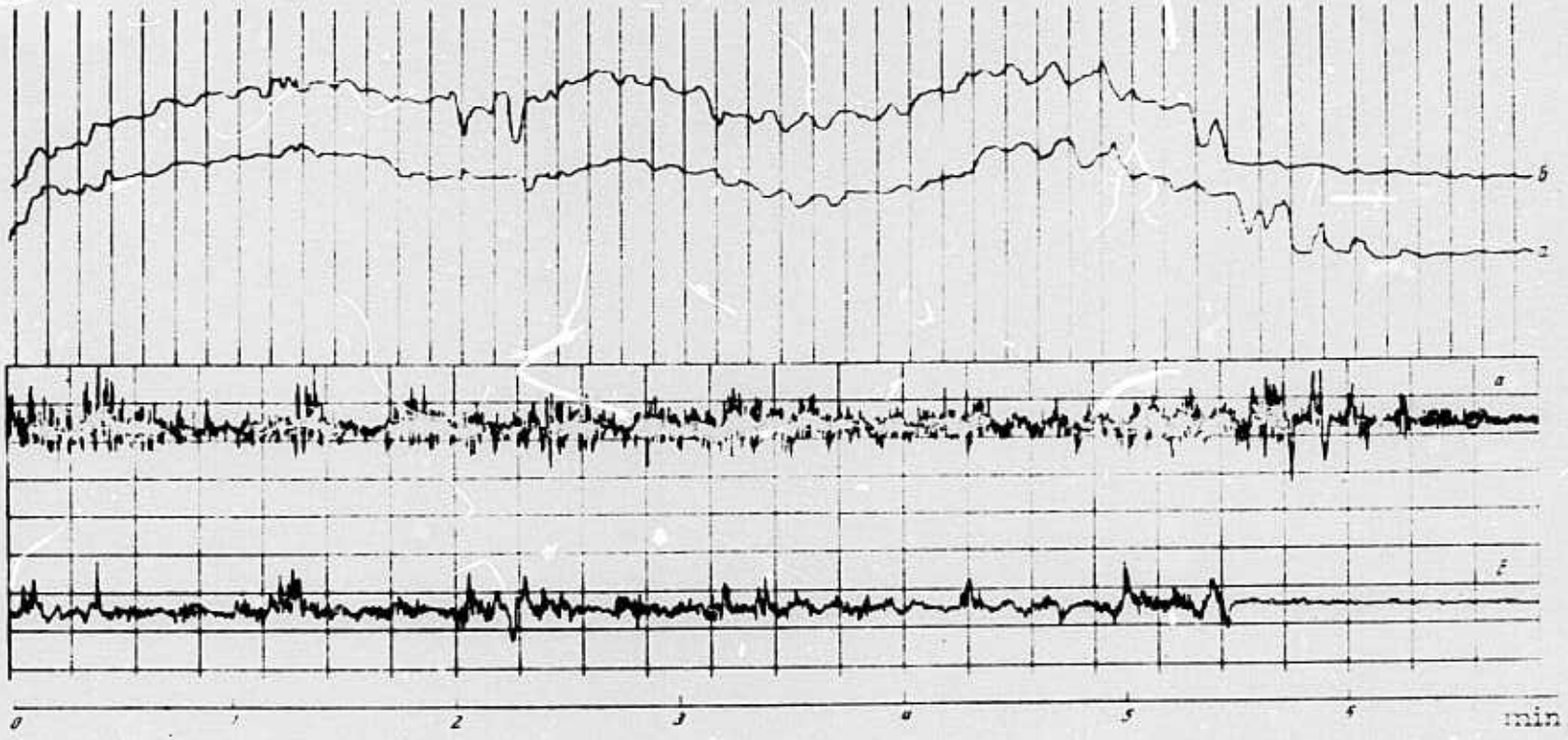

Fig. 3. Example of high- and low-frequency fluctuations of electrical conductivity measured simultaneously by two 70 cm-spaced indicators.

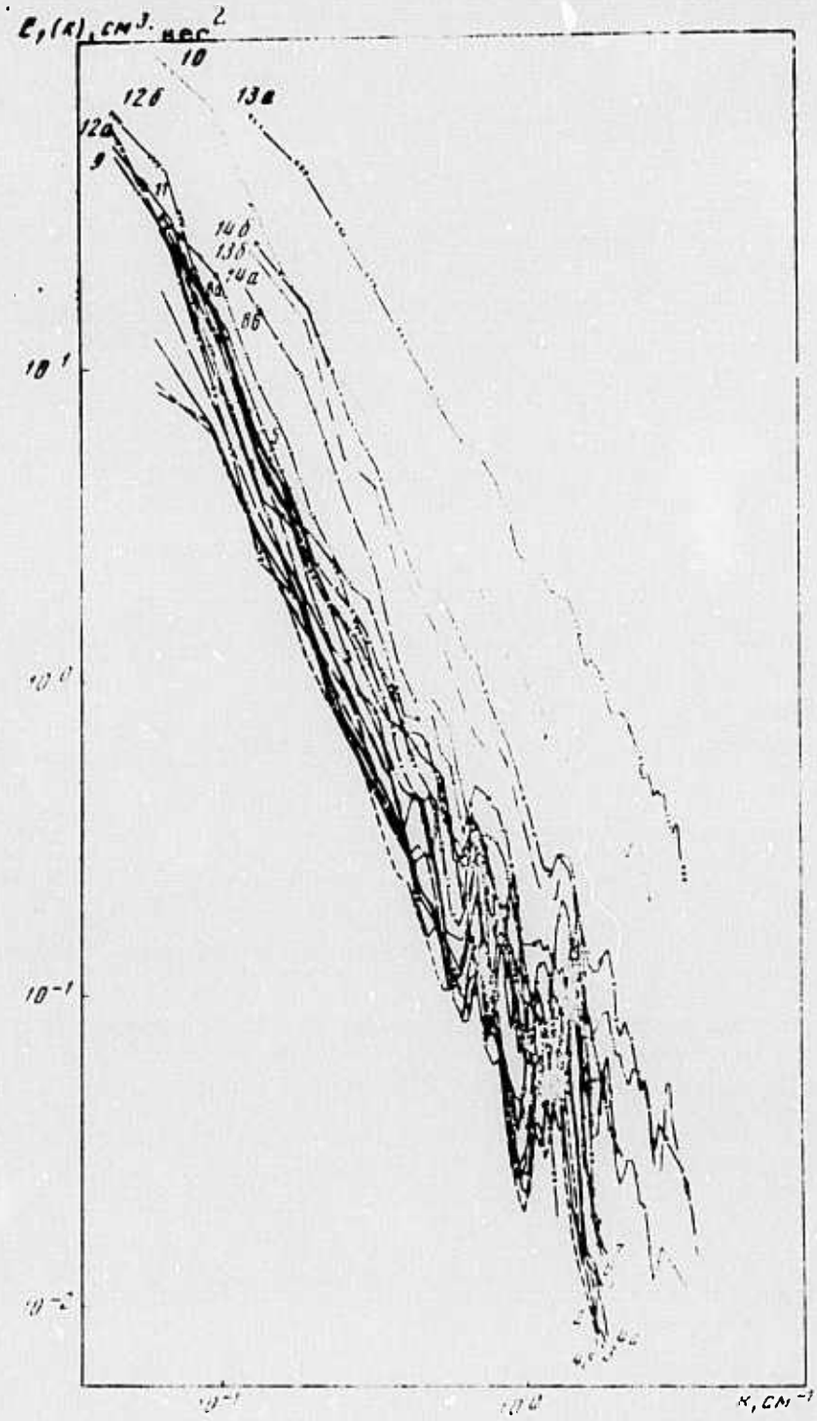

Fig. 4. Spectral densities for small-scale fluctuations of flow velocity from measurements by towed chains at 20 (1), 33(2), 55 (3), 77 (4), 94 (5), 103 (6), 121 (7), 138 (8), 141 (9), 157 (10), 160 (11), 168 (12), 195 (13), and 213 m (14).

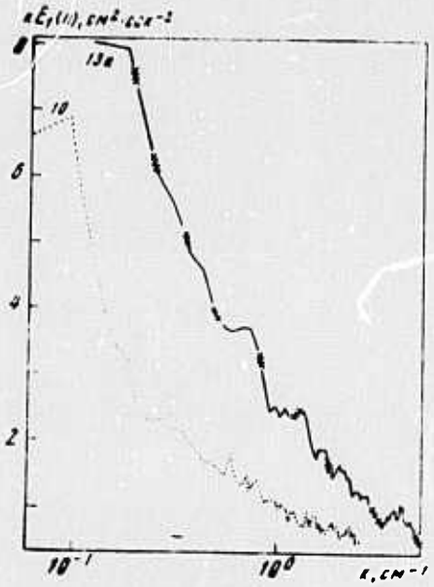

Fig. 5. Intensity spectra for small-scale fluctuations of flow velocity from measurements by towed chains.

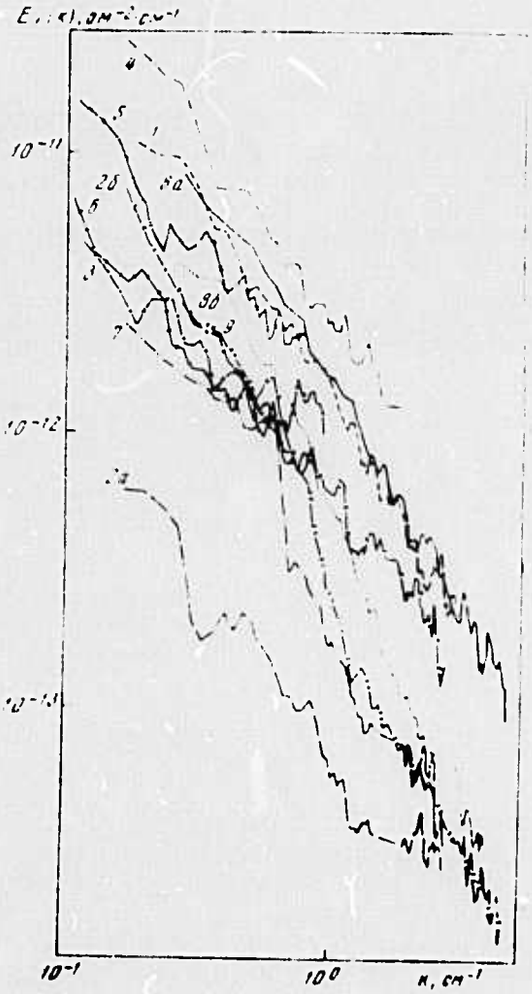

Fig. 6. Spectral densities for fluctuations of electrical conductivity from measurements by towed chains at 94(1), 138(2), 141(3), 157(4), 160(5), 168(6), 174(7), 195(8), and 213 m (9).

The dissipation rates of turbulence energy and temperature inhomogeneities were calculated to be $\epsilon = 10^{-2}$ cm^2/sec^{-3} and $N = 10^{-3}$-10^{-4} deg^2/sec, respectively. The buoyancy scale $L_* = \epsilon^{5/4}/N^{3/4}(g\alpha)^{3/2}$ was found to be of an order of magnitude equal to that of "steps" in the fine density structure.

The results of measurements of small-scale fluctuations of electrical conductivity at large depths (to 1200 m) by a Sigma probe are shown in Figs. 7-10.

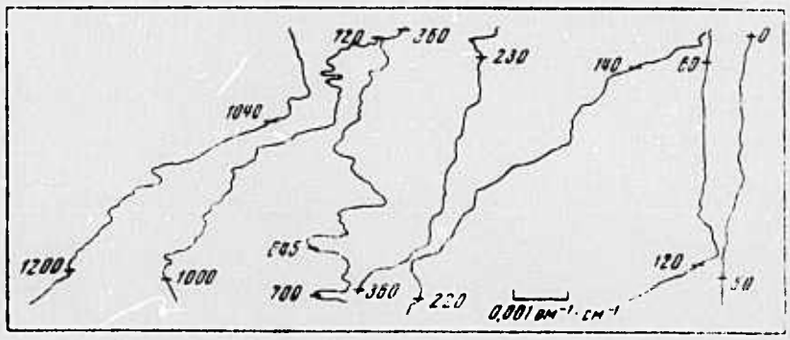

Fig. 7. Sample records of mean electrical conductivity. Numbers are depths in meters.

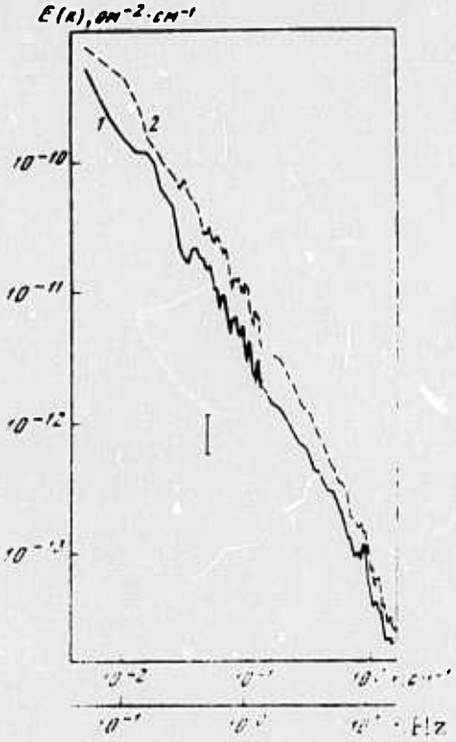

Fig. 8. Spectral densities for fluctuations of electrical conductivity at large depths.

1 - 645 m; 2 - 720 m.

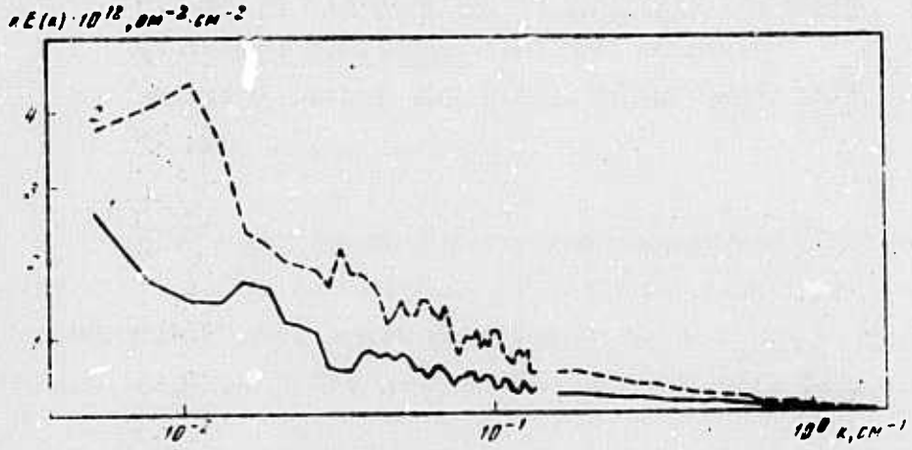

Fig. 9. Intensity spectra for fluctuations of electrical conductivity.

1 - 645 m; 2 - 720 m.

Fig. 10. Dissipation spectra for fluctuations of electrical conductivity.

1 - 645 m; 2 - 720 m.

Dotsenko, S. F. On the structure of wave motion in a flow having an arbitrary variation of density with depth. IN: Sb. Morsk. gidrofiz. issled. No. 3(62), Sevastopol', 1973, 32-41.

Stationary internal waves generated by surface pressure are analyzed in a linear formulation. Plane stationary flow of an ideal incompressible fluid with undisturbed density $\rho_o = \rho_o(z)$ is considered. The pressure exerted at the free surface of the flow is defined by

$$p_0 = f(x), \tag{1}$$

where f(x) is an even function, equal to zero at $|x| > a$ $(a > 0)$.

Fluid motion is described by the set of equations

$$u_x = -\sqrt{\nu}\,\rho_0^{-1}(p_x + p_{0x}), \qquad w_x = -\sqrt{\nu}\,\rho_0^{-1}(p_z + p_z),$$
$$u_x + w_z = 0, \qquad \rho_x - \sqrt{\nu}\,\rho_{0z} w = 0 \tag{2}$$

with boundary conditions

$$p - \zeta = 0, \qquad \zeta_x - \sqrt{\nu} w = 0 \quad \text{at} \quad z = 0,$$
$$w = 0 \quad \text{at} \quad z = -1. \tag{3}$$

Here $\nu = gHV^{-2}$; H is depth of flow; V is flow velocity (V = const); u, w, p, and ρ dynamic disturbances of horizontal and vertical velocity, pressure and density; and ξ = deviation of the free surface from z = 0. Solution of (2) and (3) is obtained in the form

$$w = \frac{i\sqrt{\nu}}{\sqrt{2\pi}} \int_{-\infty}^{+\infty} \frac{m W_1}{\Delta} f^* e^{imx}\, dm, \tag{4}$$

where $\Delta = \Delta(\lambda, \nu) = W_{1z}(\lambda, 0, \nu) - \nu W_1(\lambda, 0, \nu)$.

The poles on the integration path for the integrand in (4) are discussed in detail.

An asymptotic analysis of (4) shows that, in a linear formulation, pressure disturbances do not excite unattenuating waves at $\nu < \nu_1$. The wave motion generated at $\nu_n < \nu < \nu_{n+1}$ consists of waves exponentially attenuating at $|x| \to +\infty$, and of an unattenuating wave wake which is generated downstream from the surface pressure. The wave wake represents a sum of exactly n standing harmonic waves.

The amplitude of every k-th unattenuating wave displays k-1 zeros in the interval (-1, 0). The length of the k-th wave is greater than those of lower order wakes. Dispersion curves $m_k = m_k(\nu)$ $(k > 1)$ determined at $\nu \geq \nu_k$ rise monotonically and have common asymptotes, $m_o = \beta \nu^{1/2}$. The number of unattenuating waves at $\nu \to +\infty$ is given by

$$N(\nu) \sim \frac{1}{\pi} \omega \nu^{\frac{1}{2}}, \qquad \omega = \int_{-1}^{0} \left(-\rho_0^{-1} \rho_{0z}\right)^{\frac{1}{2}} dz, \tag{5}$$

In the case when $a(z) = -\rho_o^{-1} \rho_{0z}$ at least n-2 nodal points of $b_n(z)$ fall in the interval (z_1, z_2). At $\nu \to +\infty$ this interval narrows around z_o. Hence, with an increase of ν, every internal wave concentrates its nodal points in the vicinity of the maximum density gradient.

The author observes that the above established characteristics hold true also for wave motion generated by other types of disturbances (bottom roughness, hydrodynamic actions, etc.), as well as for any continuously decreasing function $\rho_o(z)$ which has at least one interval of monotonic decrease.

Dotsenko, S. F., and L. V. Cherkesov.
Generation of internal waves by underwater disturbances. IN: Sb. Morsk. gidrofiz. issled. No. 3 (62), Sevastopol', 1973, 19-31.

Internal waves in an ideal incompressible inhomogeneous fluid, generated by a moving immersed point source, are analyzed. The linearized problem is solved for exponential change with depth of undisturbed density, $\rho_0 = \rho_0(z)$. The numerical analysis assumes no attenuation of wave amplitude with distance from the source. Generation of waves by bottom roughness is discussed as well.

A point source with strength Q = const is assumed located at depth H_1 in the fluid layer $-\infty < x < +\infty$, $-H \leq Z \leq 0$. It moves at velocity V = const in the direction of negative x. Undisturbed density ρ_0 decreases with increase of z. For convenience, the linearized problem of stationary waves in a flow generated by point source at rest is solved. Fluid motion is described by the set of equations

$$u_x = -\sqrt{\nu}\rho_0^{-1}\rho_x, \quad w_x = -\sqrt{\nu}\rho_0^{-1}(\rho + \rho_z), \tag{1}$$

$$u_x + w_z = 0, \qquad \rho_x + \sqrt{\nu}\rho_{0z} w = 0$$

with boundary conditions

$$w_z(x,0) - \nu w(x,0) = 0, \quad w(x,-1) = 0. \tag{2}$$

Here $\nu = gHV^{-2}$; u, w, p, and ρ are disturbances of horizontal and vertical velocity, pressure and density; the source is located at (0, -h) ($-\infty < x < +\infty$, $-1 \leq Z \leq 0$, $0 \leq h \leq 1$, $h = H_1 H^{-1}$).

Analysis shows that nonattenuating wave motion is generated at a velocity V which is somewhat less than the velocity of long waves in a homogeneous fluid. Also, $u_n(z)$ and $w_n(z)$ as well as wave number m_n for an individual standing wave are independent of the disturbing factor generating it. The effect of fluid inhomogeneities on amplitude of the surface

wave A_1 ($A_n = \max |w_n(z)|$) is weak and diminishes with increase of V (see Fig. 1).

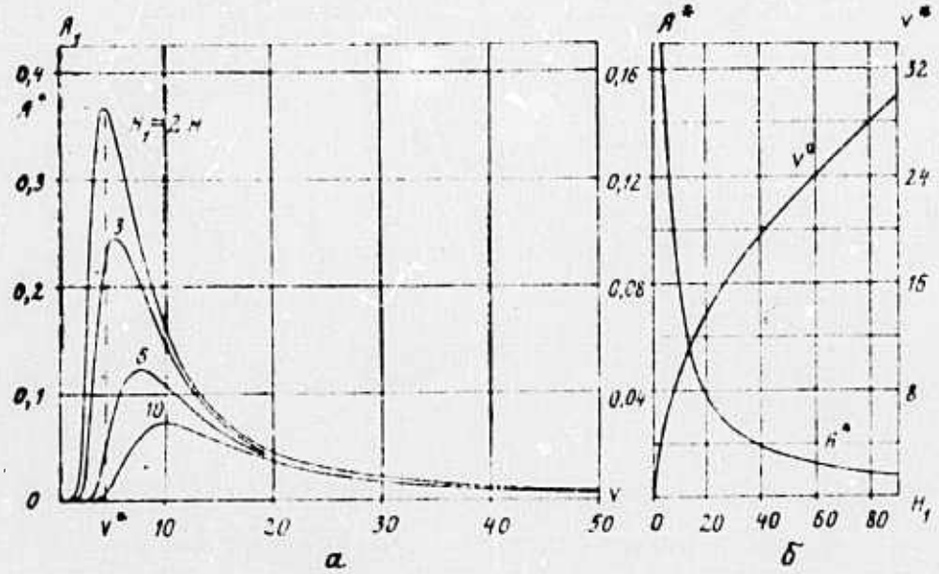

Fig. 1. Amplitude of surface wave A_1 vs. V and H_1.

Characteristics of amplitudes of individual internal waves are analyzed using expressions obtained with the Boussinesq approximation, assuming that $z = 0$ is a solid surface. Amplitudes of individual internal waves at a given z oscillate as h changes within the interval $0 \leq h \leq 1$. For every n-th wave there are $(n - 1)$ locations of the source for which it does not propagate into infinity. Amplitudes of internal waves at $\nu > \nu_n$ and given h decrease with increase of ϵ and H and decrease of V. At $\nu \to \nu_n + 0$, $A_n \to +\infty$ and $B_n \to \infty$. Hence, $\nu = \nu_n$ are resonant values and excitation of each new wave, owing to increase of ν_ϵ has a resonant nature. At $\nu_n < \nu < \nu^* = 2\nu_n$ the horizontal motion in the n-th wave is more intense than vertical, while at $\nu > \nu^*$ the opposite is true.

The net wave motion at a sufficiently large distance from the source consists of a finite number of standing waves with various lengths and amplitudes. Characteristics of A(z) and B(z) (see Fig. 2) are determined by the longest individual wave.

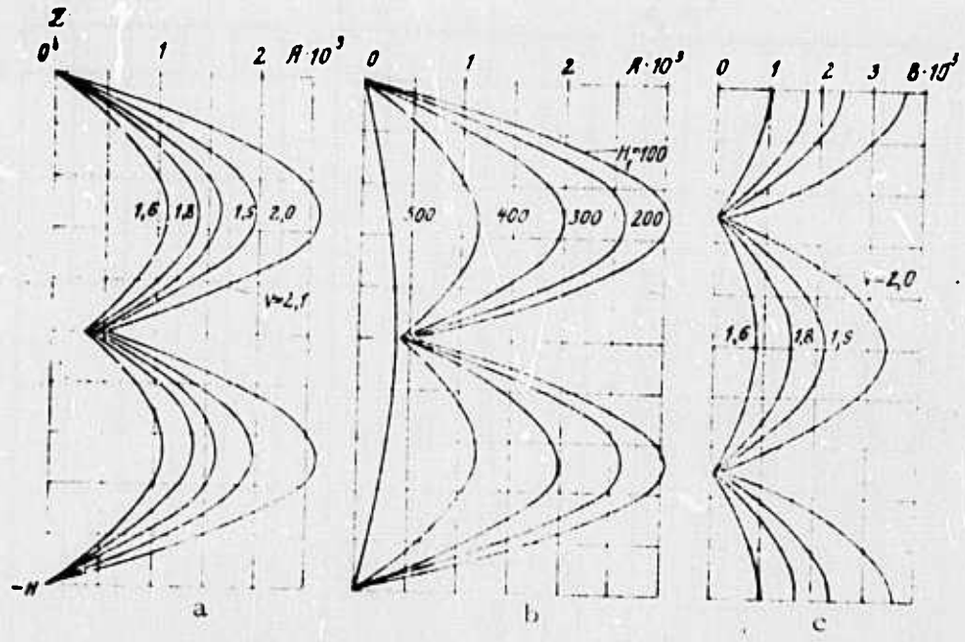

Fig. 2. Dependence of A(z) and B(z) on V and H_1.
a, b - $H_1 > 200$ m; c - V = 2.1 msec^{-1}.

Dependence of A_o = max A(z) and B_o = max B(z) on H_1 and V (see Fig. 3) are determined by the longest individual wave, namely by the N-th wave at $V_{N+1} \leq V < V_N$. Consequently, there are N-1 locations of the source for which wave motion caused by internal waves is weak.

The authors note that results on internal waves generated by moving surface pressure (Dotsenko and Cherkesov, 1971) can be applied to the case when stationary waves are generated from flow past a rough bottom:

$$z = -H + \alpha f(x), \tag{3}$$

where f(x), an even function equal to zero at $|x| > \ell$, differs slightly from z = -H.

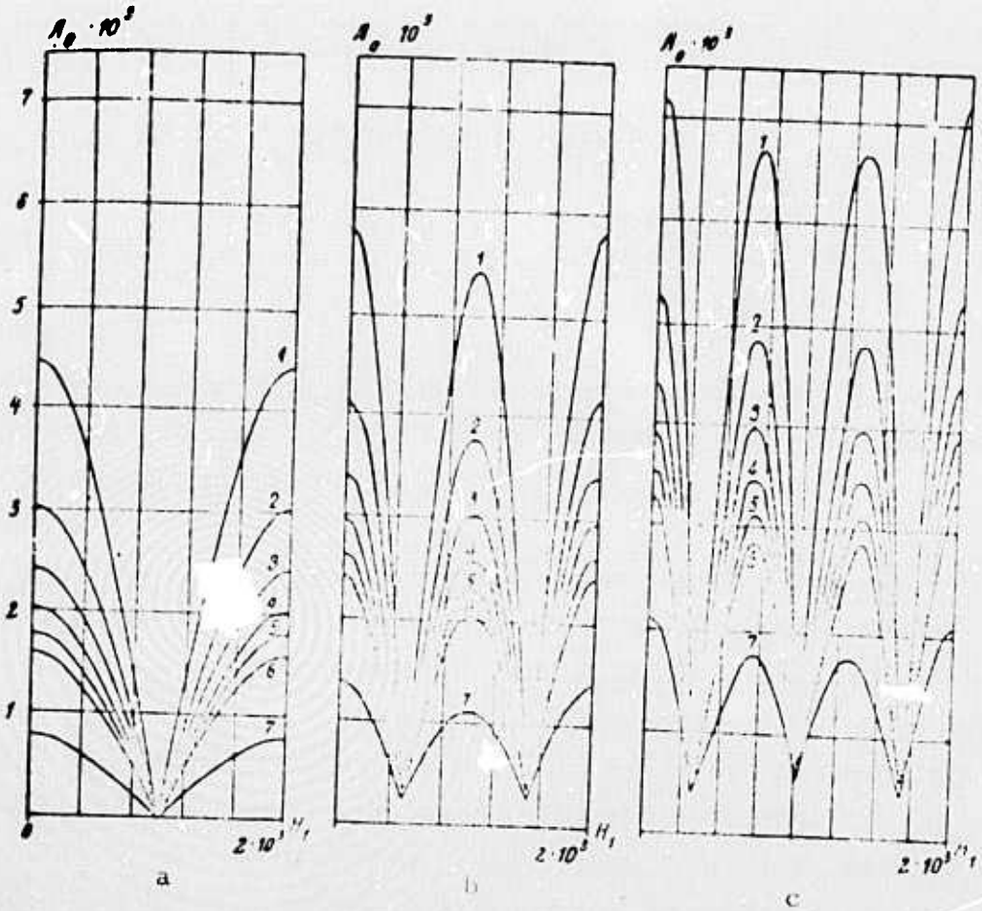

Fig. 3. Dependence of A_0 on H_1 and V.
a - N = 2; b - N = 3; c - N = 4.

Dotsenko, S. F. Internal waves excited by a source in a fluid flow with a discontinuity layer. IN: Sb. Morsk, gidrofiz. issled. No. 2(65). Sevastopol', 1974, 45-51.

Stationary waves generated by an immersed point source in a continuously stratified flow are analyzed. The following is the formulation of the problem.

Plane flow of an ideal incompressible fluid occupies the space $-\infty < x < +\infty$, $-H \leq z \leq 0$. Flow velocity V = const is in the direction of positive x. Undisturbed fluid density is

$$\rho_0 = \rho_1 \begin{cases} 1, & z_1 \leq z \leq 0 \\ \exp\left[-\kappa(z - z_1)\right], & z_2 \leq z \leq z_1 \\ \exp \kappa(z_1 - z_2), & -H \leq z \leq z_2, \end{cases} \qquad (1)$$

The disturbing source with strength Q = const is located at $(0, -\bar{H})$. Fluid motion is described by the set of equations given by Wu and Mei (Phys. Fl., v. 10, no. 3, 1967).

It is shown that wave motion generated in this case represents a sum of a finite number of standing waves. Variation with respect to z of w_s (s = 2,... n), corresponding to individual internal waves, is characterized by s-1 zeros and s extrema at $-H < z < 0$. When the source is located within either the upper $(0 < \bar{H} < h_1)$ or the lower $(h_1 + h_2 < \bar{H} < H)$ layer, the amplitude of internal waves increases as the source approaches the discontinuity layer. If the source is located within the discontinuity layer $(h_1 < \bar{H} < h_1 + h_2)$ then for every s-th internal wave there exist s-1 locations of the source $\bar{H} = Hs\ell$ (ℓ = 1, .. s-1) for which its amplitude is zero, and s locations for which its amplitude is maximum. These conclusions are illustrated in Fig. 1 which shows $\alpha(\bar{H}) = A_4(\bar{H})/A_4(0)$.

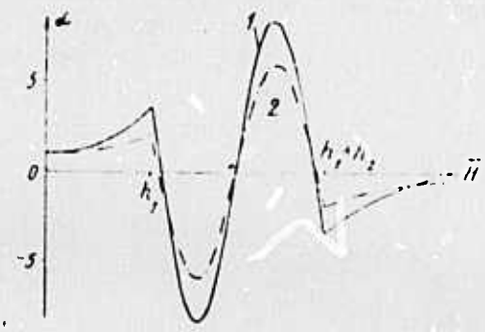

Fig. 1. Wave amplitude vs $\bar{H}$.
1 - V = 0.4 msec^{-1}; 2 - 0.43 msec^{-1}.

At sufficiently large distance from the source the wave field is composed of a finite number of standing waves with different length, amplitude and vertical profile. $A(z) = \sum_{s=2}^{n} \left| w_s(z) \right|$ for this field behaves similarly as in the case of surface disturbances. (cf. Dotsenko and Cherkesov, foregoing abstract). A_o max A(z) is reached in the discontinuity layer. When the source is located in a homogeneous layer the wave field A(z) is determined by the longest individual wave.

If the source is located in a discontinuity layer the (n - 1)-th wave becomes predominant. Fig. 2 gives $A_o(\bar{H})$ for $V = 0.5 (V_n + V_{n+1})$.

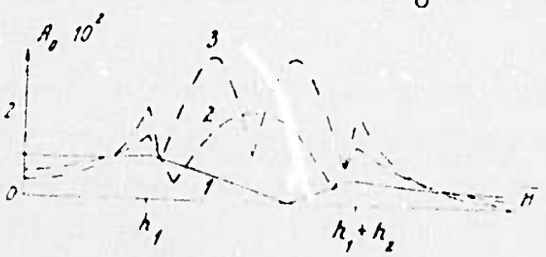

Fig. 2. A_o vs $\bar{H}$.

1 - n = 2; 2 - n = 3; 3 - n = 4.

Fig. 3 shows that if the source is located within the upper layer, internal wave amplitudes decrease with V. If the source is located within the lower layer, the most intense internal waves are generated at $V = \bar{V}_n$ which increases as the source departs from the discontinuity layer.

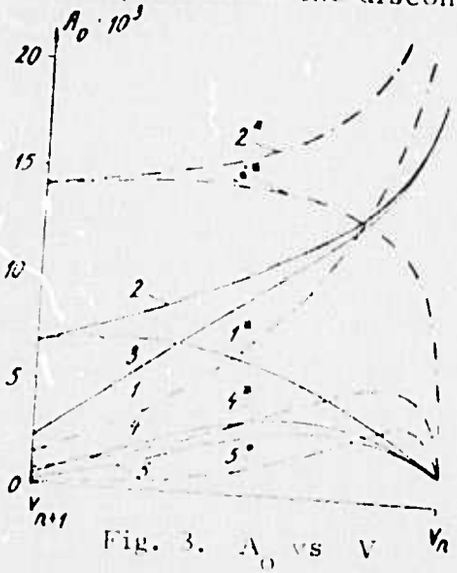

Fig. 3. A_o vs V

1-5: n = 2; 1*-5*: n = 3.

Reproduced from best available copy.

Dotsenko, S. F., and L. V. Cherkesov. On internal waves in the vicinity of a moving pressure area. IN: Sb. Morsk. gidrofiz. issled. No. 4(63). Sevastopol', 1973, 11-23.

Stationary surface and internal waves in a continuously stratified fluid, generated by a moving surface pressure area, are analyzed. Special attention is given to the wave pattern in the vicinity of the pressure area. A criterion is formulated for determining the region in which approximate analysis of the wave field is applicable.

Plane flow of an ideal incompressible fluid with undisturbed density $\rho = \rho(z)$ is considered. Surface pressure is defined by $p = af(x)$ where $f(x)$ is an even continuous function equal to zero at $|x| > a$. The linearized problem is solved for

$$f = \begin{cases} \cos \varkappa x, & |x| < \ell \\ 0, & |x| \geq \ell \end{cases} \qquad \left(\varkappa = \frac{\pi}{2\ell}, \quad f^* = \frac{2\varkappa \cos m\ell}{\varkappa^2 - m^2} \right) \tag{1}$$

A numerical analysis is made for

$$\rho_0 = \rho_1 \exp(-\varepsilon z) \qquad (0 < \varepsilon \ll 1, \quad -1 \leq z \leq 0), \tag{2}$$

The particular case of a wave field attenuating with distance is considered.

It is found that generated wave motion consists of two wave fields: one that exists both before and behind the moving surface pressure and which attenuates exponentially with distance; and a second which exists only at $x \geq -\ell$ (wave wake) and which represents a sum of a finite number of standing waves. Attenuation of the former field ($w^{(0)}$) at $|x| \to \infty$ decreases with increase of ν ($\nu_N < \nu < \nu_{N+1}$).

Characteristics of wave motion at $x \leq -\ell$ are determined for the attenuating wave field. Fig. 1a. shows the vertical profile of $\bar{w} = w(-\ell, z)/w(-\ell, z_*)$ where $z = z_*$ corresponds to $\max |w(-\ell, z)|$.

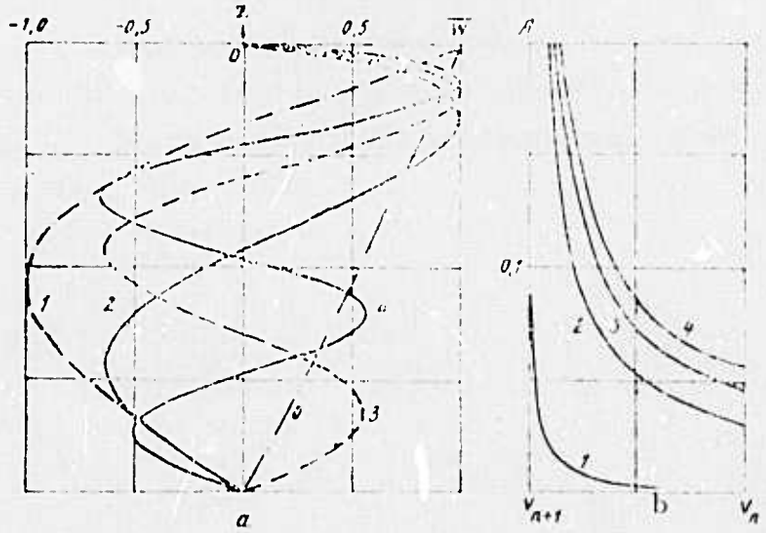

Fig. 1.

a) 0 - $V = 1.1\ V_1$; 1-4 - $V = 0.5\ (V_n + V_{n+1})$, $n = 1\text{-}4$; b) 1-4 - $n = 1\text{-}4$, respectively.

The dependence of $A = \max_z |w(-\ell, z)|$ on V ($V_{n+1} < V < V_n$) is given in Fig. 1, b. Behavior of $u(-\ell, z)$ and $\xi(-\ell, z)$ is similar to that of $w(-\ell, z)$ (see Fig. 2).

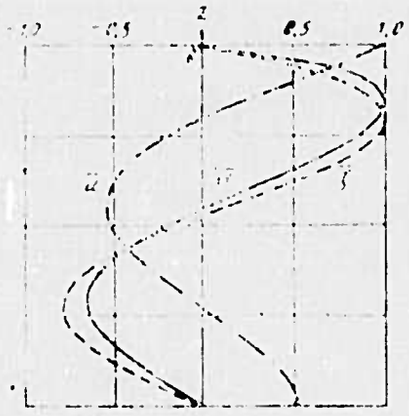

Fig. 2.

$V = 0.5\ (V_2 + V_3)$.

It can be seen that $\max_z |u(-\ell, z)|$ is reached at the free surface. Thus the arrival of the moving pressure area at a given point is preceded by deformation of the free surface and excitation of a wave field which can be significant at some v which is close to but smaller than v_N.

The dependence on ν of deflection of free surface under the pressure area, calculated by a generalized Proudman's formula, is shown in Fig. 3. Characteristics of attenuating wave field under the pressure area are shown in Fig. 4.

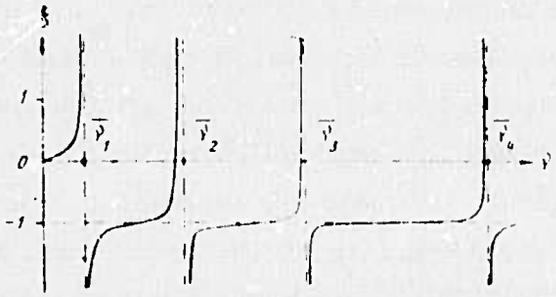

Fig. 3.

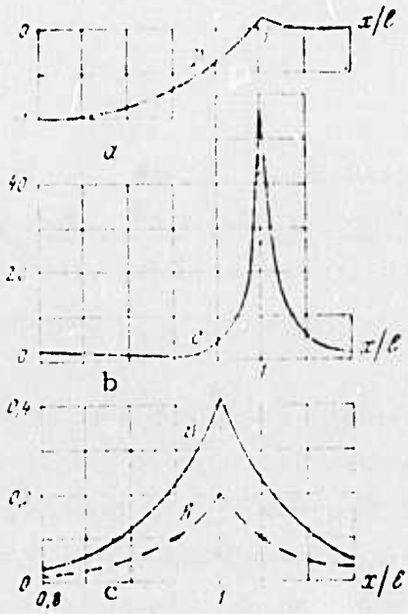

Fig. 4.

$A(x) = \max_z w^{(0)}(x, z)$;

$B(x) = \max_z u^{(0)}(x, z)$;

$C(x) = \max_z \xi^{(0)}(x, z)$;

$D(x) = \xi^{(0)}(x, 0)$.

The largest deflections of flow lines from their undisturbed position occur within the fluid (Fig. 4, b) and significantly exceed displacement of the free surface. At $\nu \to \nu_s - 0$, $B \to +\infty$ and $C \to +\infty$. Hence, $\nu = \nu_s$ are resonant values for the attenuating field. On the other hand, $\nu = \nu_s$ are resonant values for an unattenuating field (Dotsenko, 1973). Consequently parametric transformations of an attenuating into unattenuating wave and vice versa have a resonant nature. This shows that at a ν slightly smaller than ν_s, variations of wave field with respect to x and z, both under the pressure region and in close proximity to it, are determined by attenuating waves; variation of the wave field with respect to x and z as $x \to \infty$ is determined by unattenuating waves.

Grishin, G. A., and V. V. Yefimov. Wind waves on steady vertically nonuniform currents. Morskiye gidrofizicheskiye issledovaniya, no. 4, 1973, 24-42.

The problem is analyzed of surface wave disturbances caused by simultaneous effects of wind and a time-invariant translational current with a vertical gradient $\bar{U}(z)$ of average velocity. The equations of motion are solved for the flow function with allowance for wind energy transfer to the waves and seawater turbulent viscosity, ν_T. The parameter

$$\beta = \alpha\beta_0 + \alpha^2\beta_1 + \varepsilon\beta_2 + \ldots, \tag{1}$$

is introduced into the dynamic boundary condition to describe the rate of wind energy transfer. The small parameter

$$\alpha = (2\nu_T k^2/\omega_0)^{1/2} \tag{2}$$

is the characteristic of wave energy loss due to ν_T. In equations (1) and (2) $\epsilon = U_0/C_0$ is the parameter of average current effect on waves, $C_0 = \omega_0/k^{-1}$

is the characteristic phase velocity, ω_0 is the characteristic frequency of surface oscillations, k is the wave number, and U_0 is the characteristic scale of translational current. The boundary value problem is solved by the method of successive approximations in the form of the asymptotic series

$$\psi(x, t, z; \varepsilon, \varepsilon_1, \alpha) = \varepsilon_1 \sum_{j,i=0}^{\infty} \varepsilon^j \alpha^{i-1} \psi^{(ji)}, \tag{3}$$

where $\epsilon_1 = ak$ is the wave slope (a is the wave amplitude).

New characteristics of surface waves are revealed by solving the viscosity problem with allowance for the effect of a steady vertically nonuniform current. An additional factor $(1 + 2\epsilon/\varkappa + 2)$, where $\varkappa$ is a dimensionless factor, in the expression of the dispersion ratio

$$\omega = \sqrt{\frac{gk}{1+k}}\left(1 + \frac{2\varepsilon}{\varkappa+2}\right). \tag{4}$$

takes into account the effect of steady current with $\bar{U}(z)$. Both viscosity and current wave interaction result in additional vorticity of wave motion in the surface layer.

Interaction between different vortices is reflected in formulas for the normal and tangential Reynolds stresses $\overline{uw}$ which are associated with periodic disturbances of the velocity field. The components u and w of wave orbital velocity are formulated and the vertical profile of phase shear φ uw is calculated (Fig. 1).

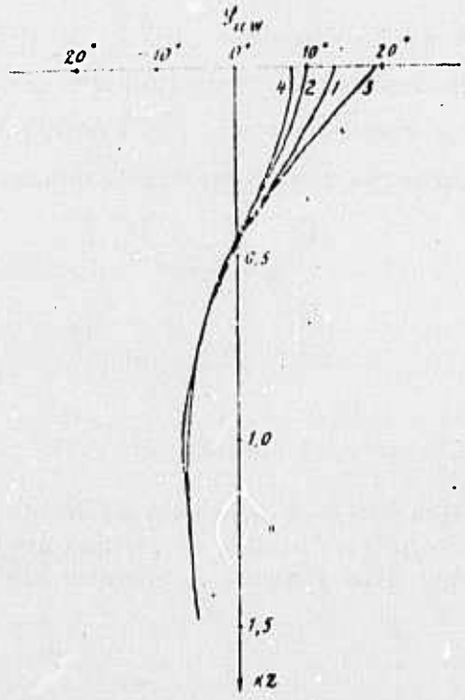

Fig. 1. Phase shear between u and w vs. depth at:

1- α = 0.3, $\kappa = \gamma$ = 1, ϵ = 0.2; 2- α = 0.3, $\kappa = \gamma$ = 1, ϵ = -0.2; 3- α = 0.3, γ = 1, κ = 2, ϵ = 0.2, and 4- α = 0.3, γ = 1, κ = 2, ϵ = -0.2. $\gamma = 1 - 2\nu_{TZ}/\nu_T$ are coefficients of turbulent viscosity which determine tangential and normal Reynolds wave stresses.

Nekrasov, V. N., and Yu. D. Chashechkin. Measuring velocity and period of internal oscillations of fluid by the method of density marks. Metrologiya, no. 11, 1974, 36-41.

The method discussed uses density marks generated by the hydrodynamic wake of freely ascending gas bubbles, together with optical

recording. It depends on an even and linear motion of gas bubbles which can be realized if $Re = 2Vr/\nu < 220$, where V is ascent rate and ν is kinematic viscosity; i.e. the optimum radius and ascent rate for gas bubbles are 0.2 cm < r < 0.0063 cm and 4 cm/sec < V < 15 cm/sec, respectively. The experimental arrangement employed is shown in Fig. 1.

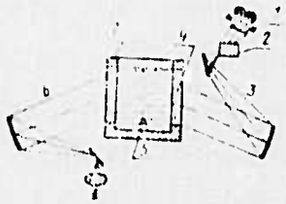

Fig. 1. Bubble tracker.

1- motion-picture camera; 2- Foucault wedge; 3, 6- shadowgraphs; 4- lateral walls of optical glass; 5- air nozzle; 7- vessel with stratified fluid.

The principal cited advantages of the use of density marks produced by gas bubbles include their long lifetime (25-30 sec) and high contrast. In addition, if several density marks are produced simultaneously they can be used in the study of a flow structure in the direction of optical axis of the shadowgraph, which is important in the case of a three-dimensional nonstationary flow.

Vlasov, Yu. N. Using optical marks in hydrodynamic investigations to obtain uniform measurements of velocity and turbulence of fluid flows. Metrologiya, no. 11, 1974, 29-36.

Theoretical and experimental aspects are discussed of the generation of optical marks (density inhomogeneities) by variance in temperature, pressure, and salinity in a small volume of fluid. Special

emphasis is given to production of optical marks by laser irradation. Errors in measuring velocity of a stationary laminar flow by the method of drift time are analyzed.

A theoretical study of the dynamics of laser-produced density inhomogeneities, which was made accounting only for thermal and electrostriction effects, showed that density change depends on laser pulse energy. Furthermore, enhancement of thermal effects and suppression of electrostriction effect is obtained by increasing absorption coefficient and pulse duration. Experiments with free-running ($\tau = 5 \times 10^{-4}$ sec) and Q-switched ($\tau = 2 \times 10^{-8}$ sec) ruby and neodymium lasers demonstrated that a free-running Nd laser ($\tau = 10^{-6} - 10^{-3}$ sec) is the most suitable for production of optical marks used in hydrodynamic studies (Fig. 1).

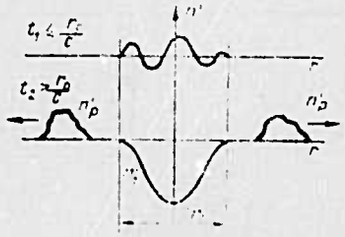

Fig. 1. Laser-induced changes of retraction in fluid at various time increments.

The relative error in measuring velocity was found to be 0.2-0.3%. This high accuracy makes it possible to use optical marks in calibration of velocity transducers.

Vorob'yev, V. P., and L. G. Palevich. Designing a recording system for studying the fine structure of the ocean. IN: Sb. Issled. izmenchivosti gidrofiz. poley v okeane. Moskva, Nauka, 1974, 155-162.

This article lists improvements introduced into the recording systems for studying the fine structure of hydrophysical fields in the ocean during the 7th cruise of the R/V Dmitriy Mendeleyev in 1971-1972. Specifications for instruments which comprised the towed measuring system (Fig. 1) employed in these measurement are listed in Table 1. Gradual enlargement of the scope of measurements and

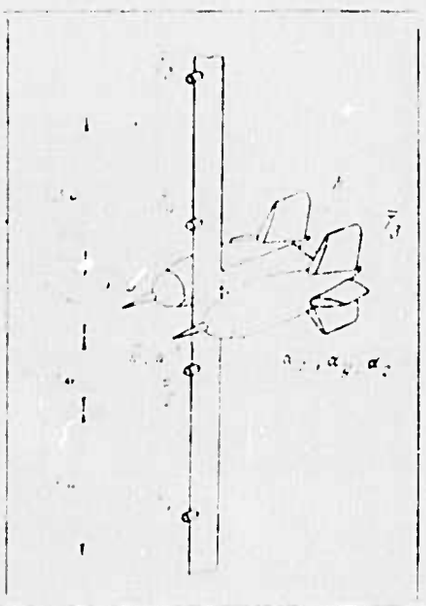

Fig. 1. Configuration of towed instrument system.

refinement of the recording system are illustrated in three block diagrams for different test areas.

Table 1

Specifications for instruments of the Institute of Oceanography, USSR Academy of Sciences

Type	Measured parameter	Symbol	Dynamic range	Frequency range
1. Hot-wire anemometer	Mean flow velocity	$\overline{u}$	1-5 m/sec	0-0.3 Hz
	Fluctuating flow velocity	u'	± 25 cm/sec	1.5-150 Hz
2. Hydroresistor	Mean flow velocity	$\overline{u}$	1-10 m/sec	0-0.3 Hz
	Fluctuating flow velocity	u'	± 25 cm/sec	1.5-1000 Hz
3. Hydroresistor	Mean electrical conductivity	σ	3000-6000 mS/m	0-1 Hz
	Fluctuating electrical conductivity	σ'	± 100 mS/m	1.5-1000 Hz
4. Thermistor	Mean temperature	$\overline{T}$	-2- +30° C	0-1 Hz
5. Film thermometer	Fluctuating temperature	T'	± 1° C	1.5-150 Hz

Reproduced from best available copy.

The most recent version of the recording system included gradient meters and an additional harmonic analyzer. The gradient meters indicate temperature gradients above and below the twin instrument pods, namely $\Delta T_B = \overline{T}_2 - \overline{T}_3$ and $\Delta T_H = \overline{T}_3 - \overline{T}_4$. These measurements enable an operator to seek a desired measuring depth and make necessary corrections in the towing depth. The bathythermogram in Fig. 2 illustrates the control of measurement depth, using preset values of $\Delta T_B - \Delta T_H$ as criteria. The additional harmonic analyzer is used to control quality of data on fluctuating parameters as regards noise introduced by shipboard systems.

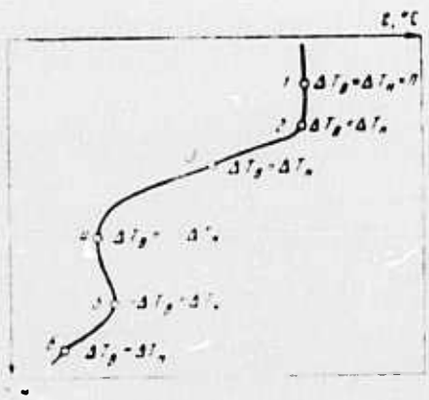

Fig. 2. Schematic bathythermogram with sections identified by gradient criteria.

Descriptions of the sensing elements, recording and display hardware are included for several test areas.

Belyaev, V. S., A. N. Gezentsvey, and R. V. Ozmidov. Intensity spectra of micropulsations of flow velocity and dissipation of kinetic energy in the ocean. IN: Sb. issled. izmenchivosti gidrofiz. poley v okeane. Moskva, Nauka, 1974, 31-41.

A description was given of $kE_1(k)$ and $k^2E_1(k)$ for small-scale fluctuations of flow velocity in the ocean. The calculations were based

on measurements in test areas V, VI and VII of the 9th cruise of the R/V Akademik Kurchatov in the Atlantic Ocean, 1971, and in test areas V, VI, and VII of the 7th cruise of the R/V Dmitriy Mendeleyev in the Indian Ocean, 1972. (This is an extension of the paper by Belyayev et al. cf. Sov. Mat'l on Int'l Wave Eff., no. 2, 1974, 13.) The measurements were carried out by a towed array of sensors of the hot-wire anemometer type, as described in the foregoing abstract by Vorob'yev et al.

Randomly selected spectra for one test area for both Atlantic and Indian Oceans are given in Figs. 1-4.

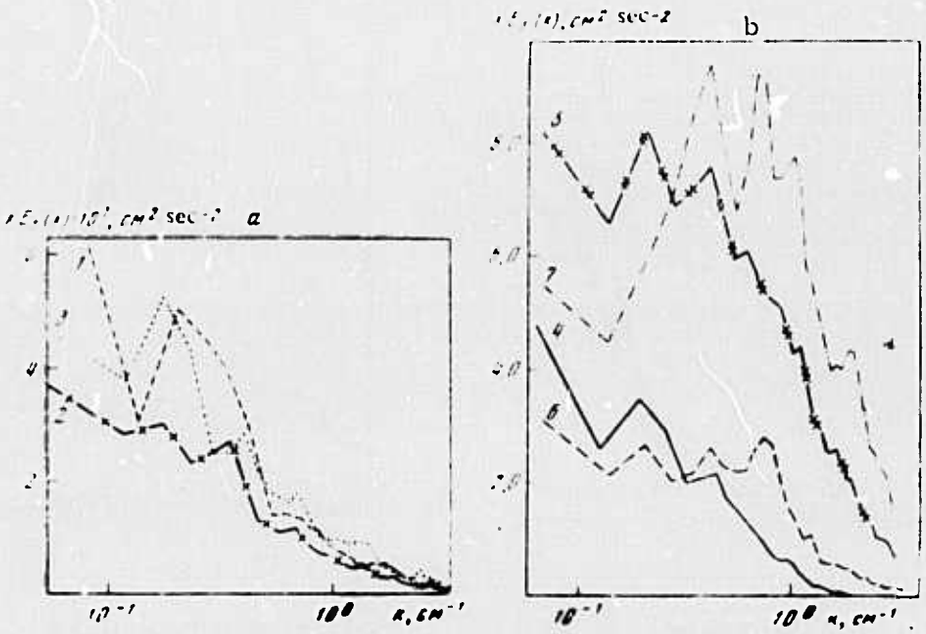

Fig. 1. Intensity spectra for fluctuations of flow velocity in test area V of the 9th cruise of the Kurchatov at depths of 30 (1), 40 (2), 50 (3), 60 (4), 70 (5), 80 (6), and 87m (7).

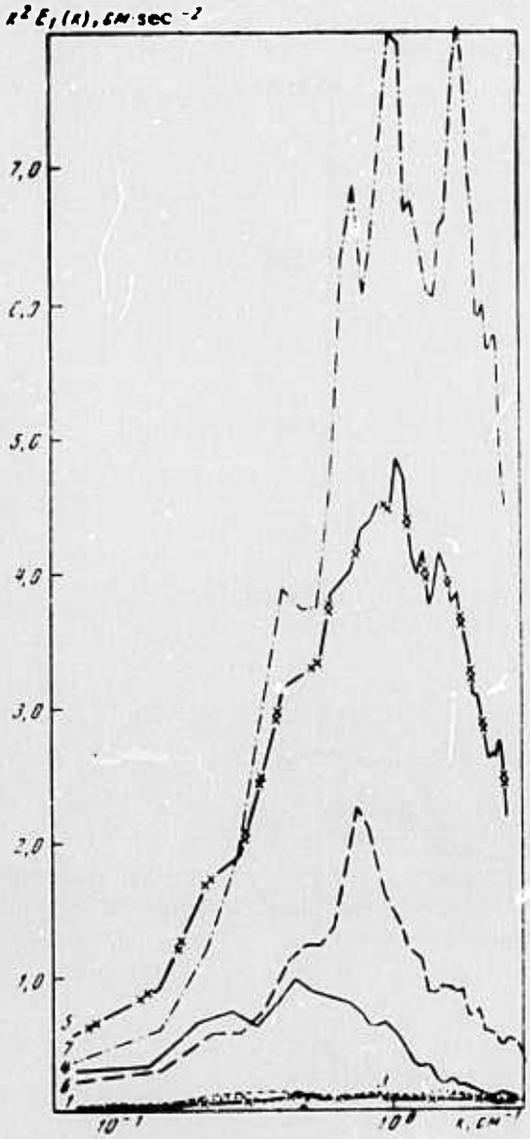

Fig. 2. Dissipation spectra for fluctuations of flow velocity in test area V of the 9th cruise of the Kurchatov. Designations as in Fig. 1.

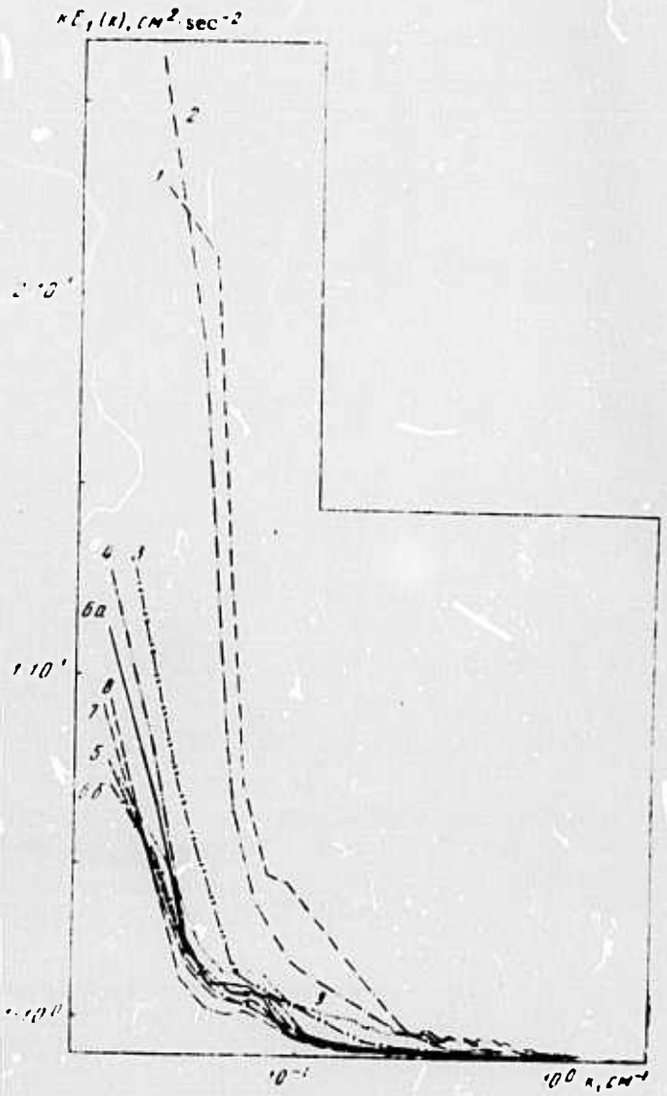

Fig. 3. Intensity spectra for fluctuations of flow velocity in test area VI of the 7th cruise of the Mendeleyev, at 80 (1), 90 (2), 104 (3), 128 (4), 136 (5), 142 (6), 150 (7), 163 (8), and 176m (9).

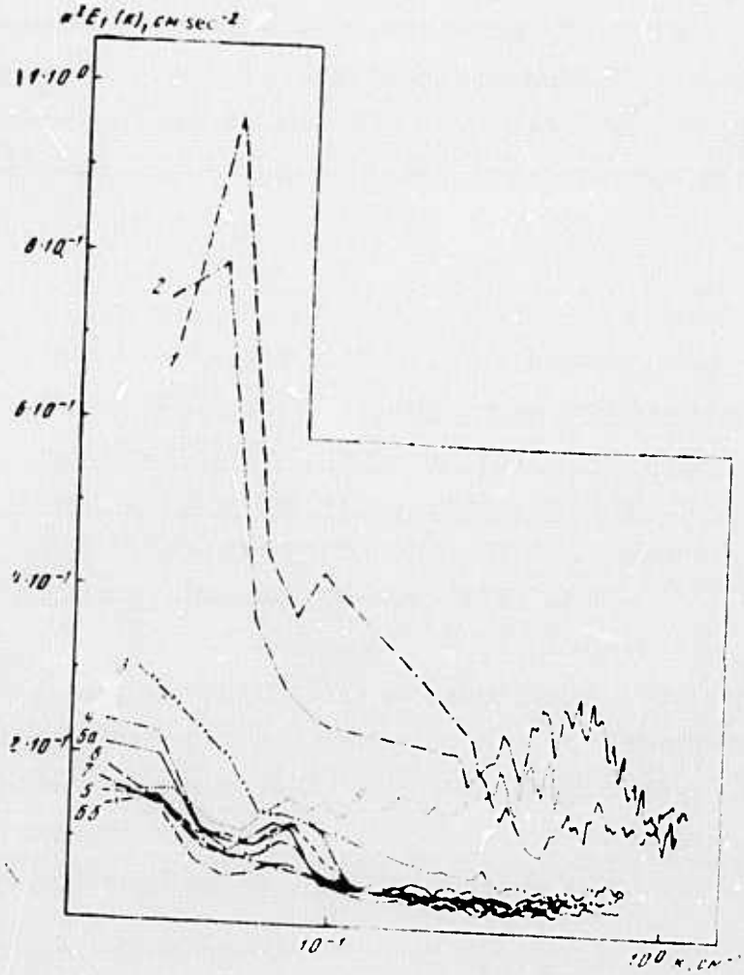

Fig. 4. Dissipation spectra for fluctuations of flow velocity in test are VI of the 7th cruise of the Mendeleyev. Designations as in Fig. 3.

The calculated dissipation rates in $cm^2 \times sec^{-3}$ are: 10^{-2}, 10^{-1}, and 10^{-1} - 10^{-2} in test areas V, VI, and VII in the Atlantic Ocean; 10^{-1} to 10^{-2} in test area V in the Indian Ocean.

A comparison of $kE_1(k)$ and $k^2E_1(k)$ for different test areas gives evidence that their shape is often a function of the general level of energy in the medium. At the same time, the position of the energy-supplying region can vary for different depths and test areas.

The authors note that the complex structure of $kE_1(k)$ and $k^2E_1(k)$ reflects a complex conjunction of mechanisms of generation of turbulence and simultaneous existence of turbulence and high-frequency internal waves (e.g. Curves 1 and 2, Fig. 3), which demands still more sophisticated recording techniques over a broader range of wave numbers.

Vorob'yev, V. P., N. N. Korchashkin, and O. N. Nikolayev. An attempt at studying the microstructure of the electrical conductivity field in the ocean by a sounding method. IN: Sb. Issled. izmenchivosti gidrofiz. poley v okeane. Moskva, Nauka, 1974, 61-65.

Sounding experiments are described in the region of the Comoro Islands, performed during the 7th cruise of the R/V Dmitriy Mendeleyev in the winter of 1972. Ten soundings at 40-60 minute intervals and descent rates of 0.7 - 1.3 m/sec were carried out by a new fast-response probe. (Fig. 1).

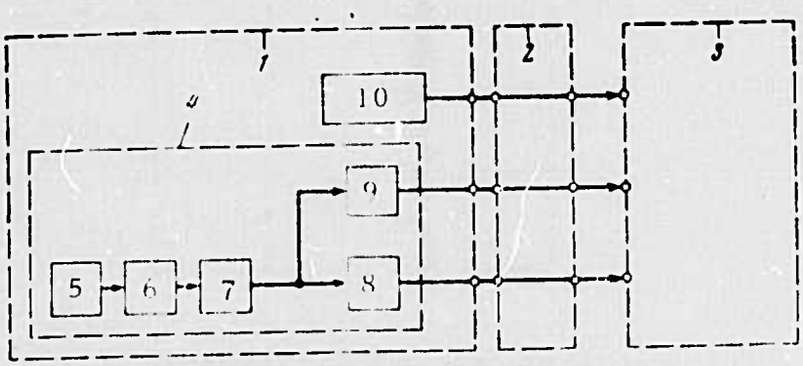

Fig. 1. Diagram of measurement of electrical conductivity in the 300 m oceanic layer.

1 - probe; 2 - three-wire cable-hawser; 3 - onboard recording unit; 4 - hydroresistor; 5 - sensor; 6 - oscillator (5 MHz); 7 - detector; 8 - amplifier; 9 - operational amplifier; 10 - DDV type pressure indicator.

The volume of sea water in the detecting element of the probe between the central and circular electrodes is approximately 3 mm^3. The electrodes are connected to oscillator 6 such that a change in electrical conductivity of sampled water changes the amplitude of the generated signal. The background noise of the measuring system is given as 3.5×10^{-4} mS/cm. The slope of the detector output is 1mv/mS/cm.

The results of measurements are briefly summarized as follows. The vertical distribution of the mean electrical conductivity has a step structure (Fig. 2). The lifetime of vertical inhomogeneities in

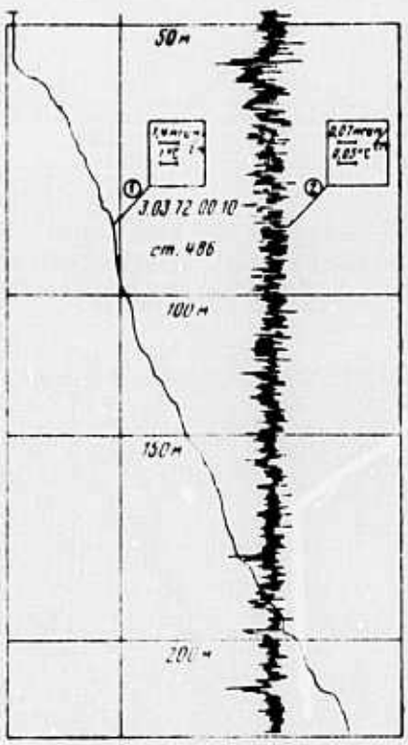

Fig. 2. Vertical profiles of mean (1) and fluctuating (2) electrical conductivity measured by the sounding method.

electrical conductivity is less than 1 hour. The dissipation rate for temperature inhomogeneities is similar for all depths, and is $5 \times 10^{-5} deg^2 sec^{-1}$. The fluctuation field of conductivity is homogeneous over the entire test 300 m layer (Fig. 3). The sharp increase of the spectral density in the upper thermocline (curve 1, Fig. 4) may indicate the presence of high-frequency internal waves.

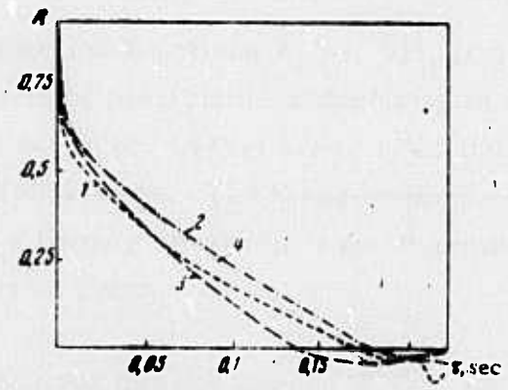

Fig. 3. Normalized correlation functions for conductivity fluctuations measured at 100 (1), 150 (2), 200 (3), and 250m (4).

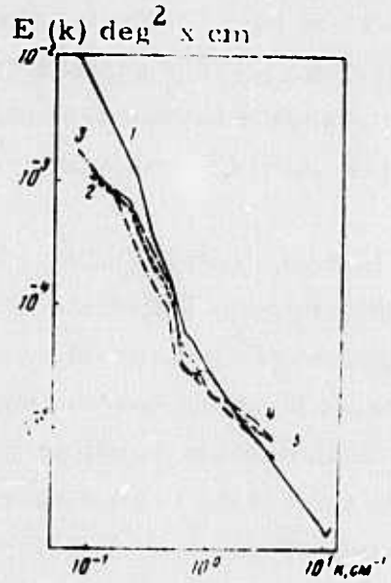

Fig. 4. Spectral densities for conductivity fluctuations at 50 (1), 100 (2), 150 (3), 200 (4), and 250m (5).

Belyayev, V. S., A. N. Gezentsvey, and R. V. Ozmidov. Spectral characteristics of pulsations of electrical conductivity field in the ocean. IN: Sb. Issled. izmenchivosti gidrofiz. poley v okeane. Moskva, Nauka, 1974, 42-49.

The spectral functions $E_1(k)$, $kE_1(k)$, and $k^2E_1(k)$ for small-scale fluctuations of electrical conductivity in the ocean were computed, using data collected in test areas I-VI and VIII of the 7th cruise of the R/V Dmitriy Mendeleyev. The measurements were carried out by towing three slightly differing arrays of fast-response sensors with an average spatial radius of 1 mm.

The spectral density curves $E_1(k)$, calculated for various test areas and depths, follows a power law, the exponent varying from -1.4 to -3 (see Figs. 1-7). The intensity spectra $kE_1(k)$ increase nearly uniformly with decrease of k (see Fig. 8) in all test areas. However, they can peak within the low wave number range at certain depth levels (see Fig. 10). The dissipation spectra $k^2E_1(k)$ are very peaked and generally do not show maxima within the considered k range. The only exception appears to be the $k^2E_1(k)$ spectra of test area VI (Fig. 11).

The authors point out that spectral characteristics of small-scale fluctuations in electrical conductivity in the upper ocean layer vary widely, irrespective of large-scale hydrological conditions. They suggest that the diverse shapes and levels of spectral functions observed, which are not correlated with large-scale hydrological conditions, indicate existence of different mechanisms of generation and decay of small-scale inhomogeneities in the electrical conductivity field.

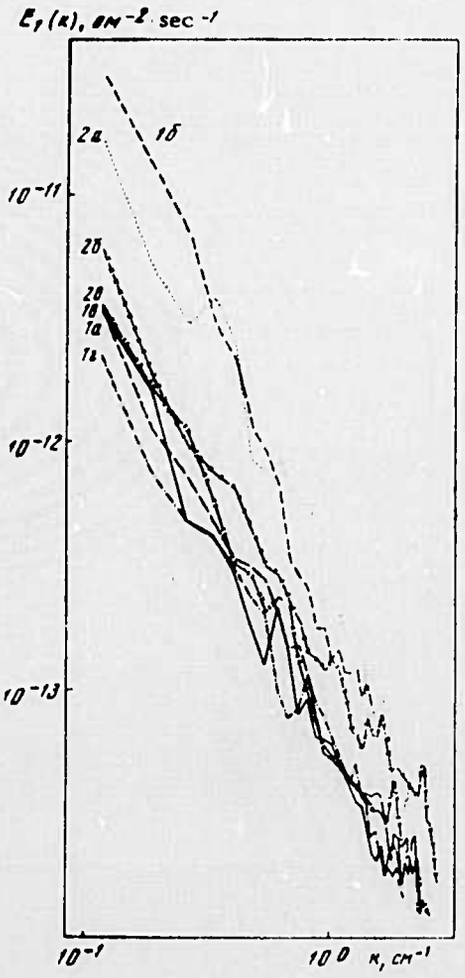

Fig. 1. Spectral density $E_1(k)$ for fluctuations of electrical conductivity in test area II in the Indian Ocean at depths of 77 (curves 1) and 120 m (curves 2). (vertical velocity gradient = 1.5 cm/sec/m).

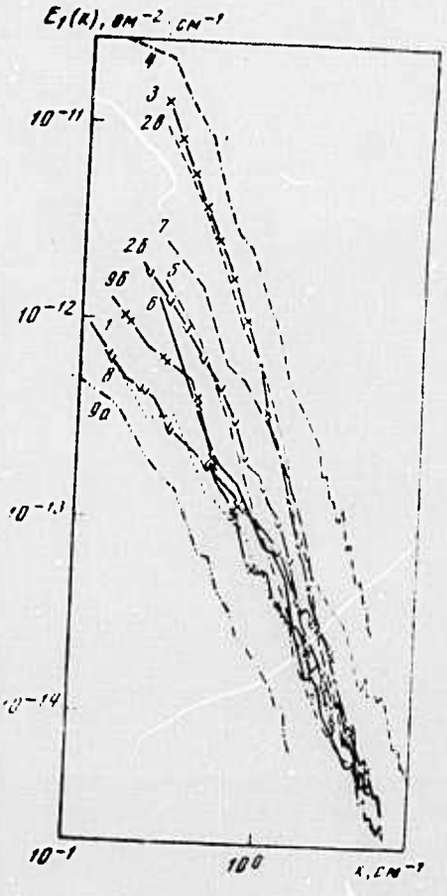

Fig. 2. $E_1(k)$ for σ' in test area IV at depths of 49 (1), 60 (2), 65 (3), 67 (4), 70 (5), 75 (6), 80 (7), 103 (8), and 120 m (9). (curves 1-7 within a homogeneous layer; curves 8 and 9 within a quasihomogeneous layer).

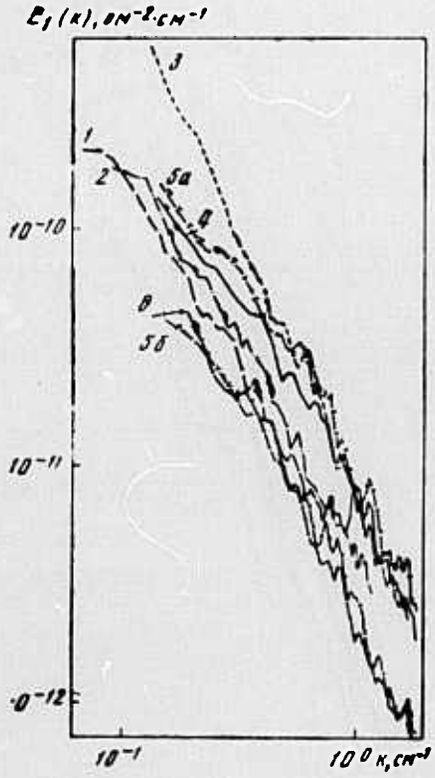

Fig. 3. $E_1(k)$ for σ' in test area VI at depths of 10 (1), 14 (2), 54 (3), 60 (4), 68 (5), and 89m (6). (curves 2-5 within constant density gradient layer; curves 1 and 6 at the upper and lower boundary of the constant density gradient layer.)

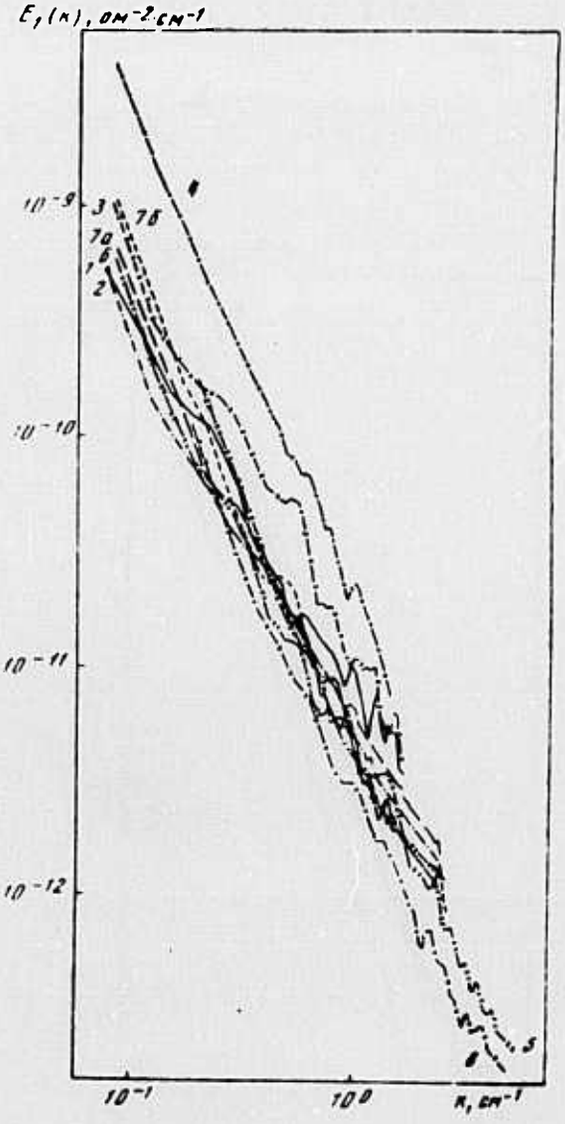

Fig. 4. $E_1(k)$ for σ' in test area VIII at depths of 55 (1), 95 (2), 110 (3), 141 (4), 145 (5), 161 (6), 170 (7), and 175m (8). (various values of density gradients)

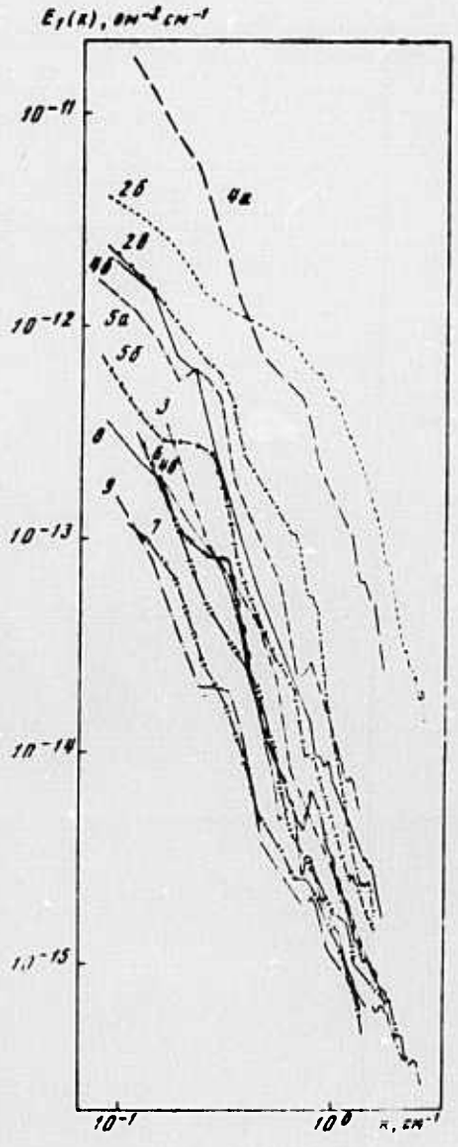

Fig. 5. $E_1(k)$ for σ' in test area III at depths of 35 (2), 52 (3), 70 (4), 72 (5), 91 (6), 103 (7), 118 (8), and 127 m (9). (various values of density gradient)

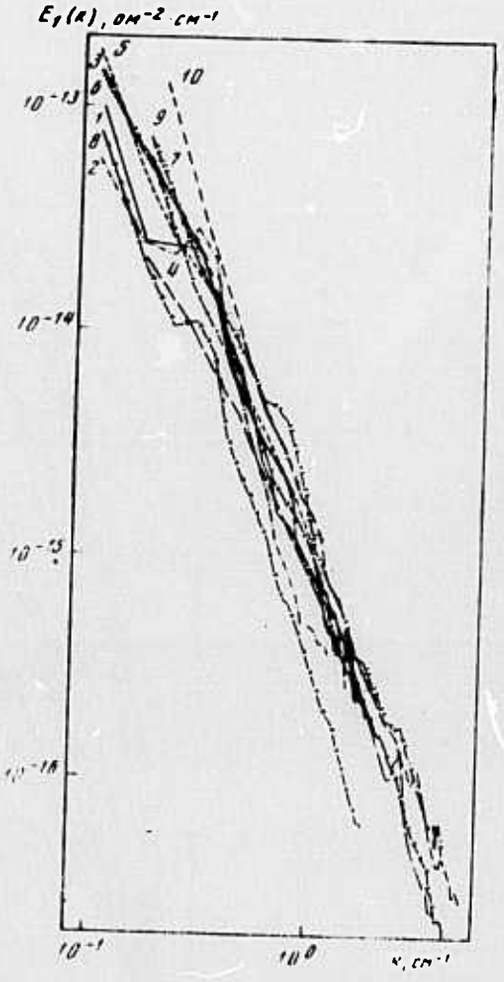

Fig. 6. $E_1(k)$ for σ' in test area V at depths of 55 (1), 80 (2), 90 (3), 100 (4), 105 (5), 115 (6), 120 (7), 129 (8), 150 (9), and 187 m (10). (curves 3-8 within density discontinuity layer; curves 9 and 10 within quasi-homogeneous layer).

Reproduced from
best available copy.

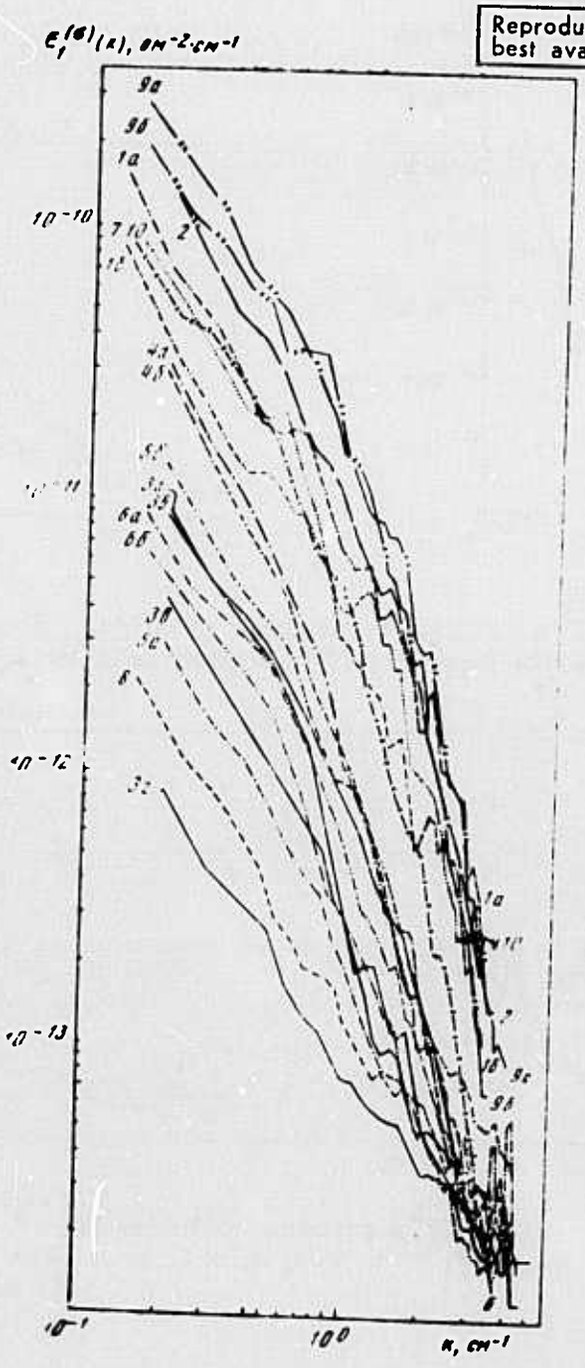

Fig. 7. $E_1(k)$ for σ' in test area VI from repeated measurements at depths of 23 (1), 45 (2), 71 (3), 75 (4), 106 (5), 125 (6), 132 (7), 146 (8), 149 (9), and 217m (10).

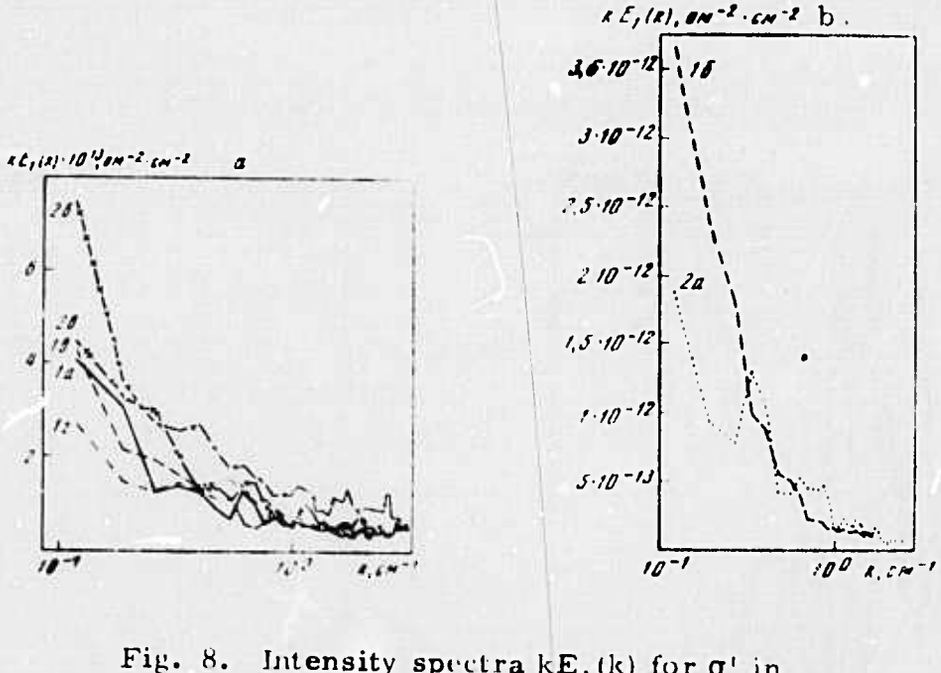

Fig. 8. Intensity spectra $kE_1(k)$ for σ' in test area II at depths of 77 (1), and 120 m (2).

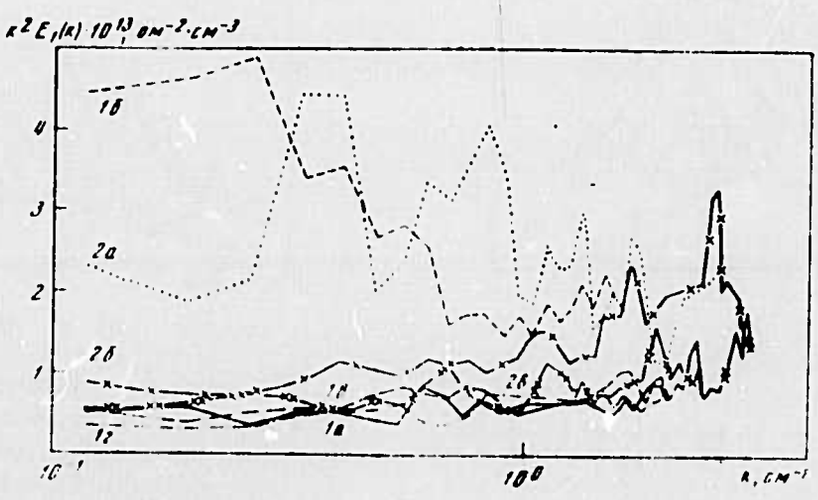

Fig. 9. Dissipation spectra $k^2E_1(k)$ for σ' in test area II at depths of 77 (1), and 120 m (2).

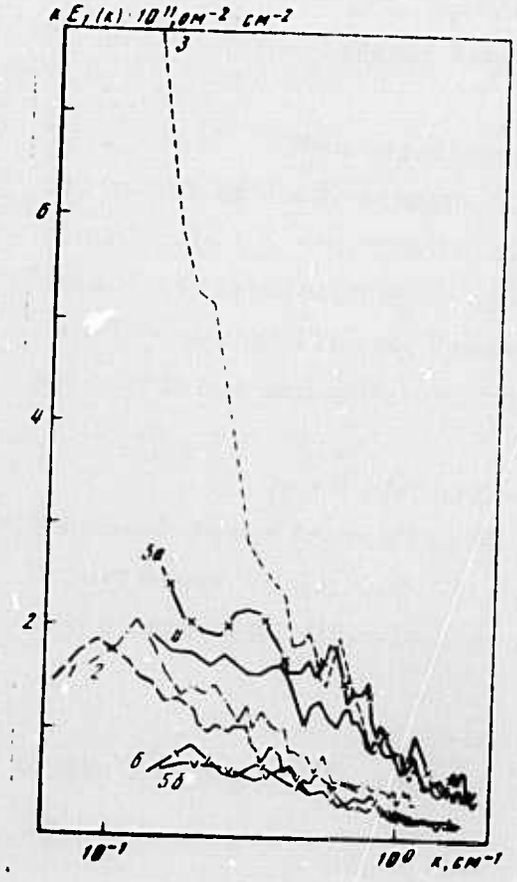

Fig. 10. Intensity spectra $kE_1(k)$ for σ' in test area VI at depths of 10 (1), 14 (2), 54 (3), 60 (4), 68 (5), and 89 m (6).

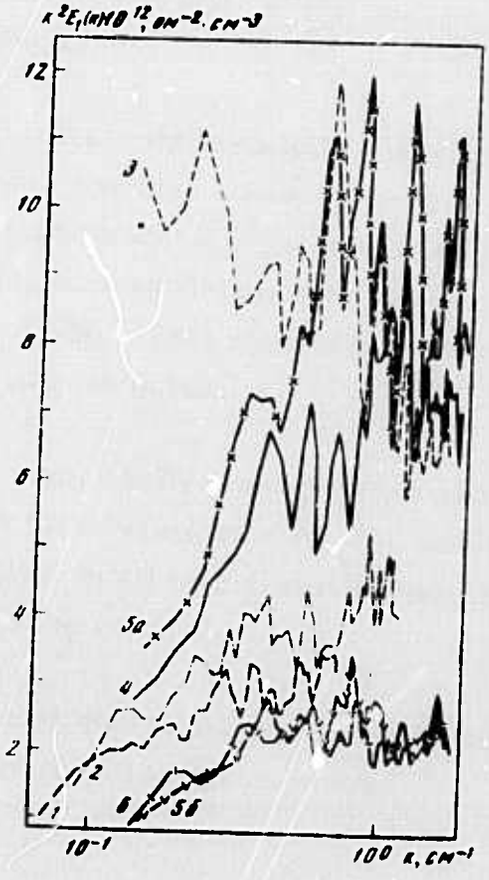

Fig. 11. $k^2E_1(k)$ for σ' in test area VI at depths of 10 (1), 14 (2), 54 (3), 60 (4), 68 (5), and 89 m (6).

Pozdynin, V. D. Statistical estimates of the parameters of small-scale ocean turbulence. IN: Sb. Issled. izmenchivosti gidrofiz. poley v okeane. Moskva, Nauka, 50-61.

Statistical data on small-scale turbulence taken during the 9th cruise of the Kurchatov in the Atlantic, are discussed. Taylor's microscale λ_o, correlation radius $r_{0.05}$, intensity $\overline{(u')}^2$, and dissipation rate ϵ of turbulence were computed using data on fluctuations of flow velocity obtained in test areas V, VI, and VII. Total numerical data for all test areas and different depth levels are tabulated

In all test areas $r_{0.05}$ is statistically homogeneous within the depth range from 30 to 80-90 m. Its mean value was 50, 39, and 38 cm in test areas V, VI, and VII, respectively. In all test areas its variability in the horizontal direction exceeds that in the vertical.

In all test areas λ_o maintains statistical homogeneity only within a thin water layer. Its statistically significant values are:

Test area	Depth, m	Taylor's microscale, cm
V ($29^{\circ}30'$S; $40^{\circ}0'$W)	30-60; 40-90	1.8; 1.1
VI ($23^{\circ}0'$S; $30^{\circ}0'$W)	30-50; 60-70	0.8; 1.3
VII ($0^{\circ}0'$; $24^{\circ}0'$W)	30-40; 140	0.9; 1.6

However, in all areas $\overline{(u')}^2$ varies widely. Its statistically significant values are:

Test area	Depth, m	$\overline{u'^2}$, cm^2/sec^2
V	30	1.01
	40-50	0.61
	50; 70; 87	18.59
	60; 80	7.41
VI	30	5.80
	40; 50; 60	3.21
	50	1.77
	40; 60; 77	0.82
VII	36; 90; 110;	1.38
	52	1.86
	73; 140	0.62

The dissipation rate calculated by

$$\varepsilon = 15\nu \frac{\overline{u'^2}}{\lambda_0^2}, \qquad (1)$$

where ν is viscosity, varies greatly and statistically significant values are found only locally. Fig. 1 gives a comparison of present results and those reported earlier by Belyayev et al. (Sov. Mat'l on Int'l Wave Eff., no. 2, 1974, 7).

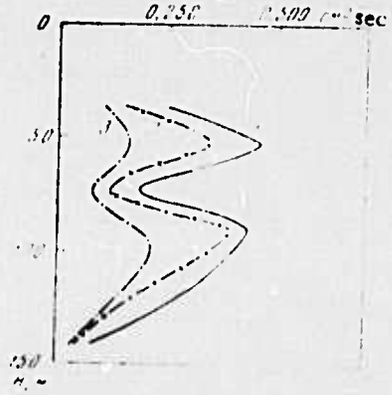

Fig. 1. Vertical profiles for the rate of dissipation of turbulence energy.

1- present results; 2- calculated using universal curve; 3- calculated by Belyayev.

A comparison of variability of the studied parameters is given in Figs. 2 and 3.

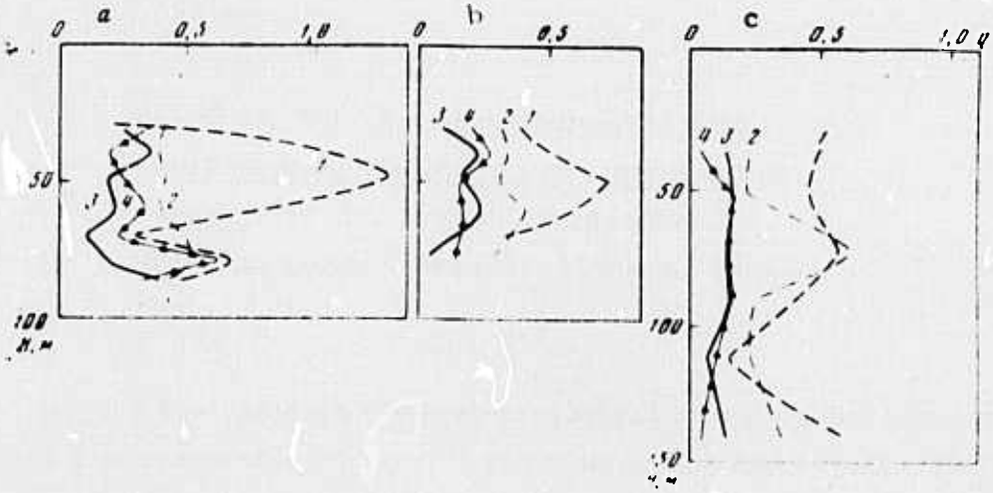

Fig. 2. Vertical profiles for the coefficient of relative variability of ϵ (1), $(u')^2$ (2), λ_0 (3) and $r_{0.05}$ (4).

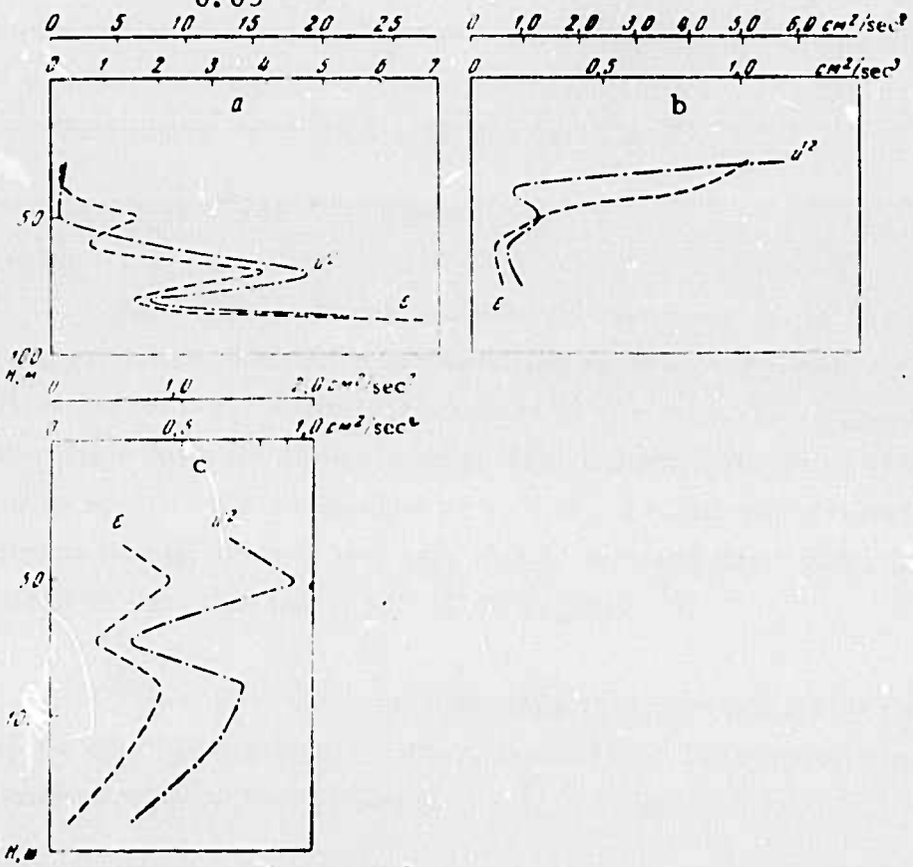

Fig. 3. Vertical profiles for $(u')^2$ and ϵ in test areas V (a), VI (b) and VII (c).

The author observes that the variation of dissipation rate ϵ is destermined mainly by the level of the turbulence energy.

Shishkov, Yu. A. Meteorological data from experimental studies of turbulence in the ocean. IN: Sb. Issled. izmenchivosti gidrofiz. poley v okeane. Moskva, Nauka, 1974, 66-71.

Requirements for meteorological observations prior to and during measurements of oceanic turbulence are discussed. The criteria for duration and periodicity of these observations are recommended.

As a criterion for periodicity of meteorological observations, the characteristic decay time T_x for oceanic turbulence in the absence of exterior sources is suggested. For a dissipation rate $\overline{\epsilon} = 10^{-2} cm^2 sec^{-3}$ and initial fluctuating velocity $v = 10$ cm sec^{-1},

$$T_x = v^2/2\overline{\epsilon} \cong 1.4 \text{ hour}. \qquad (1)$$

As a criterion for duration of meteorological observations prior to experiments, the time for dissipation of atmospheric formations which affect large-scale density structure in the ocean is suggested. Dissipation time for the kinetic energy of a 5.5 km column of the atmosphere and $v = 10$ m sec^{-1} was estimated to be 1.3 - 21.2 days, depending on the dissipation of kinetic energy per cm^2 due to surface drag and turbulent friction used in calculations (150 - 2500 erg sec^{-1}).

The author thus recommends that periodicity of meteorological observations should not exceed 1 hour, while their lead time prior to the experiments should be 7 to 10 days.

Lozovatskiy, I. D. On the balance of turbulent energy in the ocean. IN: Sb. Issled. izmenchivosti gidrofiz. poley v okeane. Moskva, Nauka, 1974, 71-75.

An estimate is made of the exchange of kinetic energy between mean and fluctuating components of motion, described in the energy balance equation

$$\frac{\partial E_t}{\partial t} + \frac{\partial}{\partial x_\alpha}\left(E_t \bar{u}_\alpha + \frac{1}{2}\overline{\rho u'_\beta u'_\beta u'_\alpha} + \overline{p' u'_\alpha} - \overline{u'_\beta \sigma'_{\alpha\beta}}\right) = \overline{\rho u'_\alpha X'_\alpha} - \rho\bar{\varepsilon}_t - \rho\overline{u'_\alpha u'_\beta}\frac{\partial u_\beta}{\partial x_\alpha}, \tag{1}$$

$$E_t = \frac{1}{2}\overline{\rho u'_\alpha u'_\alpha} \quad \text{и} \quad \overline{u'_\beta \sigma'_{\alpha\beta}} = \overline{\mu u'_\beta\left(\frac{\partial u'_\alpha}{\partial x_\beta} + \frac{\partial u_\beta}{\partial x_\alpha}\right)}, \quad \alpha, \beta = 1, 2, 3,$$

where ρ is density, $\bar{u}_\alpha$ and u'_α are mean and fluctuating velocities, p' = fluctuations of pressure, μ = coefficient of molecular viscosity, X'_α = fluctuations of exterior forces, and $\rho\bar{\varepsilon}_t = \overline{\sigma'_{\alpha\beta}\,\partial u'_\beta/\partial x_\alpha}$ is mean energy dissipation due to viscous forces. The estimate is based on "fixed" series of measurements of flow velocity at 300 m depth, measured in the Atlantic test area. The maximum length of the test series was 47 days, the averaging interval 3-8 hours.

Tabulated results of calculations are given in the article, and illustrated in Fig. 1.

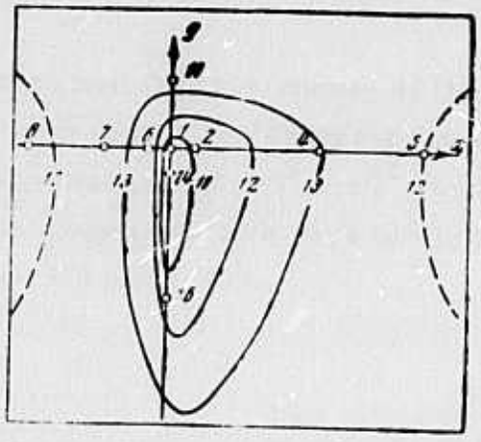

Fig. 1. Isolines of $2E_t$ (cm^3/sec^2) in the Atlantic test area. Numerals indicate measuring stations.

Results show that the exchange of energy between mean and fluctuating velocity in the considered scale range is exceeded by the transfer of energy by turbulent viscosity. The time variation of the density of turbulent energy is determined mainly by diffusion, i.e. turbulence within the considered scale range is not homogeneous. The author notes that "fixing" of time series as well as insufficient accuracy of determination of space derivatives of the velocity field may introduce errors in the results.

Vasilenko, V. M., and L. M. Krivelevich. Statistical characteristics of currents, based on observations in the Atlantic test area. IN: Sb. Issled. izmenchivosti gidrofiz. poley v okeane. Moskva, Nauka, 1974, 76-83.

Measurements of flow velocity in the tropical Atlantic during February - September 1970 were made with an Alekseyev current meter with reading intervals of 30 minutes.

The results of statistical analysis are given in Figs. 1-7.

It was observed that the energy of fluctuating velocity components decr ases with depth, the sharpest drop being below the high gradient layer. Spectral densities of $(u')^2$, $(v')^2$, and $u'v'$ in the 1-10 hours range decrease in proportion to a -1.4 to -1.8 power law, or very similarly to Ozmidov's -5/3 power law.

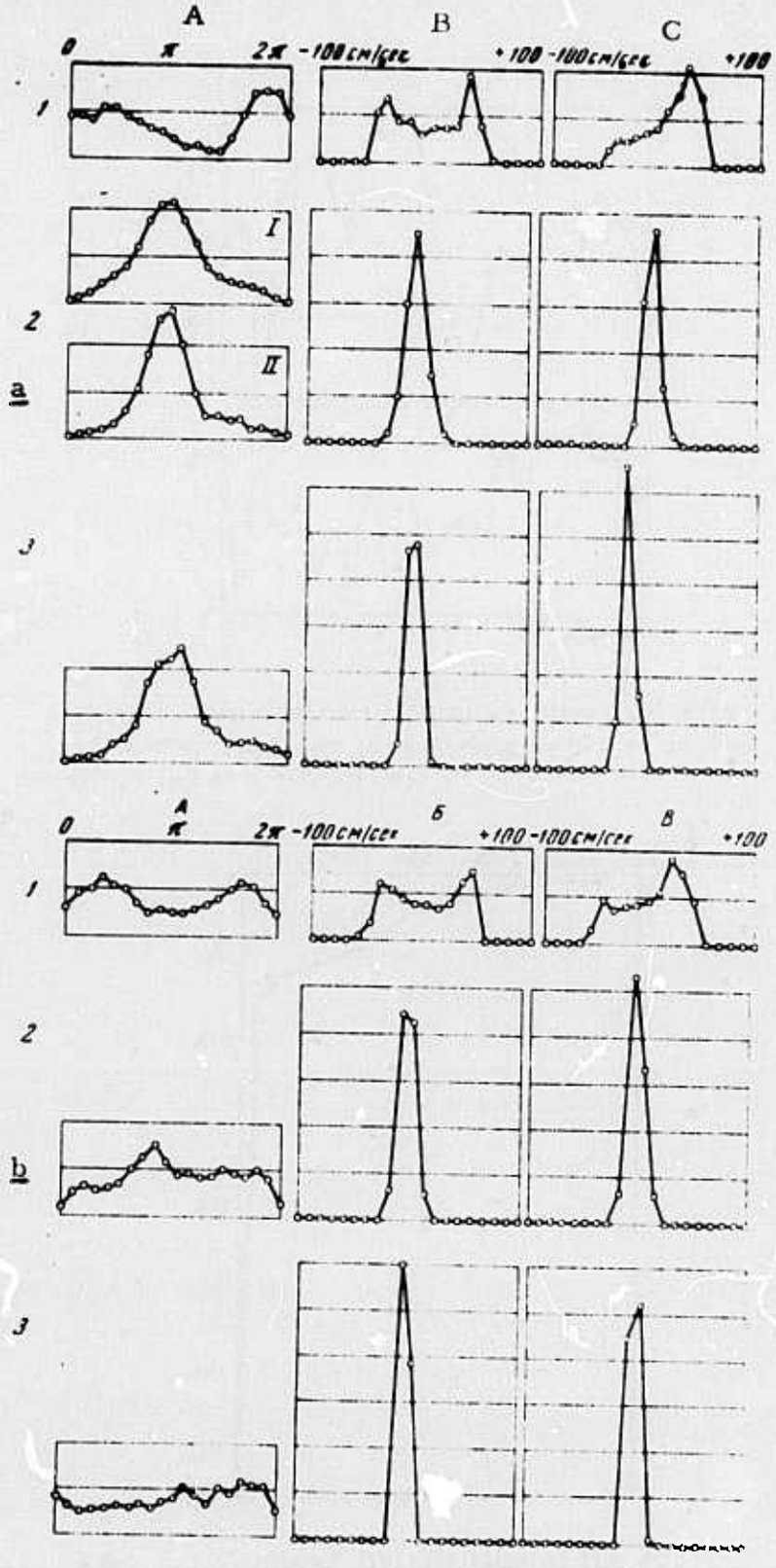

Fig. 1. Histograms of probability density for direction (A) and for magnitude of latitudinal (B) and meridional (C) components of flow velocity at depths of 25 (1), 300 (2), and 1000 m (3).

a- observations from 5/27 to 6/20; b- from 7/16 to 8/09.

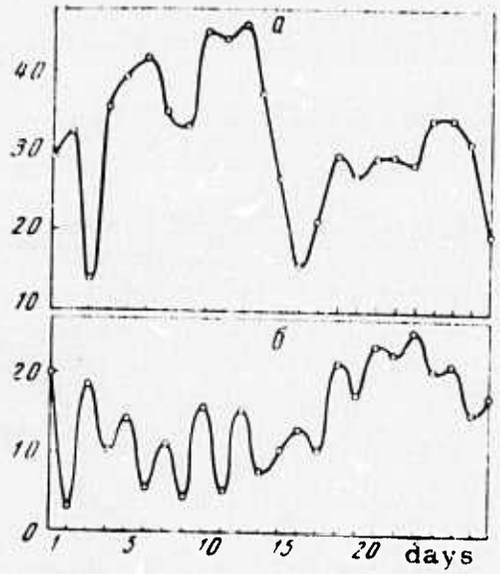

Fig. 2. Variation in 24 hour mean velocity of flow during one measuring cycle at depths of 25 (a) and 100 m (b).

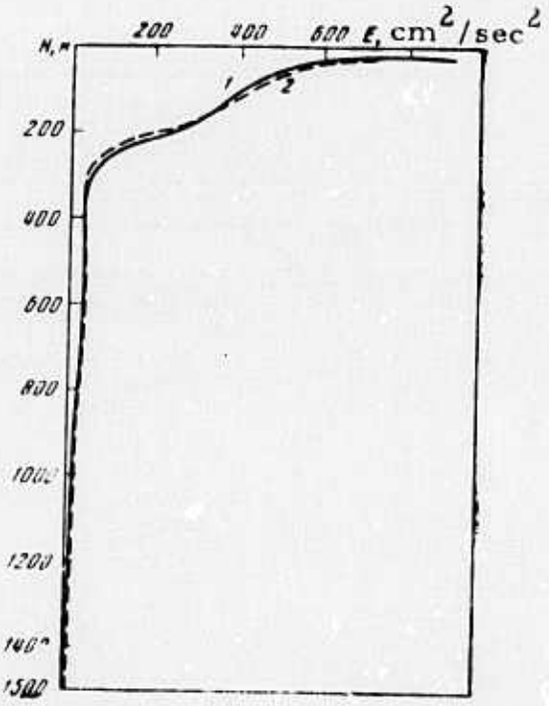

Fig. 3. Vertical distribution of the energy of u' (1) and v' (2) velocity components.

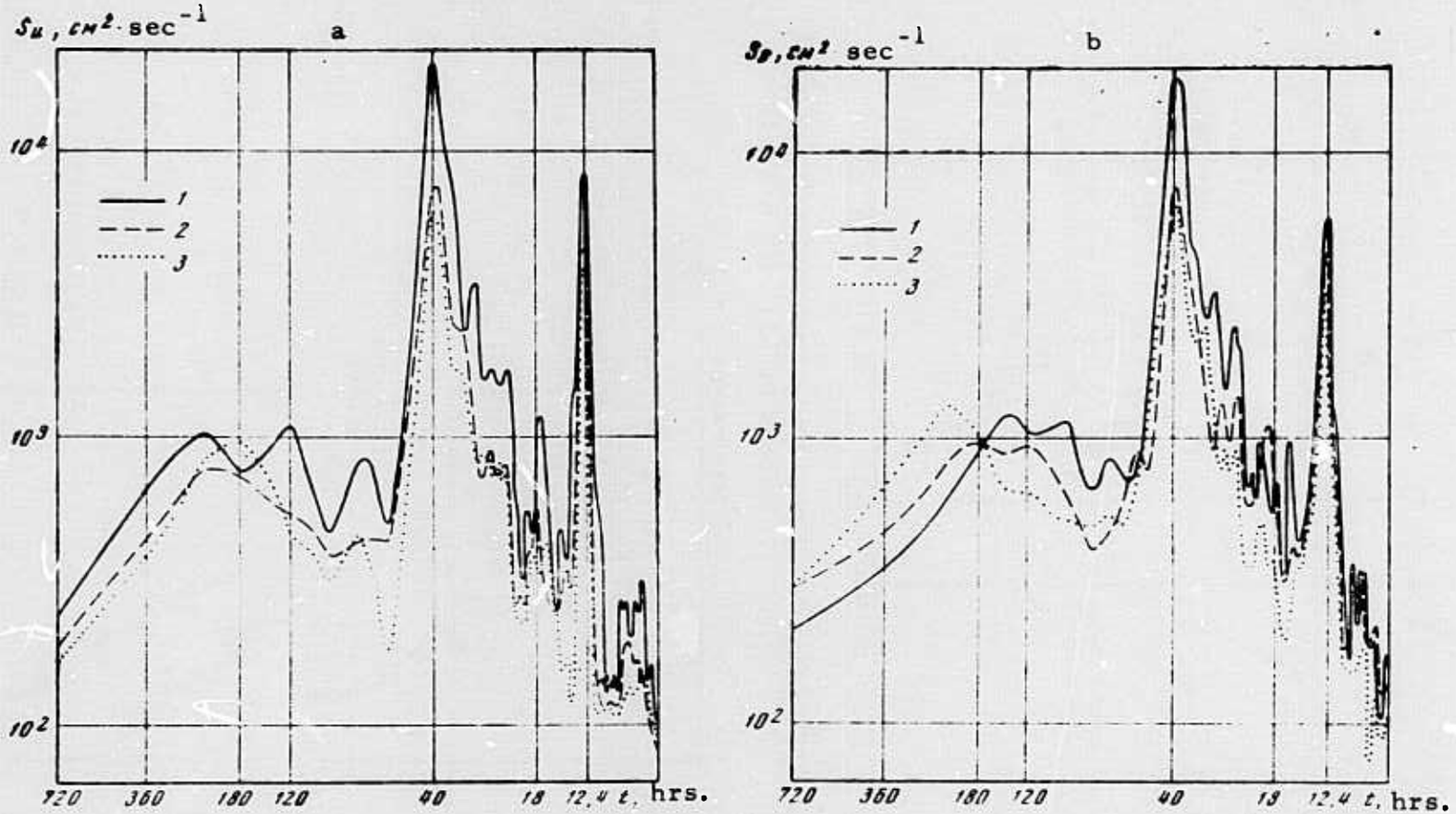

Fig. 4.

Spectral densities for latitudinal (a), and meridional (b) velocity components at depths of 200 (1), 300 (2), and 400 m (3), based on measurements at station 7.

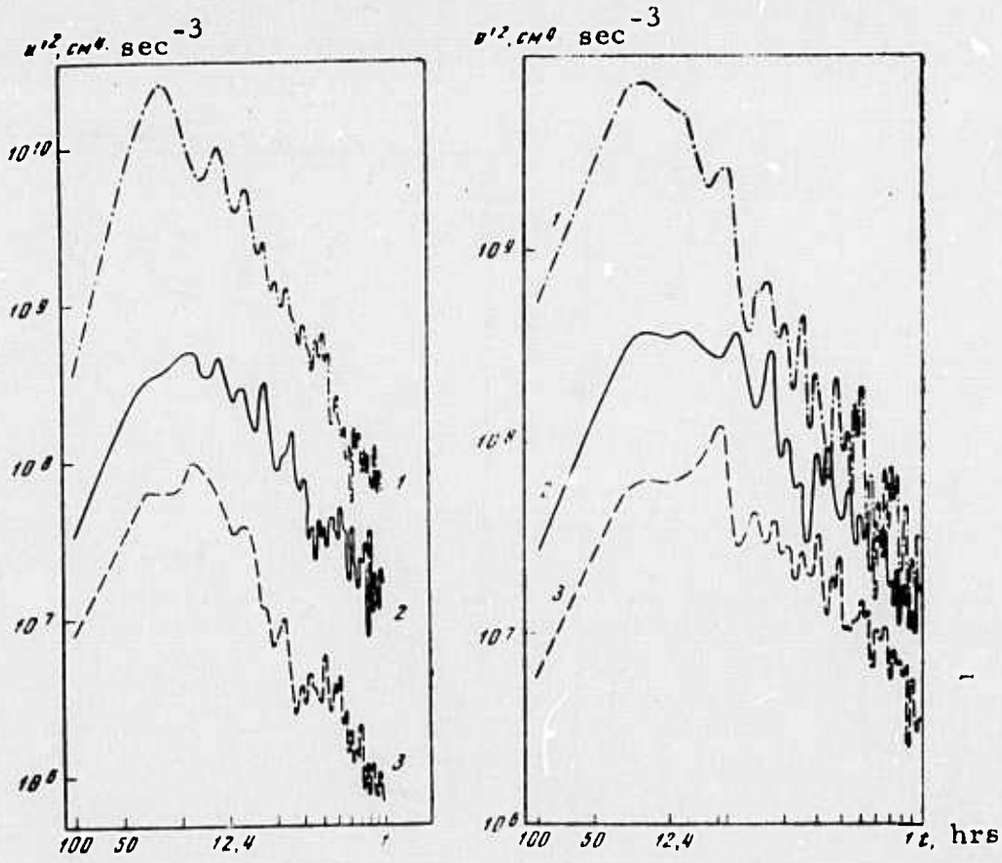

Fig. 5. Spectral densities for $(u')^2$ (a) and $(v')^2$ (b) at depths of 25 (1), 100 (2), and 500 m (3) at station 10.

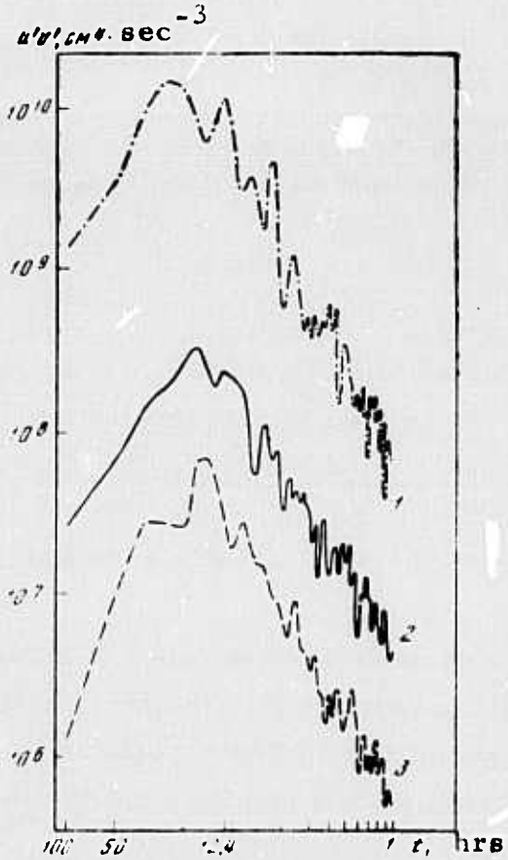

Fig. 6. Spectral densities for u'v' at depths of 25 (1), 100 (2), and 500 m (3) at station 10.

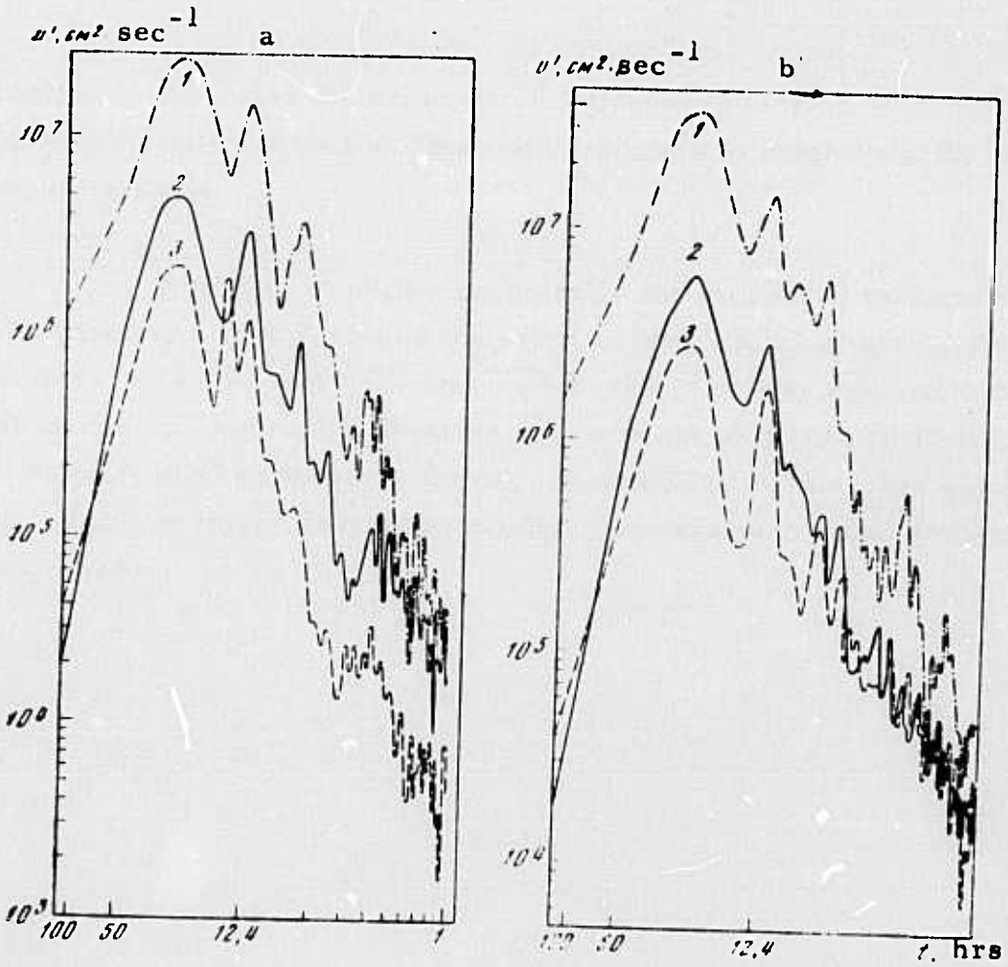

Fig. 7. Spectral densities for u' (a) and v' (b) velocity components at depths of 25 (1), 100 (2), and 500 m (3) at station 10.

Benilov, A. Yu., and I. D. Lozovatskiy.
On the inertial interval in spectra of turbulence in a stratified fluid (Heisenberg - Monin model).
IN: Sb. Issled. izmenchivosti gidrofiz. poley v okeane. Moskva, Nauka, 1974, 83-91.

The effects of ocean stratification on the inertial interval in the turbulence spectra are determined analytically. The solution of the equations for balance of turbulence energy and intensity of temperature inhomogeneities in spectral form (Monin and Yaglom, 1965) is obtained in

parametric form, using the generalized Heisenberg closing as proposed by Monin (1962) for a turbulent flow with gradients of mean velocity and temperature fields.

Results are shown graphically and compared to those of other authors who have analyzed the effect of stratification on turbulence parameters. The present authors conclude that a proper evaluation of experimental vs. theoretical findings requires not only data on fluctuations in the velocity and temperature fields, but also data on the mean gradients of these fields at the measurement points. To date such measurements have not been made.

parametric form, using the generalized Heisenberg closing as proposed by Monin (1962) for a turbulent flow with gradients of mean velocity and temperature fields.

Results are shown graphically and compared to those of other authors who have analyzed the effect of stratification on turbulence parameters. The present authors conclude that a proper evaluation of experimental vs. theoretical findings requires not only data on fluctuations in the velocity and temperature fields, but also data on the mean gradients of these fields at the measurement points. To date such measurements have not been made.

Ivanov, Yu. A., Ye. G. Morozov, and A. S. Samodurov. Internal gravity waves in the ocean. IN: Sb. Issled. izmenchivosti gidrofiz. poley v okeane. Moskva, Nauka, 1974, 91-98.

A review is given of the results of experimental and theoretical studies of internal gravity waves in the ocean, as recently reported in Soviet and Western publications. The following is a summary of the Soviet results only.

The energy distribution for fluctuations of temperature and flow velocity shown in Fig. 1 was obtained by Brekhovskih et al. (1971) who analyzed extended series of measurements in the Atlantic test area. Ivanov and Morozov (1974) suggested that fluctuations of hydrophysical fields in the

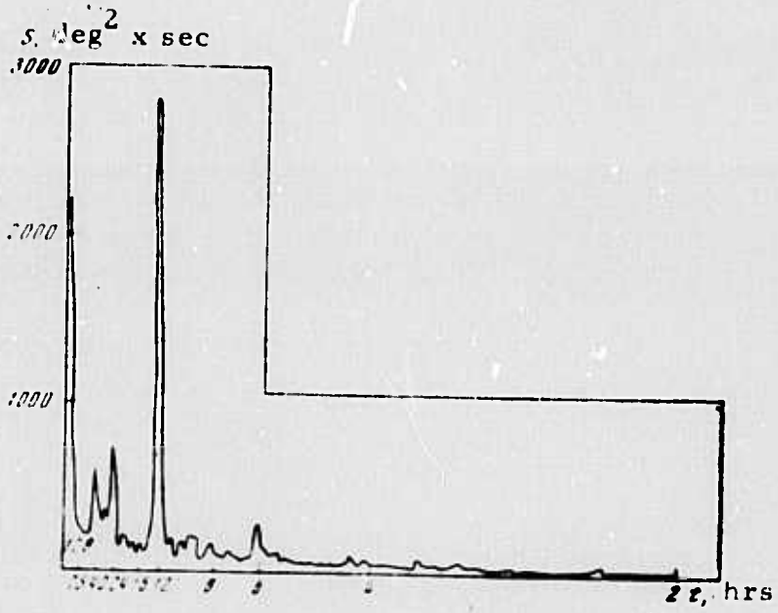

Fig. 1. Spectral density of temperature fluctuations at a depth of 200 m (Atlantic test area, 1970). Length of the series = 5 months, reading intervals = 30 min.

ocean with tidal periods are determined by internal gravity waves with wavelength of 110-120 km, and a constant propagation direction. The following table gives, as an illustration of that suggestion, coherence and phase shift for temperature fluctuations with periods of 12 hours, measured at 1000 m depth at 8 stations in Atlantic test area 70. Furthermore, they

L, miles	5	20	30	50	70	80
H	0.88	0.85	0.83	0.85	0.77	0,73
$\Delta\varphi$, deg	18	56	100	156	264	320

suggest that fluctuation of the hydrophysical fields with frequencies near to the inertial ones, which are characterized by a relatively rapidly decreasing coherence, may be caused by undulating motion with a wavelength of 25 miles and a south-southeast propagation direction.

Fluctuations of hydrophysical fields in the ocean within a period range of 10 min. to 12 hrs were studied in numerous characteristic regions (Ivanov and Morozov, 1973). Location of measurement areas in the tropical Atlantic and some results of the measurements in the upper thermocline are given in Figs. 2-6.

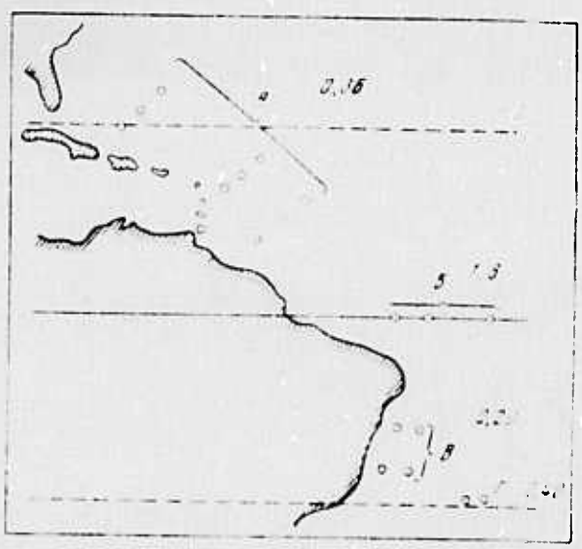

Fig. 2. Location of measurement areas.
Numerals indicate maximum standard dispersion.

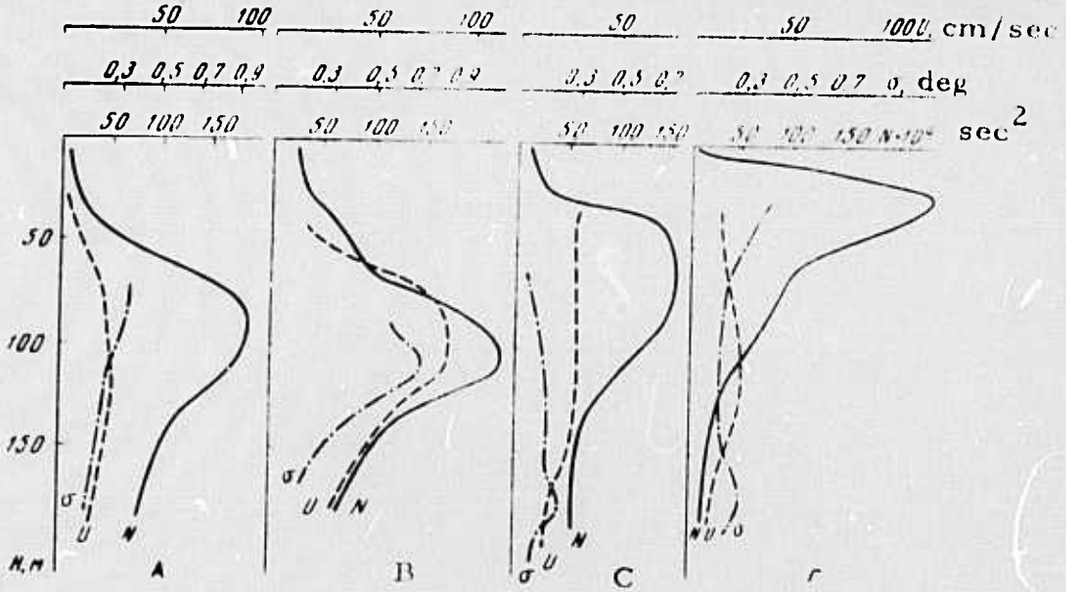

Fig. 3. Vertical profiles of the Vaisala-Brunt frequency, flow velocity, and rms deviation for the temperature fluctuations in the tropical Atlantic. A-Г are test areas of Fig. 2.

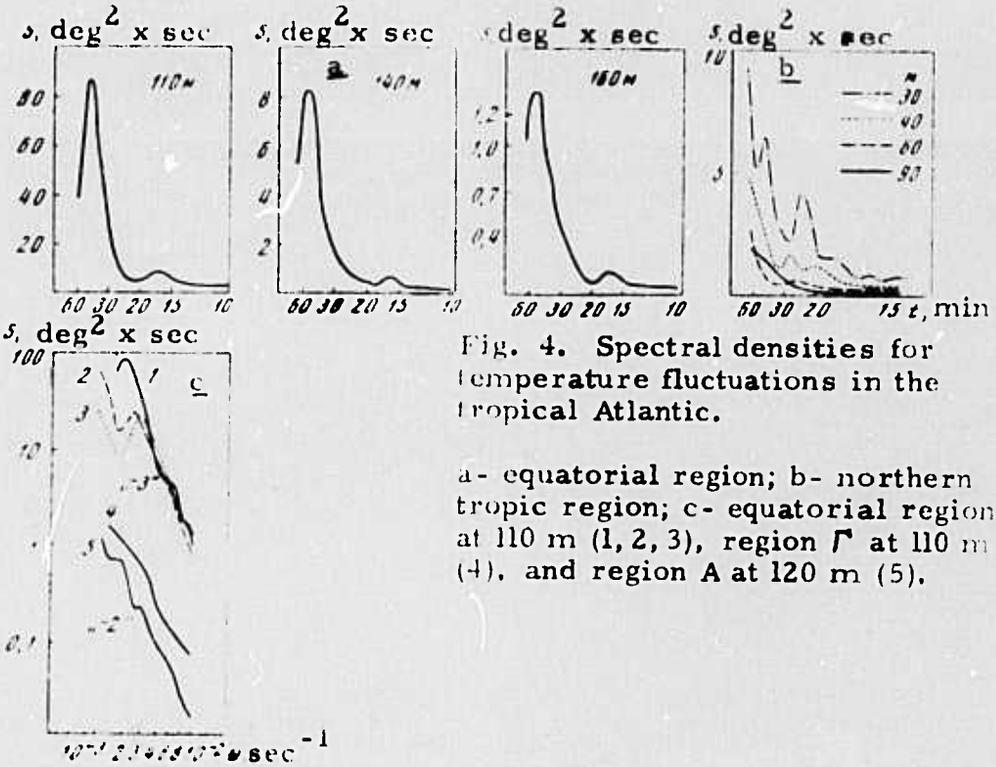

Fig. 4. Spectral densities for temperature fluctuations in the tropical Atlantic.

a- equatorial region; b- northern tropic region; c- equatorial region at 110 m (1, 2, 3), region Г at 110 m (4), and region A at 120 m (5).

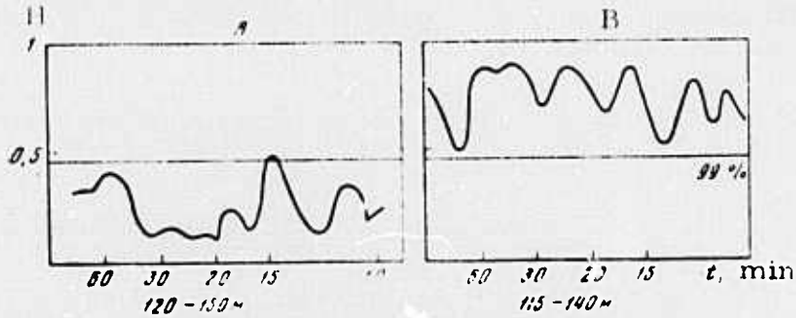

Fig. 5. Coherence functions for temperature fluctuations at different depths.

region A - small dispersion; region B - large dispersion.

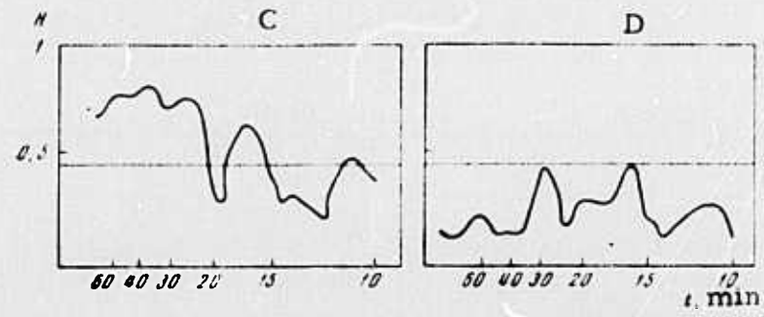

Fig. 6. Coherence functions for fluctuations of temperature and flow velocity at 110 m.

As can be seen in Figs. 3-6 the most intense fluctuations in the considered frequency range, which were observed in the equatorial Atlantic with large vertical velocity shear, possess statistical characteristics of wave motions. However, in the regions with small vertical velocity shear and dispersion, fluctuations of hydrophysical fields are determined by non-stationary internal waves and turbulent motions. Numerous measurements conducted in the Black Sea, Atlantic Ocean, and Indian Ocean revealed intermittency in the energy of temperature fluctuations as illustrated in Fig. 7.

A theoretical study of breaking of internal waves was attempted by Morozov (to be published) by calculating variation of potential energy in the 50-250-m layer during passage of a wave train. He found that the increase of potential energy amounts to 10% of energy exchange during complete

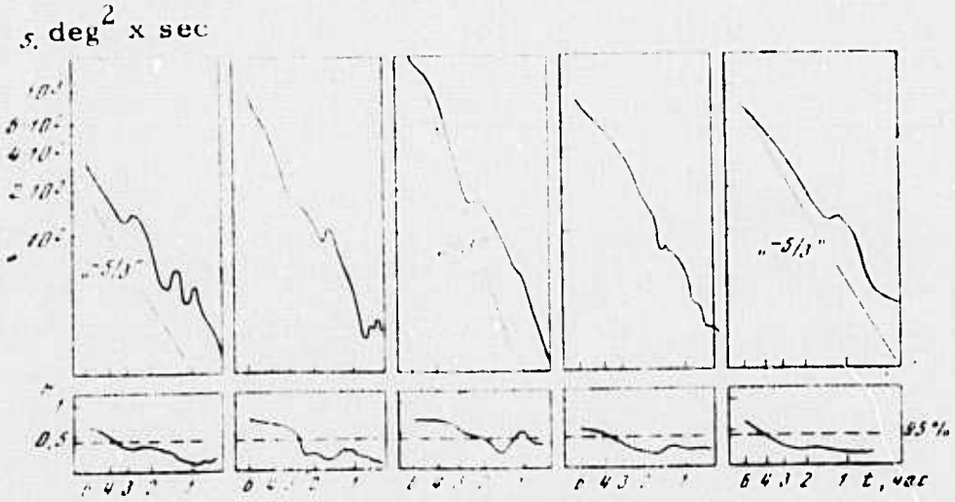

Fig. 7. Spectral densities for temperature fluctuations at 125 m, and coherence functions for fluctuations at 125 and 150 m (Northwest Indian Ocean).

mixing in that layer. However, calculations were made by averaging bathymetric series measured before and after the passage of a wave train, which may induce an error in the results. Samodurov (to be published) studied instability of internal waves in the case when N = N(x). He showed that the amplitude of internal waves increases and their wavelength decreases on approaching the point where $N(x_0) = w$ (w is frequency of waves).

It was concluded that the results of experimental studies show that internal gravity waves are generated by instability of a stratified flow with vertical velocity shear. The theoretical studies show that the breaking of internal waves is determined by the overall energy of wave motions, on one hand, and by inhomogeneities in the medium on the other.

Samodurov, A. S. On the generation of internal wave trains in the ocean. IN: Sb. Issled. izmenchivosti gidrofiz. poley v okeane. Moskva, Nauka, 1974, 99-108.

The author suggests that a possible mechanism for the generation of trains of internal waves (secondary waves) is an instability of finite-amplitude (primary) internal waves. The problem of infinitesimal disturbances in a stratified fluid was solved in the vicinity of the critical point $\bar{u}(y_o, z_o) = c_o$, where $\bar{u}$ is horizontal particle velocity in primary waves, and c_o is phase velocity. An expression for the period of secondary waves in the real ocean is proposed. A numerical estimate of secondary wave periods is compared to measured periods of short internal waves in the Strait of Gibraltar (Zigenbein, 1969).

Karabasheva, E. I., and V. T. Paka. Observation of internal waves in the Central Atlantic. IN: Sb. Issled. izmenchivosti gidrofiz. poley v okeane. Moskva, Nauka, 1974, 108-114.

An analysis is given of temperature data acquired in one of the test areas during the 8th cruise of the R/V Akademik Kurchatov in 1970. The measurements were performed by a towed vertical chain of 20m-spaced sensors at a speed of 8-10 knots along 10 mile long tacks in an eight-pointed star pattern. The vertical profiles of T, S, and σ_t for the region tested (16^{o}N; 33^{o}W) are shown in Fig. 1.

The two-dimensional temperature structure in the Central Atlantic is illustrated in Fig. 2. It was observed that temperature structures

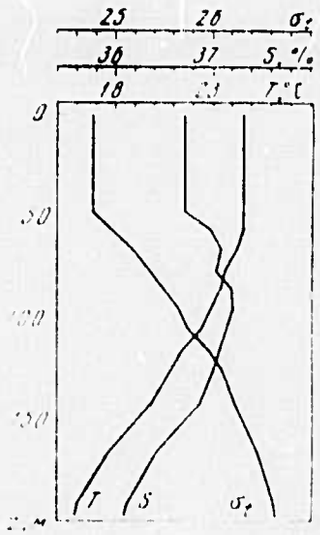

Fig. 1. Vertical profiles of T, S, and σ_t in the Central Atlantic (16°N; 33°W).

along other tacks were similar to that shown in the figure, although observed temperature fluctuations are not cophasal. Statistical characteristics of fluctuations in the depth of the 20.5°C isotherm and of fluctuations of temperature within the layer are shown in Figs. 3-5.

It was concluded that the energy spectra in Fig. 5, which are proportional to k^{-3}, indicate the presence of internal waves in the ocean. These short-period internal waves can be considered as stationary and isotropic to a first approximation.

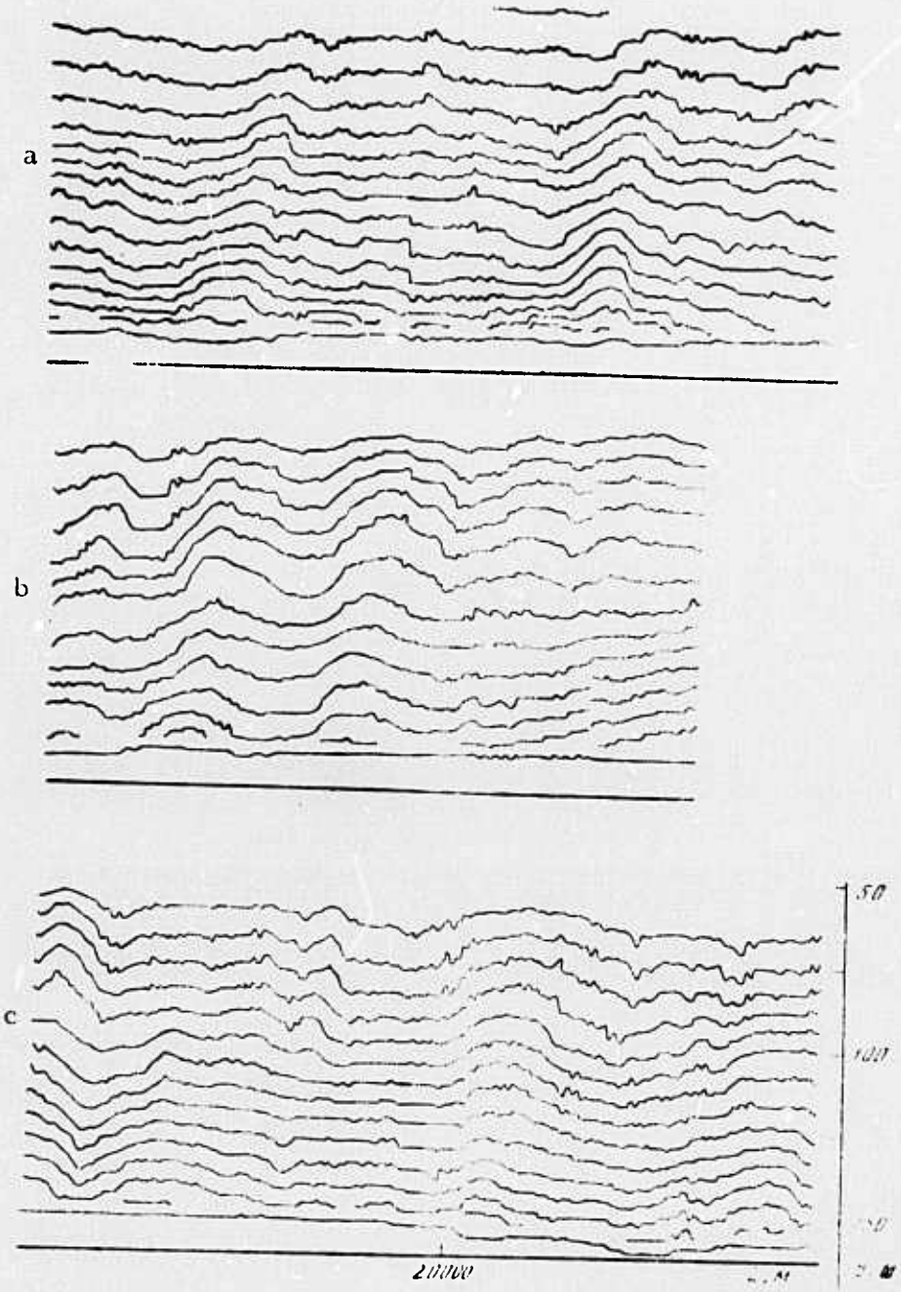

Fig. 2. Two-dimensional temperature structure along a 45° tack.

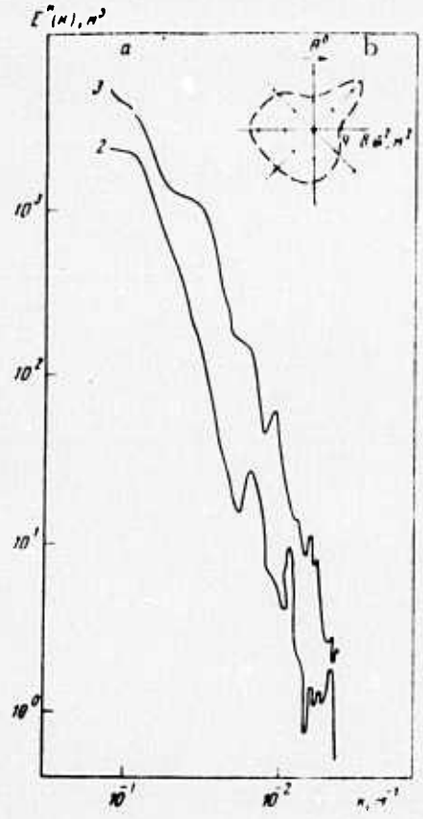

Fig. 3. Spectra (a) and standard dispersion (b) for fluctuations in depth of the 20.5°C isotherm. Numerals indicate tacks.

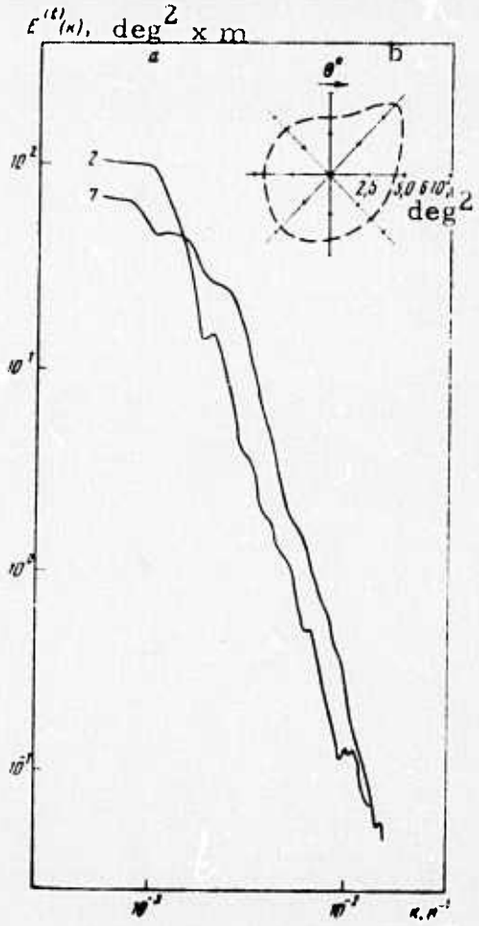

Fig. 4. Spectra (a) and standard dispersion (b) for temperature fluctuations averaged over depths.

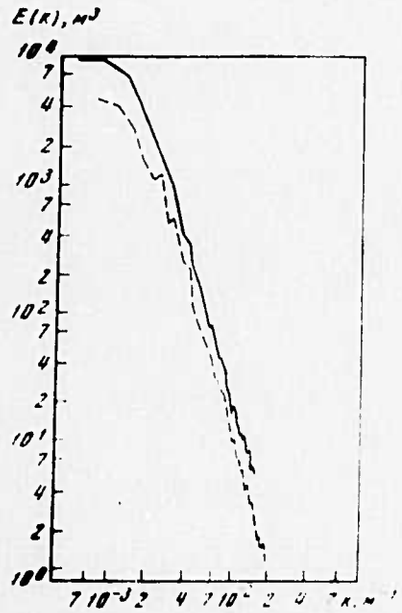

Fig. 5. Spectra for fluctuations in depth of the 20.5°C isotherm, averaged over all depths and directions (solid line) and over all directions (dashed line).

Benilov, A. Yu. On the spectrum of Reynolds stress. IN: Sb. Issled. izmenchivosti gidrofiz. poley v okeane. Moskva, Nauka, 115-122.

An expression is derived for the spectrum of the Reynolds stress in a statistically stationary and horizontally homogeneous turbulent flow, assuming a locally homogeneous turbulence. The results of numerical analysis of the spectral function derived are compared to experimental data for the atmosphere.

The expression for spectral function was derived using Monin's form for the equation of conservation of turbulent energy, Heisenberg's form for the inertial transfer of turbulent energy and the tensor of the Reynolds stress in the form

$$-\overline{u_i'u_j'} = K(k_0)\varepsilon_{ij}, \qquad \varepsilon_{ij} = \frac{\partial U_i}{\partial x_j} + \frac{\partial U_j}{\partial x_i}.$$

An analysis of the derived expression showed that, if the three-dimensional spectrum of the Reynolds stress in the inertial interval can be approximated by $-E_{uw} \sim k^{-m}$, than the exponent m should satisfy the inequality $m \geq 7/3$.

Results of numerical calculations and their comparison with experimental data are given in Figs. 1 and 2.

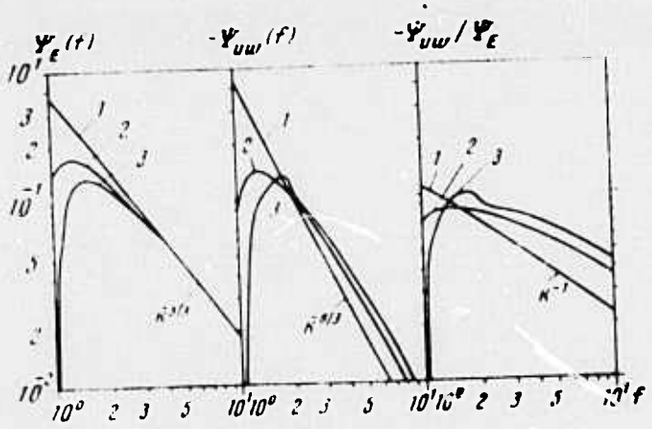

Fig. 1. Effect of the parameter ψ_σ^1 (1) on dimensionless spectra of energy and Reynolds stress. Curves 1-3: ψ_σ^1 (1) = 1/2, 1, and 2, respectively.

$$\psi_\sigma = \left(\frac{\partial U}{\partial z}\right)^{-2} \sigma_{uw}^2$$

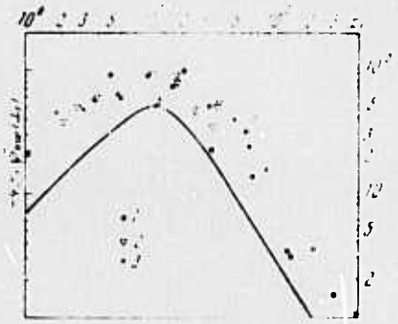

Fig. 2. Function $x_1 \psi_{uw}(x_1)$ calculated for $\psi_\sigma(1) = 2$ at $\mu = n = 1/2$

$$\bar{\Psi}_{uw}(x_1) = \int_{x_1}^{\infty} x^{-1} \psi_{uw}(x)\, dx.$$

Experimental data according to Zubkovskiy and Koprov (1969):

1 - z = 16 m, $\bar{U}$ = 4.7 m/s; 2 - 8 m, 4.4 m/s; 3 - 2.5 m, 4.1 m/s.

Aleksandrov, A. P., and E. S. Vaydruk. Measurement of the parameters of an aerated sea layer as a method for the remote study of near-surface vertical turbulence. IN: Sb. Issled.izmenchivosti gidrofiz. poley v okeane. Moskva, Nauka, 1974, 122-128.

The thickness of an aerated sea layer, d, was measured by the method of ultrasonic echo-sounding as indicated in Fig. 1. The measuring

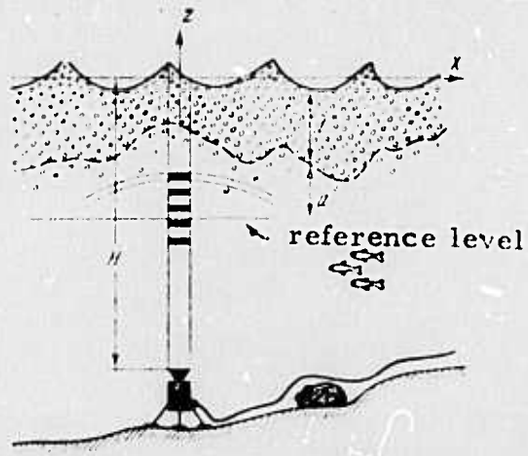

Fig. 1. Echo-sounding experiment

system was mounted on the sea bed at a water depth of 20 m and offshore distance=1 km. The diameter of the ultrasonic beam used was 1 m; the diameter of scattering element was 10 cm.

It was possible with this technique to identify large-, medium- and small-scale fluctuations of the thickness of the aerated layer. Large-scale fluctuations in d of the order of about 10 cm/sec were suggested to be associated with turbulent motions (see Fig. 2). Statistical characteristics of these fluctuations are shown in Figs. 3-5. The characteristic vertical turbulence scale was found to be proportional to wind velocity, mean wave height, and water depth.

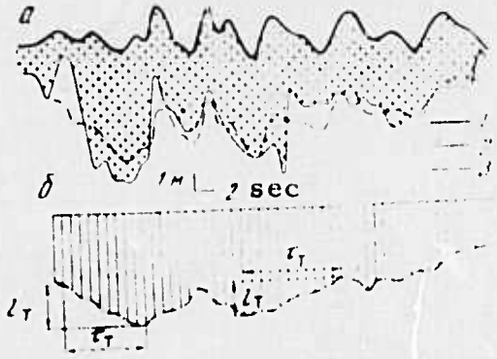

Fig. 2. Determining vertical turbulence scale ℓ_T from fluctuations of d.

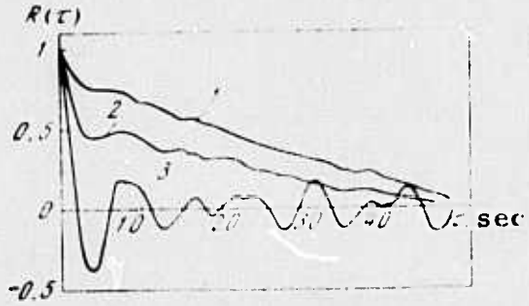

Fig. 3. Typical autocorrelation functions for fluctuations of d (1), elevation of the base of the aerated layer a (2), and elevation of the sea surface H(3).

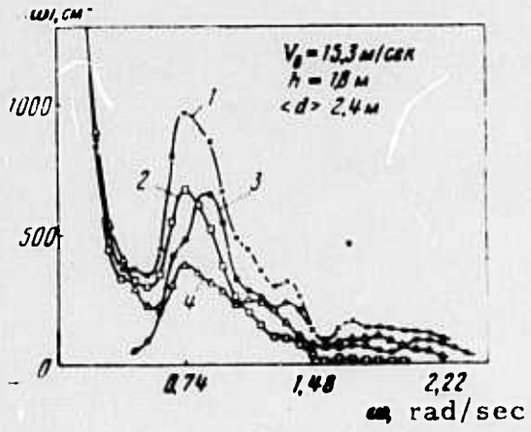

Fig. 4. Typical spectral functions of a (1 and 2), H(3), and d(4).

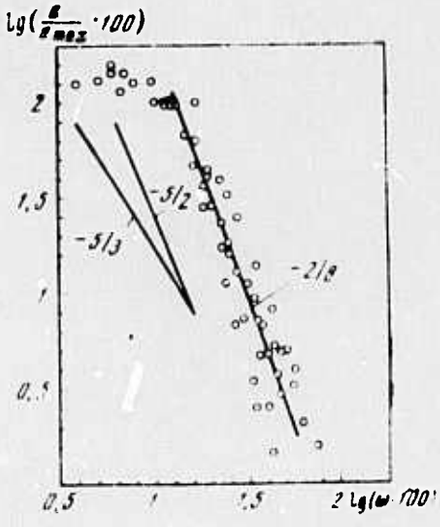

Fig. 5. Averaged spectral function for fluctuations of a.

The results of the present experiment thus confirm the feasibility of studying local turbulence in a near-surface sea layer up to several meters thick by means of remote acoustic measurements of parameters of the aerated layer.

Konovalov, Ye. A., and V. N. Yasenskiy. Some problems in the use of structural functions for determining parameters of anisotropy of a turbulence field. IN: Sb. Issled. izmenchivosti gidrofiz. poley v okeane. Moskva, Nauka, 1974, 129-131.

An attempt is made to express geometric parameters of elliptical anisotropy of an arbitrary two-dimensional turbulent field in the terms of structural functions. Some assumptions used in the analysis were tested experimentally.

The two-dimensional normalized structural function for fluctuations of a turbulent field $\rho(x, y)$ was given in the form

$$D(\xi, \eta) = \frac{\overline{[\rho(x, y) - \rho(x + \xi, y - \eta)]^2}}{D(\infty)}. \qquad (1)$$

where ξ, η are displacements in the x and y directions, and $D(\infty)$ is the structural function in the region of saturation.

A simplified form of the structural function is shown in Fig. 1.

In order to express (1) in terms of the geometric parameters of elliptical anisotropy $\beta = \xi_k / \eta_k$ (β = anisotropy coefficient, ξ_k and η_k = intervals of structural correlation), the following assumptions were made:

$$D(\xi, 0) = k_\xi \xi^{\gamma_\xi}, \qquad D(0, \eta) = k_\eta \eta^{\gamma_\eta}, \tag{2}$$

$$D(\xi_k, 0) = k_\xi \xi_k^{\gamma_\xi} = 1, \qquad D(0, \eta_k) = k_\eta \eta_k^{\gamma_\eta} = 1. \tag{3}$$

where k_ξ and k_η are scale factors in the x and y directions.

Using (3) and expressing the semiaxes of an arbitrary section of surface (1) $D_i(\xi_i, \eta_i) = \text{const}$ as

$$\xi_i = D_i^{1/\gamma_\xi} \xi_k, \qquad \eta_i = D_i^{1/\gamma_\eta} \eta_k. \tag{4}$$

yields

$$\frac{\xi^2}{(D_i/k_\xi)^{2/\gamma_\xi}} + \frac{\eta^2}{(D_i/k_\eta)^{2/\gamma_\eta}} = 1. \tag{5}$$

$$\beta = \frac{\xi_k}{\eta_k} = \frac{k_\eta^{1/\gamma_\eta}}{k_\xi^{1/\gamma_\xi}}. \tag{6}$$

Calculated structural functions for fluctuations in the two-dimensional field of electrical conductivity in an immersed jet, which were measured in hydrodynamic test stand, are shown in Fig. 2.

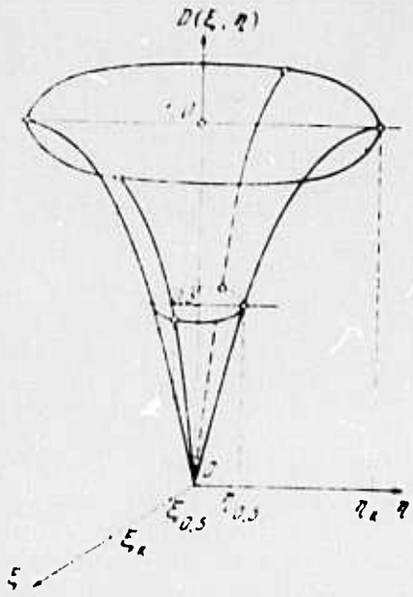

Fig. 1. Schematic of two-dimensional structural function.

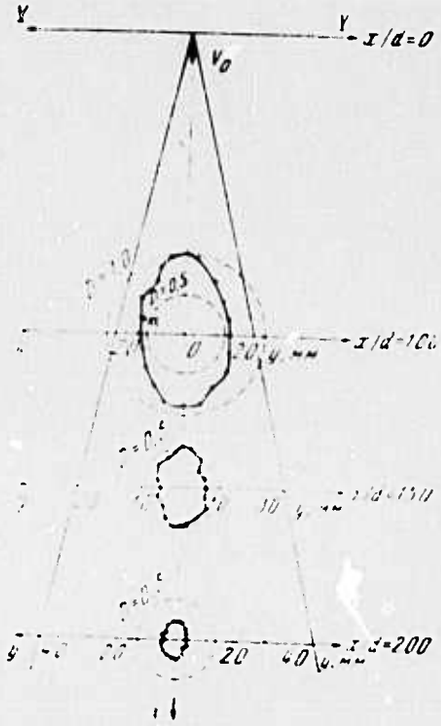

Fig. 2. Structural functions for fluctuation of electroconductivity field of an immersed jet at different distances from the source.

Karabashev, G. S., and R. V. Ozmidov. Study of admixture diffusion in the sea by means of luminescent tracers and a towed sensor. IN: Sb. Issled. izmenchivosti gidrofiz. poley v okeane. Moskva, Nauka, 1974, 135-144.

A description is given of instruments and configurations used in measurements of concentration of a luminescent dye tracer in the sea. The article includes some results of measurements conducted in the Black and Baltic Seas.

An optical schematic of the fluorimeter employed is shown in Fig. 1. Its specifications are: measuring range 5×10^{-10} - 1×10^{-6} gr/mℓ

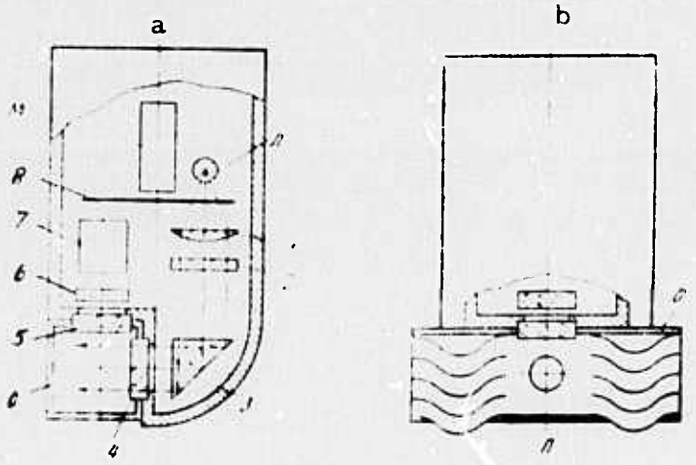

Fig. 1. Optical layout of towed fluorimeter (a), and cross-section of screen 0 (b).

for uranin and 1×10^{-9} - 5×10^{-6} gr/mℓ for rhodamine C; drift 0.2 sec; power drain 80 w; duration of continuous operation 7 hrs; depth range, 0-100 m. The space-time distribution of the tracer concentration in a dyp patch or ribbon was measured by towing the fluorimeter across them at different depths, or by locating the

fluorimeter at a fixed distance from a continuous source. Different arrangements for measurements are shown in Figs. 2-4. Graphical results illustrating both vertical and horizontal dye diffusion are included.

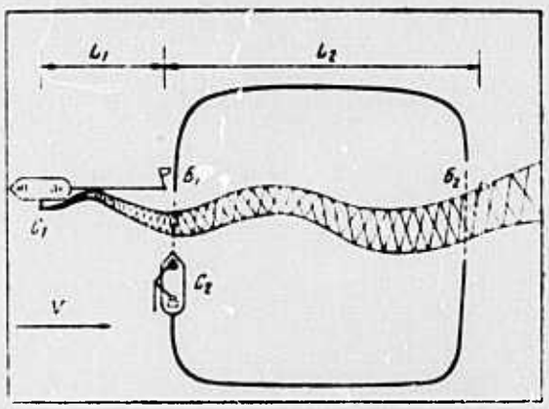

Fig. 2. Schematic of arrangement with a continuous source of tracer.

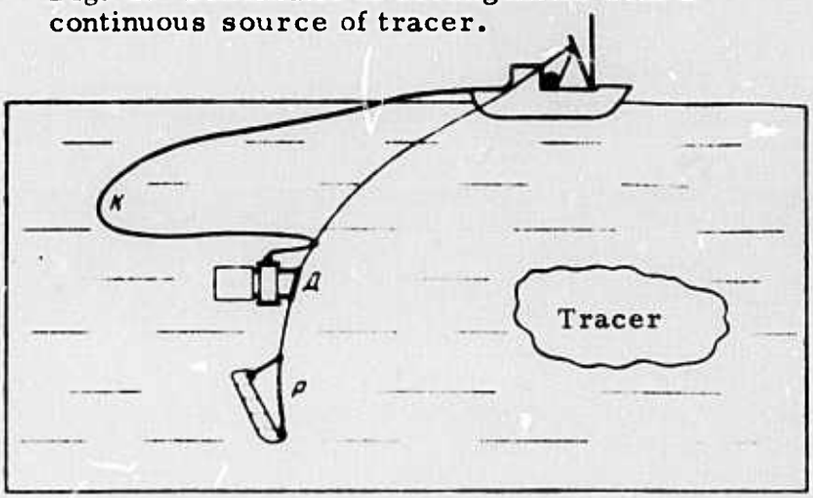

Fig. 3. Depth control of the towed fluorimeter.

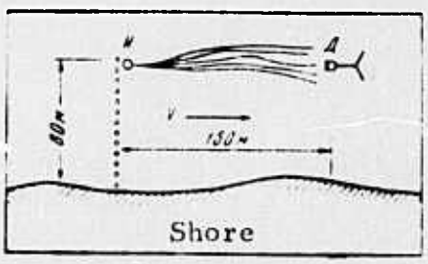

Fig. 4. Test arrangement with fluorimeter mounted at a fixed distance from a continuous source of tracer.

Goroshko, V. I. Turbulent diffusion of dye tracer in a sea coastal zone. IN: Sb. Issled. izmenchivosti gidrofiz. poley v okeane. Moskva, Nauka, 1974, 145-150.

This article studies the spatial distribution of dye tracer concentration in a coastal zone, for the case of variable coefficients of eddy diffusion. The problem is solved in the framework of a semiempirical theory of turbulent diffusion.

Calculations of the field of tracer concentration S(x, y, z) generated by a stationary point source $M_o(0, y_o, z_o)$ was made by the Fourier method. It was assumed that water depth in the coastal zone is constant and turbulent transport in the x-direction (i.e. parallel to the coastline) is negligible. The article includes results of numerical calculations of relative tracer concentration $S_* = \frac{Sdh^{a+1}}{N(1-\alpha)k_1}$, where N is source strength for the shallow-water coastal zone (h = 2.5 m) and a point source placed at (0, 45, 0.5).

Calculated results are shown in Figs. 1 and 2.

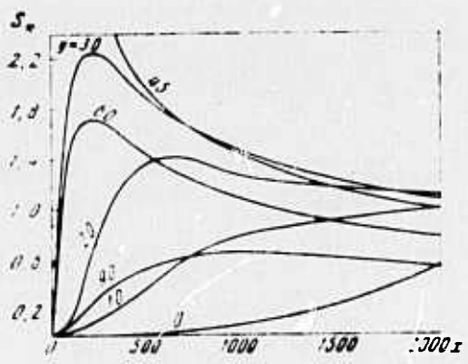

Fig. 1. Distribution of tracer concentration parallel to the coastline.

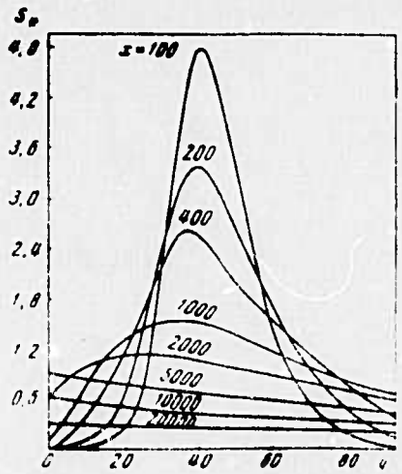

Fig. 2. Distribution of tracer concentration perpendicular to the coastline.

As seen in Fig. 2 the maxima on the tracer concentration distributions occur nearer the coastline as x increases. This fact is explained as being caused by a more rapid scattering of the dye on the seaward side of the source (y > 45) owing due to larger coefficients of eddy diffusion.

Dobroklonskiy, S. V., and M. L. Pyzhevich. An example of calculation by indirect methods of vertical velocity of flow and vertical coefficients of turbulence viscosity in the ocean. IN: Sb. Issled. izmenchivosti gidrofiz. poley v okeane. Moskva, Nauka, 1974, 150-155.

Computations on turbulent viscosity are reported, using data on flow velocity, temperature, and salinity from three buoy stations (Fig. 1) obtained during the 51st cruise of the R/V Vityaz in 1972.

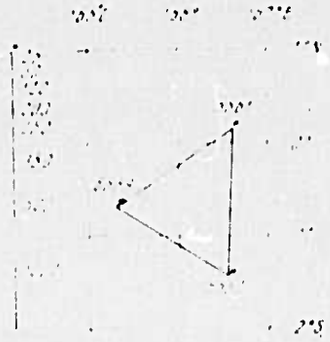

Fig. 1. Location of buoy stations with indicated measurement depths.

The following formulas were derived for calculations:

$$w = \frac{\frac{\partial v}{\partial z} X(z) - \frac{\partial u}{\partial z} Y(z)}{u \frac{\partial v}{\partial z} - v \frac{\partial u}{\partial z}}, \qquad (1)$$

$$v = \frac{vX(z) - uY(z)}{u \frac{\partial v}{\partial z} - v \frac{\partial u}{\partial z}}$$

It is emphasized that the interpretation of present results can reflect only general trends in distributions of w and ν.

Nabatov, V. N., V. T. Paka, and V. I. Shkurenko. On the use of hot-wire anemometers in a flow with temperature fluctuations. IN: Sb. Issled. izmenchivosti gidrofiz. poley v okeane. Moskva, Nauka, 1974, 162-174.

An analysis is given of error in measurement of flow-velocity fluctuations by hot-wire type anemometers in the presence of temperature fluctuations. Laboratory measurements by a multiple or "three-heat" method are described, and results of separation of spectra of velocity and temperature fluctuations are given.

Measurements in grid-produced turbulent flows both with and without temperature fluctuations were made simultaneously by type DISA-55D01 and Stolypin (hydroresistor) hot-wire anemometers. The sensitive element in the latter instrument is a micro-electrode hydroresistor which detects electrical conductivity in a small water volume. Response of the hydroresistor hot-wire anemometer is given in Fig. 1.

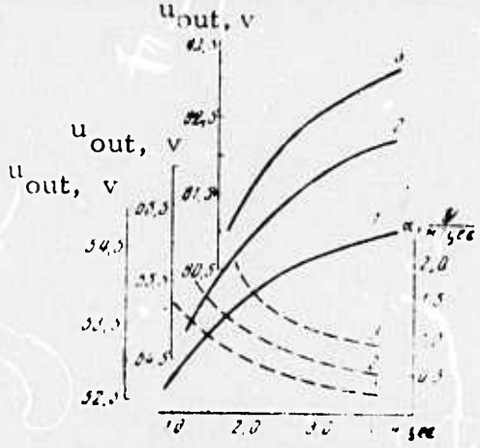

Fig. 1. Calibration (solid lines) and sensitivity (dashed lines) curves for hydroresistor hot-wire anemometer at a supply voltage of 10(1), 12(2) and 15V(3).

The minimum mean velocity required is 0.3-0.5 m/sec at 10 V, ~1.0 m/sec at 12 V, and ~1.5 m/sec at 15 V supply. Sensitivity to velocity and temperature fluctuations, α and β, for both instruments are given in Table 1.

Table 1

Sensitivity	DISA - 55 DOI hot-wire anemometer				Hydroresistor hot-wire anemometer		
	10°C	20°C	30°C	40°C	10 V	12 V	15 V
α, V/m/sec	2.55	2.55	2.55	2.55	0.46	0.81	1.43
β, V/deg	1.50	0.75	0.48	0.34	0.30	0.33	0.36

A comparison of spectra for velocity pulsations measured simultaneously by the two instruments is given in Fig. 2.

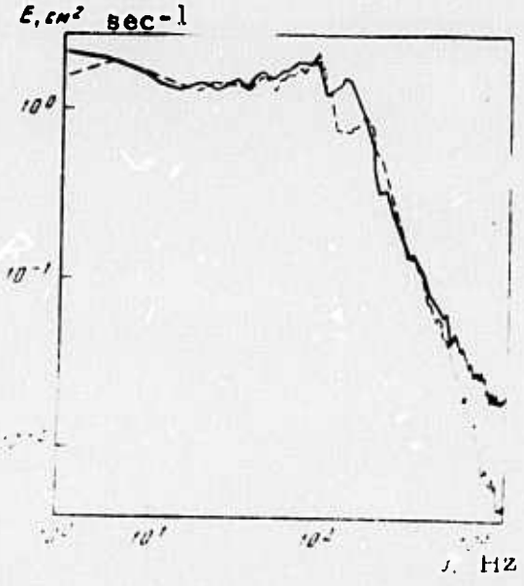

Fig. 2. Spectra for velocity pulsations measured by DISA-55DOI and hydroresistor hot-wire anemometers.

It was concluded that hot-wire type anemometers can give reliable measurement of energy and structural characteristics of velocity fluctuation fields in the presence of temperature fluctuations, if measurements are made by the "three-heat" method. The hydroresisto-type hot-wire anemometer which, in addition to high sensitivity and resolution, has exceptional mechanical reliability and contamination stability, appears to be a better prospect for the study of ocean turbulence than the DISA instrument.

Pluzhnikov, V. M., and M. S. Khlystunov. Frequency-responsive piezoelectric pressure indicator for oceanological research. IN: Sb. Issled. izmenchivosti gidrofiz. poley v okeane. Moskva, Nauka, 1974, 175-197.

Physical principles and design of a frequency responsive piezoelectric depth (pressure) indicator are discussed in detail. The sensitive element of this instrument is a piezoelectric, preferably quartz, resonator with an AT cut. Metrological characteristics of the quartz resonator are analyzed and the theory of both monolithic and segmented types of this sensor as a depth (pressure) indicator is developed. Errors introduced in measurements by separate structural elements are evaluated numerically for a segmented-type instrument. Figs. 1 and 2 illustrate the two constructions.

It is concluded that high accuracy ($\sim 0.002\%$), large dynamic range (10^4-10^6), linearity, digital output, and small overall dimensions make the piezoelectric depth indicator very prospective for the study of oceanic fine structure.

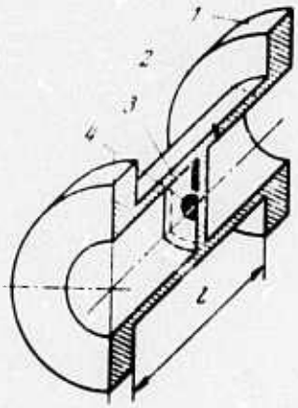

Fig. 1. Monolithic pressure sensor. 1, 2 - β-quartz cylinder and end flanges; 3- resonant transducer; 4- electrode.

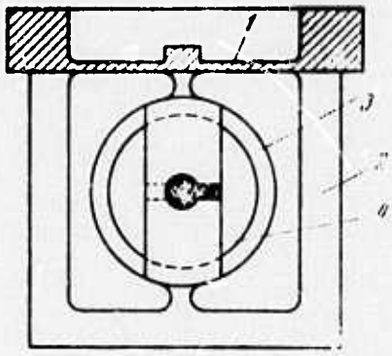

Fig. 2. Segmented sensor. 1, 2 - steel flange and base; 3 - elastic element; 4 - piezoelement support.

Ganson, P. P., A. V. Khokhlov, and V. F. Sytnikov. Some results of studies of thermohaline structure by a towed measuring system. IN: Sb. Mor. gidrofiz. issled. No. 1 (64), Sevastopol, 1974, 177-183.

A study of the thermohaline structure within the 50-100 m deep ocean layer was conducted during the 4th and 5th cruises of the R/V Akademik Vernadskiy in the equatorial region of the Pacific and Indian Oceans, and the northeast part of the Arabian Sea. Measurements were performed by the Nyrok-2 system operating in both towed and sounding regimes.

In the Pacific the two-dimensional thermohaline structure along the 155°E meridian is characterized by pronounced low-frequency fluctuations in the depths of isotherms and isohalines within the high-density gradient layer (130-160 m). Spectra for these fluctuations are characterized by an inertial interval within the 55-90 m range. However, corresponding spectra along the 170°E meridian display numerous peaks, which may indicate either the presence of internal waves or the fine structure of the Cromwell current.

In the Indian Ocean along the 56°E meridian, isotherms and isohalines are horizontal and fluctuate only slightly over the entire depth range, which is characterized by a uniform easterly current. Here the maximum vertical gradients through 130 m are 0.06° C/m and 0.02 0/00/m. Along the 75°E meridian (in the region of the Southwest Monsoon Current, and the Equatorial Countercurrent partially shielded here by the Maldive Islands) the isotherm is horizontal and low, respectively, on its southern portion, gently deepening and becoming higher (0.45°C/m) in its norther portion. The depth of maximum salinity, which coincides with the upper boundary of the high temperature gradient layer, decreases slowly northwards. On the 85° meridian the maximum vertical gradients coincide with the boundary between the Monsoon Current and Equatorial Countercurrent. Local homogeneous zones are nevertheless found in the vicinity of this boundary. The presence of local homogeneous zones is manifested in the spectra of temperature and salinity fluctuations. Fig. 1 illustrates one observed homogeneous zone.

In the Arabian Sea, a notable feature of the thermohaline structure in the area under study was an inversion layer, located above the high-gradient layer. Its generation may be associated with southerly transfer of high-salinity water. The thickness of this layer was found to fluctuate more intensely in the lateral than along the mean flow direction (Fig. 2).

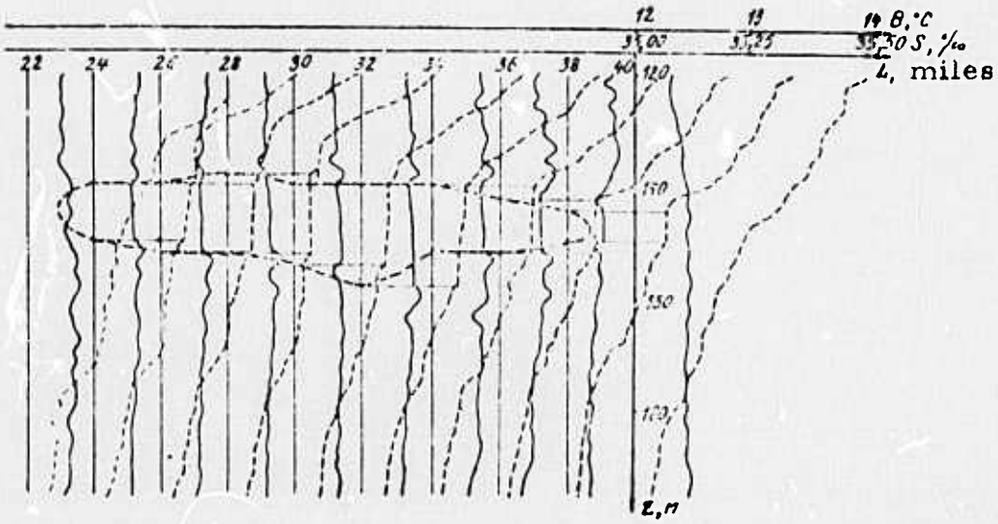

Fig. 1. Planar section of a homogeneous zone, Indian Ocean. Solid lines = salinity, dashed lines = temperature.

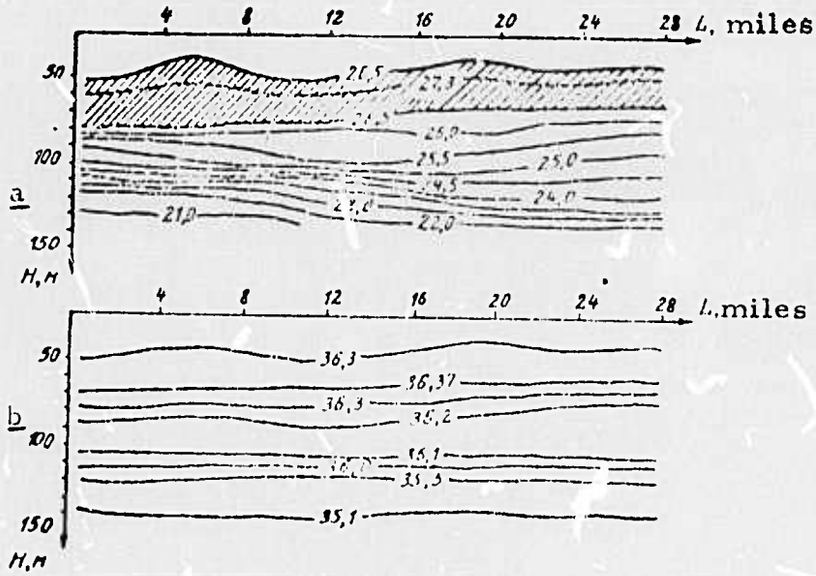

Fig. 2. Two-dimensional structure of inversion layer in the direction perpendicular to the mean flow, Arabian Sea. a - temperature, b - salinity.

Kats, A. V., and V. M. Kontorovich.
Theory of weak turbulence of waves on the surface of a fluid. ZhPMTF, no. 6, 1974, 97-106.

Weakly turbulent distributions of capillary waves in shallow water are analyzed, as well as conjugacy and interaction of turbulent spectra in different self-similar regions. Wave spectra were developed from the kinetic equation for wave number which describes a random wave aggregate in the theory of weak turbulence. In the development of the equation for N(k), impermissible decaying processes in the gravity region were excluded from the Hamiltonian by means of canonic transformation. Equations of motion and matrices describing the interaction of waves in a finite-depth fluid were then obtained in Hamiltonian variables.

An expression for weakly turbulent distribution of capillary waves, corresponding to a constant energy flux P over the turbulent spectrum was obtained in the form

$$N = P^{1/3}\left(\frac{k}{\omega}\right)^{1/2} k^{-4}(kh)^{1/2} \sim P^{1/3}k^{-4}, \quad h^{-1} \gg k \gg k_0 \tag{1}$$

The expression for weakly turbulent wave distribution in the transition from the gravity to capillary region ($k \sim k_0$), corresponding to a constant energy flux and $k_0 k \gg 1$, then becomes

$$N = P^{1/3}k^{-4}F\left(\frac{P}{Vk^3}, \frac{k}{k_0}\right), \quad F(x, y) = \begin{cases} 1, & y \ll 1 \\ x^{1/3}, & y \gg 1 \end{cases} \tag{2}$$

Finally, the weakly turbulent distribution of gravity waves in deep water, induced by capillary waves, was obtained in the form

$$N_q \simeq P^{1/3}\left(\frac{k_0}{\omega_0}\right)^{1/2} k_0^{-4}\left(\frac{q}{k_0}\right)^{9/4}, \quad \omega_0 \equiv \omega(k_0) \tag{3}$$

Thus the decaying spectrum in the capillary region $N_k \sim k^{-17/4}$ induces an increasing spectrum in the gravity region $N_q \sim q^{9/4}$.

Gorodetskiy, A. K., A. P. Orlov, A. I. Pashkov, and V. N. Stolyarov. On relationship of radiation and kinetic temperature of the surface water layer. IN: Sb., TROPEKS-72. L., Gidrometeoizdat, 1974, 511-519. (RZhGeofiz, 8/74, #8V92). (Translation)

The results are given of measurements of radiative water temperatures in the tropical Atlantic, taken on the 13th cruise of the R/V Akademik Kurchatov. The radiative capacity of the water surface was determined in the range of 2 to 45° down from horizontal. The radiative (T_r) and kinetic (T_w) temperatures of the surface water layer, measured from a drift vessel, were compared. The mean values of $\overline{\delta T} = \overline{T_r - T_w}$ and their corresponding standard deviations are: (-)0.55° and 0.2° at an elevation angle α = (-)45°; the mean value of δT at α = -90° is estimated to be (-)0.25°.

The angular dependences of the effective radiative capacity of the ocean-atmosphere system, $\epsilon(\alpha)$, and the radiative capacity of the water surface, $\epsilon'(\alpha)$, were determined from the angular dependence of the radiation of the water surface, taking into account the reflected radiation of the atmosphere. The dependence $\epsilon'(\alpha)$ is characterized by an increase at small angles. Estimates are given of the rms slope angles of waves for cloudless-sky cases, which confirm the possible use of measurements of natural ocean radiation for determining characteristics of sea waves.

Physics of the sea and atmosphere: Conference proceedings, February 1974. (Mosk. o-vo ispyt. prirody. Sekts. fiz.) M., Nauka, 1974, 97 pp. (RZhGeofiz, 10/74, #10B30 K).

Papers given at this conference are listed. Those of possible pertinence include:

Microconvections during evaporation and ice formation (A. V. Shumilov);

Study of temperature fields of an absorbing medium in a radiating system of arbitrary structure (Yu. A. Surinov);

Results of the hydrodynamic theory of finite-amplitude waves (Ya. I. Sekerzh-Zen'kovich);

Calculation of heights, periods, profile parameters and power spectra of wind waves (L. A. Korneva);

Temperature waves in a stratified sea (Vo Van Lan' and A. A. Pivovarov).

Cherkesov, L. V. Some problems in the study of the generation of internal waves in the ocean. Okeanologiya, no. 6, 1974, 1130-1131.

This paper reviews the results of theoretical studies on generation of internal waves in the ocean, conducted during recent years in the Laboratory for Wave Theory of the Marine Hydrophysical Institute of the Soviet Academy of Sciences. All the problems were considered in linear approximations.

The following wave generators are considered: 1) disturbances of atmospheric pressure periodically varying in time, applied to a restricted stationary area of a sea surface; 2) periodically shifting surface pressures, $p_o = a \cos (kx-\sigma t)$ within the range $|x| \leq \infty$, $|y| < b$, where k is wave number, σ = frequency, a = amplitude of the pressure wave, and b = width of the band where pressure is applied; 3) time-independent baric disturbances occupying a limited region and moving at a constant velocity; 4) bottom obstacles with small elevations (hills or ridges) as well as periodic oscillations of a portion of the bottom.

For each above type of wave source the following density models are considered: a) density discontinuity at the interface between two finite-depth layers with constant densities; b) continuously varying density from the free surface to the bottom; c) continuously varying density in the upper layer, constant in the lower; d) continuously varying density in the middle layer, constant densities in the upper and lower ones; e) continuously varying density in the upper and lower layers, with a larger gradient in the upper one.

For all the indicated sources and density models, rigorous analytical solutions are obtained and on the basis of these solutions further analytical and numerical studies were completed, providing explanations for the effects of the form and parameters of sources and density models of internal waves.

For models (b), (c), (d), and (e), periodic steady-state wave motions were studied. For model (a), development of the wave process, from an undisturbed-state fluid through periodic steady-state or time-independent waves, was studied. In addition, for this model the solution to the problem of generation of internal waves by surface waves for the case of an arbitrary change of the basin depth and depth of the upper layer was obtained.

Gurvich, A. S., and N. S. Time. Study of turbulence microstructure by means of lasers. Okeanologiya, no. 6, 1974, 1128-1129.

This paper was given at the April 12, 1974 Seminar on Geophysical Hydrodynamics at the Oceanographic Commission, Soviet Academy of Sciences. The paper deals with optical methods for the study of turbulent structures in different scale ranges. These methods are based on the relationship between statistical characteristics of refractive index

fluctuations and fluctuations in the parameters of visible light waves. Since temperature fluctuations play a dominant role in determining fluctuations of the refractive index for waves in the optical range, a study of the refractive index is equivalent to the study of temperature.

The authors describe phenomena accompanying propagation of waves in a turbulent medium, and on the basis of a simple model of inhomogeneities in the refractive index field, the basic patterns in fluctuations of the parameters of light waves are inferred.

Particular attention was paid to the methods for measuring the structural constant C_n^2 for refractive index, which is the main characteristic of the spectrum in the inertial interval. Various methods for measuring the average value of C_n^2 over an optical path have been developed at the Institute of Atmospheric Physics. Specifically, simple and suitable apparatus was developed for fast C_n^2 measurements. Gradient measurements, which were previously used, have a lower accuracy and give average values over larger time intervals and at a single point of a path.

Among the methods proposed to measure the temperature field structure in the scale range comparable to that of Kolmogorov, the following are mentioned: determination of internal scale from measurements of dispersion of light intensity fluctuations; and determination of spectral shape in the dissipation region, from measuring frequency spectra of fluctuations in log intensity along the axis of a wide light beam. The latter method, developed by the authors, is a unique one, and gives results over the temperature spectrum in the viscous interval.

In the solution of this problem, difficulties have arisen in solving the equation relating the above mentioned quantities. The equation appeared to be incorrect, and for its solution the method of statistical

regulation was applied. Fig. 1 gives a comparison of a one-dimensional normalized temperature spectrum obtained from optical measurements

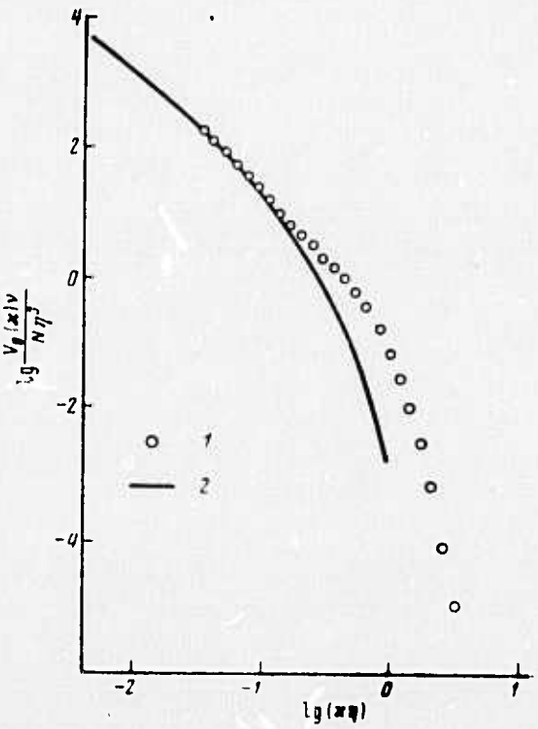

Fig. 1. One-dimensional spectrum of temperature fluctuation.

1 - from optical measurements;
2 - from resistance thermometer

and as measured by a resistance thermometer (Boston, 1972). Spectrum 1 is attenuated less rapidly in the region of high frequencies than spectrum 2. This can be attributed to the distorting effect of the sensor on the structure of turbulent flow.

In conclusion the prospects for applying optical methods to the study of turbulence in different scale ranges are discussed. Present photographic techniques are judged inadequate to meet requirements of the problem of small-scale turbulence.

Vo Van Lan', and A. A. Pivovarov. Temperature waves in a stratified sea. IN: Sb. Fiz. morya i atmosfery. Moskv, Izd-vo Nauka, 1974, 68-72. (RZhGeofiz, 11/74, #11 V114). (Translation)

The effect of density stratification on propagation of temperature waves is explained, using a one-dimensional equation of turbulent thermal conductivity. The vertical density profile and its time variations are assumed given. The form of the source or heat flow function [$Q(z, \tau)$ where τ is time] corresponds only to the absorption of radiated solar energy. Temperature, Q and density ρ as functions of depth and time are represented as sums of the average diurnal and annual values and their corresponding standard deviations.

It is found that, if $\rho(z)$ is linear and the turbulent exchange steady, the amplitude profile for temperature waves is the opposite of the density profile, and the phase shift of temperature waves is independent of the density profile. The results hold true qualitatively for other density profiles as well.

Navrotskiy, V. V. Vertical structure of mesoscale temperature pulsations. IN: Sb. Atlantich. gidrofiz. poligon-70. M., Nauka, 1974, 283-304. (RZhGeofiz, 11/74, #11 V115). (Translation)

Measurements of temperature made by a towed sensor chain are described. The results of statistical analysis of spatial temperature fluctuations are given as follows. 1) The vertical structure of temperature pulsations in the upper ocean layer reflects the effects of the simultaneous

presence of turbulence and internal waves. The effect of turbulence in the process of exchange of disturbance energy sharply diminishes downward from the upper boundary of [this] stratified layer. 2) Maximum energy of observed internal waves with $\lambda \approx 80$ m is found in the zones of maximum shear of the average flow, which suggests the possibility for generation of internal waves by shear. 3) Collapse of internal waves leads to a deepening of the upper boundary of the stratified layer and the formation of a layer with a slight inversion or with zero gradient of the average temperature, with substantial temperature pulsations during its formation. 4) In the case of weak nonlinear interaction, the theory of random linear systems can be used and interactions described by such characteristics as transfer functions (modulus and phase). In the case of significant nonlinear interactions it is more expedient to analyze only the correlation, which makes it possible to evaluate integral scales of inhomogeneities and integral rates of disturbance propagation.

Borshchevskiy, Yu. T., E. M. Litvinenko, and V. G. Nakhanchuk. Transfer processes in a turbulent boundary layer with low concentration of a dispersed phase. IN: Teor. osnovy khim. tekhnol. no. 4, 1974, 507-516. (RZhMekh, 11/74, #11B367). (Translation)

On the basis of boundary layer equations, formulas are developed by the parametric method for instantaneous and averaged fields of velocity distribution, concentration, and temperature in a turbulent boundary layer. It is shown that the method applied is suitable for the study of other flow forms.

Kartvelishvili, N. A., and G. P. Kumsiashvili. Quality of natural waters and the problem of turbulence. IN: Sb. Vzaimodeystviye poverkhnost. i podzemn. stoka. Vyp. 2. M., Mosk. un-t, 1974, 88-99. (RZhMekh, 11/74, #11B1143). (Translation)

The Reynolds equations for three-dimensional flow of a turbulent nonisothermic fluid composed of several components are developed. Different methods of closing of moment equations are considered. It is suggested that, in the case of a three-dimensional flow for which it is difficult to determine average velocity gradient ("nonprismatic" flow, in the authors' terms), the tensor of turbulent stresses may be represented as the sum of stresses arising due to the presence of flow walls, and caused by variation in average velocity over the channel cross-section as well as by stresses due to curvature and spiraling of flow lines.

Borshchevskiy, Yu. T., I. M. Fedotkin, M. N. Chepurnoy, and V. E. Shnayder. Calculation of heat exchange in turbulently discharging fluid films. Minsk, 1974, 13 pp. (RZhMekh, 12/74, #12 B957 DEP). (Translation)

On the basis of a power law distribution of velocity, major hydrodynamic parameters of turbulently discharging fluid films are determined, which agree well with published experimental data in the range of $10^3 < Re < 10^5$.

Nekrasov, V. N., and Yu. D. Chashechkin. Measurement of the period of free internal oscillations of a fluid. IN: Tr. VNII fiz.-tekhn. i radiotekhn. izmereniy, no. 14(44), 1974, 69-73. (RZhMekh, 12/74, #12B1360). (Translation)

A procedure for determining the period of free internal oscillations in a fluid by a method of "density" marks, and an analysis of measurement errors, are given.

Vlasov, Yu. N., and Yu. D. Chashechkin. Flow visualization for measurements of velocity and turbulence of a fluid. (Review). IN: Tr. VNII fiz.-tekhn. i radiotekhn. izmereniy, no. 14(44) 1974, 23-29. (RZhMekh, 12/74, #12B1365). (Translation)

Methods for visualizing flows presently used in hydrodynamics are considered. The methods are separated into five groups: 1) dyed fluids; 2) discrete microparticles; 3) electrolytic; 4) luminescence-photolytic; and 5) optical. Descriptions of accuracy and applicability limits are given for each method.

Anuchin, V. P., A. M. Gusev, Yu. G. Pyrkin, and M. M. Khapayev. Problem of near-bottom density currents on the continental shelf. IN: Sb. Fiz. morya i atmosfery. M., Nauka, 1974, 90-95. (RZhGeofiz, 11/74, #11V69). (Translation)

Turbulence characteristics of near-bottom density currents on the continental shelves and their effect on the vertical profile of average flow velocity have been studied. Taking into account small changes in the width of these currents, the authors consider them approximately as plane-parallel flows of higher-density fluid along the sloping surface of a lower-density one. The motion of the fluid occurs because of the gravity component parallel to the sloping bottom. It is shown that the vertical profile of average flow velocity can be inferred from the obtained distribution of turbulent stress. A calculation method is proposed enabling one to determine turbulence characteristics without using direct measurements of velocity pulsations. (cf. Anuchin et al., Sov. Mat. on Int. Wave Eff., no. 3, Apr. 1975, 86).

Gol'dshtik, M. A., and V. N. Stern. Model self-oscillations and turbulence. IN: Sb. Probl. teplofiz. i fiz. gidrodinamiki. Novosibirsk, Nauka, 1974, 17-25. (RZhMekh, 12/74, #12B1044). (Translation)

Model self-oscillations in a viscous flow, sinusoidal with respect to uniform coordinates and time, are considered. Such a model enables illustration of the characteristics a turbulent flow would have in the case of a "cut-off" cascade process. It is shown that self-oscillations describe at least qualitatively correctly the mechanism of nonlinear instability and properties of two-dimensional turbulence in a perpendicular magnetic

field. They appear to be useful in construction of the average velocity profile in the case of a developed turbulent flow.

Yampol'skiy, A. D. On inertial pulsations in a flow velocity field. IN: Sb. Atlantich. gidrofiz. poligon-70. M., Nauka, 1974, 189-192. (RZhGeofiz, 11/74, #11V60). (Translation)

Characteristics of inertial pulsations in a velocity field were studied, using observations from a test area. Pulsation intermittency and the possibility for a statistical approach to the study of inertial motions were discussed. Findings are 1) inertial pulsations are closely related to the average flow fields, particularly to their horizontal gradients, and consequently to sea water density; 2) a theoretical study of inertial pulsations is useful only in the framework of nonlinear models; 3) construction of orbits for the analysis of inertial pulsations is not presently recommended; 4) observations should enable evaluation not only of the average flow field and its horizontal gradients, but also of the density field and its gradients. The latter is required for the analysis of pressure gradients which are apparently an important condition for the existence of inertial pulsations in a velocity field.

Hydrophysical and hydrooptical studies in the Atlantic and Pacific oceans. Results of studies during the 5th cruise of the R/V Dmitriy Mendeleyev. In-t okeanol. AN SSSR. M., Nauka, 1974, 328 pp. (RZhF, 12/74, #12D815 K). (Translation)

Part I of this monograph reviews the methodology of hydrophysical studies in the ocean. The second and third parts deal with

light absorption and light scattering mechanisms in sea water; space-time variability of the optical characteristics in waters of the Atlantic and Pacific; and generation of luminescence fields from natural and artificial sources. In the fourth part, factors affecting optical properties of ocean waters are discussed.

Potetyunko, E. N. Natural oscillations of an infinite-depth viscous fluid. IN: Sb. Mat. analiz i yego pril. T. 6. Rostov-na-Donu, Rostov. un-t, 1974, 158-161. (RZhMekh, 11/74, #11B616). (Translation)

The functional dependence on wave number of the roots of a secular equation is obtained, for the problem of surface waves on an infinite-depth viscous fluid. Asymptotic expressions, previously known, are obtained as a partial solution of the problem. The dependence obtained can be used in solving problems of nonstationary wave motions.

Sovershennyy, V. D. Model of the absolute viscosity at the wall in a turbulent boundary layer. Minsk, 1974, 15 p. (RZhMekh, 11/74, #11B862 DEP). (Translation)

A formula is proposed for absolute viscosity, intended for the calculation of flow in a boundary layer, including regions of laminar, transitional and turbulent flow regimes. Calculated results are compared to experimental data obtained for various flows (with injection and suction; with a pressure gradient). Satisfactory agreement of calculated and experimental values demonstrates the universality of the proposed formula and constants associated with it.

Shvab, V. A. Model of turbulence generation in a "gradient" flow. IN: Sb. Materialy 4-y nauch. konf. Tomsk. un-ta po mat. i mech. T. 2. Tomsk, Tomsk. un-t, 1974, 115-116. (RZhMekh, 12/74, #12B1052). (Translation)

A model of turbulence generation is studied in which displacements occur as a result of mechanical degeneration of turbulence and periodic weakening of the turbulent portion of tangential stresses. Displacements in an ideal fluid are interpreted as discontinuities in the direction of the averaged motion. These are the cause of vortex disturbances which periodically regenerate turbulent motion.

Kutateladze, S. S. Problem of turbulence. Tr. XIII Mezhdunar. kongr. po istorii nauki. Sekts. 5, 1971. M., Nauka, 1974, 274-276. (RZhMekh, 12/74, #12B1046). (Translation)

A short summary of this paper is given containing the main historic facts together with the author's views on the importance of the problem of turbulence.

Brekovskikh, L. M. (ed). Akustika okeana (Acoustics of the ocean). Akust. in-t AN SSSR. Moskva, Izd-vo nauka, 1974, 695 p. (RZhF, 11/74, nos. 11Zh645 K - 11Zh654).

This is a collection of articles on ocean acoustics with the following breakdown:

I. Ageyeva, N. S. et al. Oceanological characteristics pertinent to ocean acoustics, pp. 5-78.

Chapter 1: Velocity and absorption of sound in the ocean. Chapter 2: The ocean bottom. Chapter 3: Sound-scattering ocean accumulations. Chapter 4: The ocean surface. Chapter 5: Internal waves. Chapter 6: Random inhomogeneities of ocean strata.

II. Brekhovskikh, L. M. Elements of the theory of an acoustical field in the ocean, pp. 79-162.

Chapter 1: Ray theory of an acoustic field in the ocean. Chapter 2: Acoustic characteristics of the surface and bottom of the ocean as plane boundaries. Chapter 3: Waveguide propagation of sound. Chapter 4: The underwater acoustic channel. Chapter 5: Anti-waveguide propagation.

III. Ageyeva, M. S. Acoustic field of a concentrated source in the ocean, pp. 163-229.

Chapter 1: Ray patterns. Chapter 2: Acoustic field of aqueous rays. Chapter 3: Acoustic field of bottom rays. Chapter 4: Experimental studies of an acoustic field in the ocean. Chapter 5: Experimental characteristics of an acoustic field.

IV. Lysanov, Yu. P. Sound scattering by uneven surfaces, pp. 231-330.

Chapter 1: Sound scattering at a surface with small-size scale roughness. Chapter 2: Sound scattering at a surface with large-scale roughness.

V. Andreyeva, I. B., and S. D. Chuprov. Reflection and scatter of sound by a disturbed sea surface, pp. 331-394.

Chapter 1: Fluctuations of a signal reflected by a disturbed ocean surface. Chapter 2: Acoustic field, retransmitted by the surface in mirror and near-mirror directions. Chapter 3: Method for experimental study of back-scatter of sound by a sea surface. Chapter 4: Experimental characteristics of surface back-scatter.

VI. Volovov, V. I., and Yu. Yu. Zhitkovskiy. Reflection and scatter of sound by the ocean bottom, pp. 395-490.

Chapter 1: Sound reflection from the ocean bottom. Experimental methods. Chapter 2: Statistical characteristics of reflected signals. Chapter 3: Relationship of characteristics of reflected signals with general relief of the bottom. Chapter 4: Frequency and angular dependences of characteristics of reflected signals. Chapter 5: Sound scatter by the ocean bottom. Chapter 6: Analysis and processing of experimental data. Chapter 7: Sound scatter in regions with a flattened-out relief. Chapter 8: Sound scatter in regions with a rough relief. Chapter 9: Determining morphometric characteristics of the ocean bottom and the effective reflection coefficient.

VII. Andreyeva, I. B. Scatter in sound-scattering ocean layers, pp. 491-558.

Chapter 1: Characteristics of sound scattering within ocean water. Chapter 2: Mechanism of sound scattering by organisms Chapter 3: Scattering of acoustic waves by a sound-scattering layer. Chapter 4: Methods of field experimental investigations. Chapter 5. Results of field measurements in the ocean.

VIII. Chuprov, S. D., and R. F. Svachko. Acoustic field in an ocean with random inhomogeneities taken into account, pp. 559-614.

Chapter 1: Scattering at random inhomogeneities and acoustic fields in the ocean. Chapter 2: Signal fluctuations during sound propagation in the ocean.

IX. Furduyev, A. V. Ocean noise, pp. 615-691.

Principal experimental and technical data on characteristics of natural noise fields in the ocean are explained. Chapter 1 contains descriptions of fields from different sources and methods of their study; it considers main characteristics of noise from thermal, industrial and biological sources and sources under an ice cover. Chapter 2. describes properties of dynamic ocean noise, examines the principal hypotheses on noise sources, and gives experimental data on distribution of noise sources in the ocean, as well as on statistical energetic characteristics of a noise field and their correlation with hydrometeorological measurement conditions.

Sturova, I. V. Wave motion, originating in a stratified fluid during flow around a submerged body. ZhPMTF, no. 6, 1974, 80-91.

Problems of two- and three-dimensional waves, excited by source and sink of equal intensity which are submerged in a density-stratified free-surface fluid, are solved in a linear formulation by the method of integral transformation. In the two-dimensional case the problem reduces to consideration of flow around a closed symmetrical oval; in the three-dimensional case - an axisymmetrical oval. The solution to the three-dimensional problem was found for a general as well as for the simplified case of a submerged body at great depth in a weakly stratified fluid. The effect of internal waves was studied by numerical analysis of the general solution in the two-dimensional case and the simplified solution in the three-dimensional case.

Numerical analysis in the two-dimensional case was performed by Simpson's method. The results showed that surface waves will be appreciable only if submergence depth is small, and their amplitude increases significantly with increase of body elongation. Although the profile of the free surface changes insignificantly in the presence of internal waves, disturbances of horizontal velocity reach maximum at the free surface. Internal waves also attenuate very slowly with depth. At body radius R = const. amplitudes of internal waves increase with body elongation almost in direct proportion, while their phases remain unchanged.

A comparison of computation using the general solution for the three-dimensional case (excluding the component describing local effects) and those using a simplified solution for a dipole showed that phases of internal waves in these cases coincide, while amplitudes differ. The author notes that the thickness of the layer in which internal waves are excited is much smaller in the three-dimensional than in two-dimensional case.

Protasov, S. N. Diurnal variation of the temperature in the surface and near-water layers of the sea and the atmosphere in the case of time-varying coefficients of turbulent heat exchange. VMU, no. 5, 1974, 619-622.

An analytical solution for diurnal variation of sea surface temperature was found, under the following assumptions: the temperature of the water and the air is defined only by vertical turbulent heat exchange, which is for both of them maximum during nighttime and minimum during daytime hours; at the surface of a uniform-density sea there occurs absorption of incident radiant flux, expenditure of heat of evaporation, outgoing radiation, and heat exchange with the atmosphere. Numerical solutions were found for diurnal variation of temperature in the surface sea layer for both time-varying and constant turbulent exchange, using experimental data obtained in the Black Sea during April 5-8, 1966.

Calculated results are shown in Figs. 1 and 2. The calculations were made using the following expressions developed by Voskanyan et al., 1970 and Voskanyan et al., 1967, respectively for the 1-8 m surface sea layer:

$$\hat{K}_1(\tau)\ [\text{cm}^2\ \text{sec}^{-1}] = 3{,}429\,(1 + 0{,}6027 \cdot \sin(\omega\tau + 0{,}5375) + 0{,}1695 \sin(2\omega\tau - 0{,}9322)), \quad (1)$$

$$I_0(\tau)\ [\text{cal cm}^{-2}\ \text{sec}^{-1}] = 8{,}37 \cdot 10^{-3}(1 + 1{,}406 \cdot \sin(\omega\tau + 4{,}582) + 0{,}3237 \sin(2\omega\tau + 1{,}276) + 0{,}1882 \cdot \sin(3\omega\tau + 1{,}164)). \quad (2)$$

and for $K_1 = 0.16\ \text{cm}^2\text{sec}^{-1}$, $C_2 = 1\ \text{cal gr}^{-1}\text{deg}^{-1}$, $C_p = 0.24\ \text{cal gr}^{-1}\text{deg}^{-1}$, $\rho_1 = 1.29 \times 10^{-3}\ \text{gr cm}^{-3}$, $\rho_2 = 1\ \text{gr cm}^{-3}$, $h_1 = 10^4\ \text{cm}$, $h_2 = 10^3\ \text{cm}$, $f_1 = 19.2^\circ\text{C}$, $f_2 = 21.2^\circ\text{C}$, $L = 590\ \text{cal gr}^{-1}$, $\mu_o = 0.7 \times 10^{-4}\ \text{deg}^{-1}$, $\mu_1 = 30\ \text{cm}^{-1}$, $R = 3.5 \times 10^{-3}\ \text{cal cm}^{-2}\ \text{sec}^{-1}$.

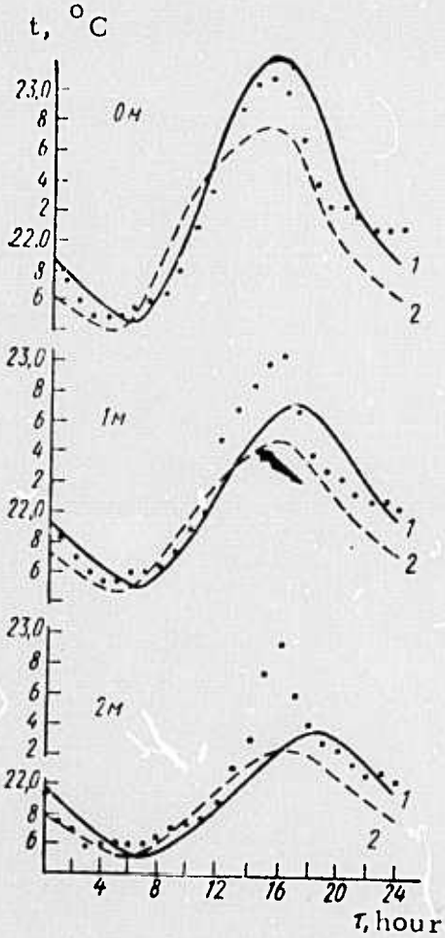

Fig. 1. Diurnal variations of water temperature at various depths for K = K(τ) (1) and K ≠ K(τ) (2). Data points after Voskanyan et al., 1967.

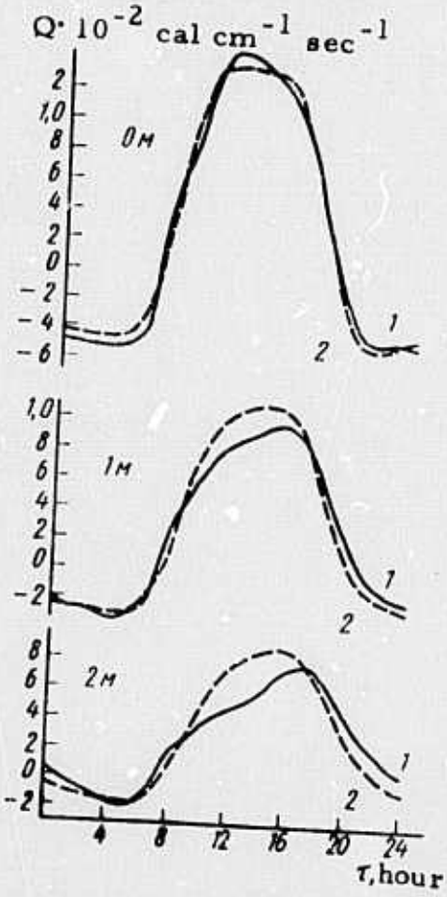

Fig. 2. Diurnal variations of heat flow at various depths for K = K(τ) (1) and K ≠ K(τ) (2).

Baum, V. A., and O. Bekmuradov. On the measurement of coefficient of turbulent diffusion. IAN Turk, no. 4, 1974, 112-113.

The authors consider theoretical aspects of the dye tracer technique for measuring coefficient of turbulent diffusion in a fluid flow.

Specifically, they examine the limitations of an approximate formula defining relative spread in dye concentration, which assumes that turbulent diffusion in the longitudinal direction is negligibly small compared to convective transfer. Since this assumption does not always hold true, the authors develop criteria which determine when longitudinal diffusion needs to be taken into account.

Bukatov, A. Ye., and L. V. Cherkesov. Effect of ice cover on internal waves in a continuously stratified sea, generated by atmospheric disturbances. Problemy Arktiki i Antarktiki, no. 43-44, 1974, 106-111.

The authors examine the effect of an ice cover on waves generated by atmospheric excitation, in a sea with stratified density. An analytical solution is found in a linear approximation for the following model of density and atmospheric pressure:

$$\rho(z) = \begin{cases} \rho_0 = \text{const} & \text{при } z_1 \leqslant z \leqslant 0 \\ \rho_0 \exp[-k(z - z_1)] & \text{при } z_2 \leqslant z \leqslant z_1 \\ \rho_0 \exp[-k(z - z_2)] & \text{при } -H \leqslant z \leqslant z_2, \end{cases} \tag{1}$$

$$p_0 = af(x, y)\cos \sigma t. \tag{2}$$

where $z_1 = -H_1$, $z_2 = -(H_1 + H_2)$.
A numerical solution was found for

$$f(x) = \begin{cases} \cos^2 \frac{\pi x}{2l} & \text{при } |x| \leqslant l \\ 0 & \text{при } |x| > l \end{cases} \tag{3}$$

and $H_1 = 20$ m, $H_2 = 60$ m, $H_3 = 2 \cdot 10^3$ m, $l = 10^5$ m, $E = 3 \cdot 10^7$ n/m^2, $\gamma = 0.34$, $\rho_1 = 870$ kg/m^3, $O_m \leq h \leq 5$ m, 4.5×10^{-2} s^{-1} $\leq \sigma \leq 7 \times 10^{-1}$ s^{-1}, $O \leq \epsilon = kH_2 \leq 10^{-2}$.

It was found that pressure p_o generates only one progressive undamped wave in an ice-covered, continuously stratified sea when $\sigma^2 > kg$ and $\sigma > 2\omega$ (2ω is the Coriolis parameter). This wave is an ordinary surface wave whose amplitude attenuates with depth. Density stratification affects wave motion only weakly, either in water or ice. The effect of an ice cover depends on its characteristics and oscillation frequency σ (see Table 1).

Table 1

Phase velocity ν, m/s	Wave length λ, m	Ice thickness h, m	σ x 10
48.23	1514	5	2
48.53	1524	3	2
49.04	1539	0	2
32.25	675.2	5	3
31.03	672.0	3	3
32.69	684.5	0	3
27.27	285.4	5	6
21.86	228.8	3	6
16.35	171.1	0	6

However, at $2\omega < \sigma < (kg)^{1/2}$ the pressure p_o generates a superposition of an infinite spectrum of undamped waves. The zero harmonic is also an ordinary surface wave attenuating with depth and weakly affected by ice cover and density stratification. Harmonics with $n \geq 1$ are internal waves whose $v_n \to 0$, $\lambda_n \to 0$ when $n \to \infty$. These waves do not depend on characteristics of the ice cover, while they increase substantially with ϵ.

As far as the wave amplitude is concerned, it is not affected by ice cover, while density stratification affects essentially its depth dependence. Depth dependence of the amplitude of the horizontal velocity component is illustrated in Fig. 1 and Table 2.

Table 2

$\epsilon \cdot 10^3$	$\overline{B}(0)$	$\overline{B}(z_2)$
0	6,97	6,97
2	166,00	11,70
5	251,00	13,70

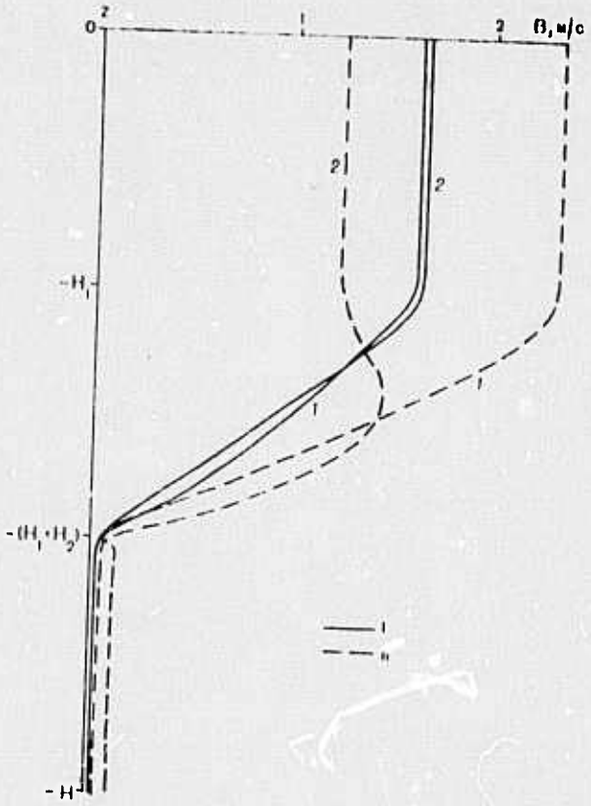

Fig. 1. Depth dependence of the amplitude of horizontal velocity component.

1 - $\sigma = 2.9 \times 10^{-4}$ s^{-1}; 2 - $\sigma = 1.45 \times 10^{-4}$ s^{-1}; I - $\epsilon = 2 \times 10^{-3}$; II - $\epsilon = 5 \times 10^{-3}$.

Kirichek, A. D., and Yu. D. Mikhaylov. Results of an experiment with luminescent tracer in studying turbulent diffusion in the sea. Trudy GOIN, no. 122, 1974, 79-89.

An experiment with an instantaneous source of tracer was conducted in the southeast portion of the Baltic Sea on July 14-15, 1972 on board the R/V's Okeanograf and Yurate. The experimental process is described in detail.

The following are the main results obtained:

1. The coefficient of horizontal turbulence K_ℓ ranges from 10^{-4} to 10^{-5} cm^2/sec. The dependence of K_ℓ on the turbulence scale ℓ can be satisfactorily approximated by a 3/4 power law, as seen in Fig. 1.

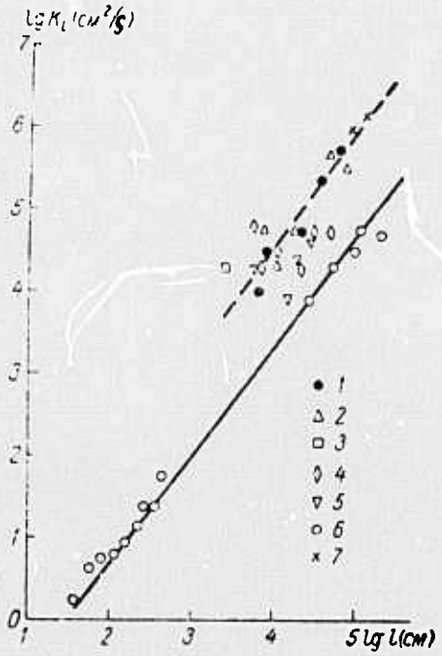

Fig. 1. Dependence of coefficient of horizontal turbulence on turbulence scale.

1-5 - present experiments; 6 - after Ozmidov, 1968; 7 - estimated from dissipation of turbulent energy.

2. The dissipation rate of tracer concentration at the center of the tracer patch depends strongly on hydrological conditions. Its time dependence can be approximated by a power law with exponent in the range of 0.9-3.5.

3. The maximum depth of tracer penetration does not exceed 10 m. The penetration depth coincides with the upper boundary of the seasonal thermocline, and corresponds to an approximate depth of wind mixing ($\sim$ 13 m).

The results obtained made it possible to hypothesize the existence of a thin surface layer with circulation cells which are apparently elements of vortices with horizontal axes. A hypothetical scheme of coastal circulation, based on present results and additional data on temperature, salinity, and flow at different water levels, as well as on wind conditions, is shown in Fig. 2.

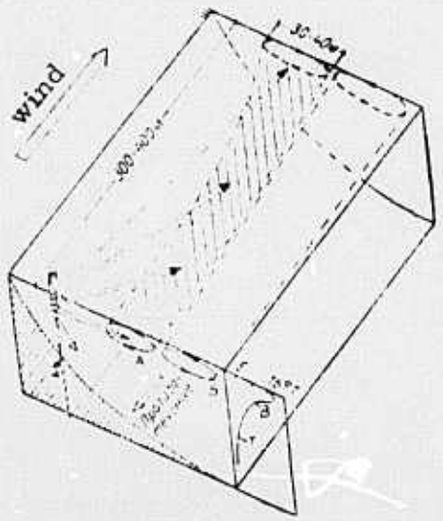

Fig. 2. Hypothetical scheme of water circulation in the coastal region, from experimental data.

A - tracer patch 1-2 hours after release; Б - undercurrent; B - vortex with horizontal axis; Г - Ekman spiral.

Davidan, I. N., T. A. Pasechnik, and V. A. Rozhkov. Determining components of the equation of wave energy balance in spectral form, and some model calculations of probability characteristics of wind waves. Trudy GOIN, no. 122, 1974, 59-78.

The authors develop expressions describing the generation and propagation of wind waves. The problem is attacked through a wave

energy balance equation in spectral form:

$$\frac{DS}{Dt} \equiv \frac{\partial S}{\partial t} + v_x \frac{\partial S}{\partial x} + v_y \frac{\partial S}{\partial y} + k_x' \frac{\partial S}{\partial k_x} + k_y' \frac{\partial S}{\partial k_y} = \mathfrak{S}, \tag{1}$$

The equation is solved analytically as well as numerically, using experimental data obtained in the Atlantic Ocean west of the Iberian Peninsula (see Table 1, Fig. 1).

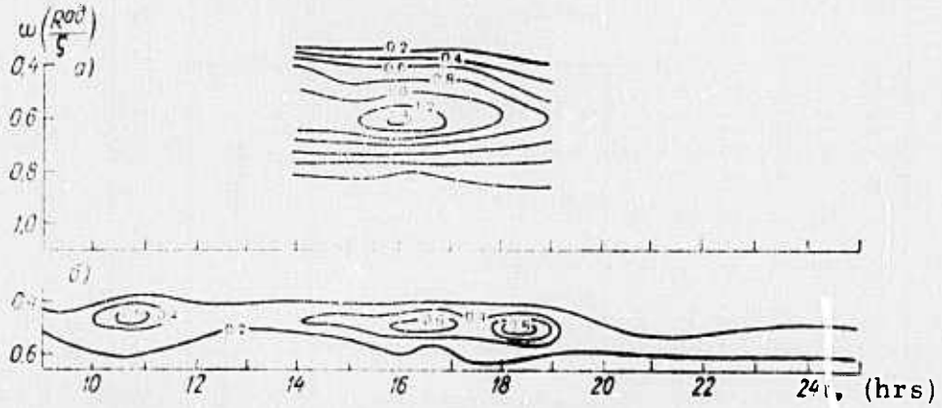

Fig. 1. Spectral density $S(\omega, t)$ (m^2 sec) for wind waves observed by the R/V's Okeanograf (a) and Aysberg (b) in 1969.

The source function $\mathfrak{S} = \mathfrak{S}(x, y, t, \omega, \theta)$ was determined using approximations for spatial spectra of ocean wind waves based on experimental data (Davidan et al., 1971; Davidan, 1967) for two cases: a stationary inhomogeneous process for which case Eq. (1) takes the form

$$\frac{\partial S}{\partial t} = \mathfrak{S}(S), \tag{2}$$

and a nonstationary homogeneous process, for which case

$$\mathfrak{S} = \sum_{i=1}^{7} \mathfrak{S}_i + \sum_{i=1}^{4} \mathfrak{S}_i'. \tag{3}$$

The results of calculations are shown in Fig. 2. It was shown that the source function can be sufficiently well approximated by a 4th order polynomial whose coefficients are functions of V, ω, and θ.

Table 1

Wind conditions and statistical characteristics of sea waves in the Atlantic Ocean on October 8, 1969

Time, hour	R/V "Aysberg"											R/V "Okeanograf"							
	Wind		Visual obs.							Instr. obs.		Wind		Visual obs.				Instr. obs.	
			ww	swell I			swell II							ww	swell				
	Velocity, m/s	Direction, °	Height, m	Flight, m	Period, sec	Direction, °	Height, m	Period, sec	Direction, °	Dispersion, m^2	Frequency at spectr. peak, rad/sec	Velocity, m/s	Direction, °	Height, m	Flight, m	Period, sec	Direction, °	Dispersion, m^2	Frequency at spectr. peak, rad/sec
09	5.8	130	0.5	2	12.5	320	1.5	10	260	0.12	0.48	0	-	0	1.5	8	280	0.26	0.48
12	3.7	130	0.25	2	14	310	1.5	11	260	0.10	0.48	0	-	0	2.0	12	280	-	-
15	1.2	180	0.25	2	13	300	1.5	10	260	0.15	0.48	3.0	160	0.25	3.0	14	280	0.45	0.51
18	0	-	0	2	13	300	1	10	260	0.25	0.49	6.0	210	1.0	3.0	14	280	0.29	0.54
21	1.0	80	0	2	13	300	-	-	-	0.14	0.55	2.0	160	0.25	2.0	12	280	-	-
24	1.6	130	0	1.5	13	300	-	-	-	0.14	0.51	6.0	160	1.0	2.0	-	250	-	-

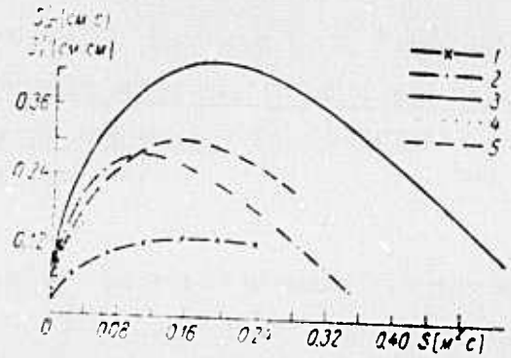

Fig. 2. Source function for a stationary inhomogeneous (1, 2, 3) and nonstationary homogeneous (4, 5) process.

1 - V = 10 m/sec, $\theta = O^{\circ}$, w = 0.9 rad/sec; 2 - 14, 20, 0.9; 3 - 14, 0, 0.9; 4 - 10, 0, 1.5; 5 - 10, 0, 0.9.

Analytical solutions of Eq. (1) were found for a dead swell and for waves in deep water generated by a uniformly steady wind. Numerical solutions to Eq. (1) were then found, using the approximation of a two-layered differential scheme. Experimental data were modeled in three variants: a) in accordance with the analytical solution for a dead swell, assuming that energy propagates in one direction only; b) in accordance with the analytical solution for a dead swell and an empirical expression for angular distribution of wave energy (Davidan et al., 1971); and c) in accordance with Eq. (1), where the right side of the equation is taken after Barnett, 1968.

It is concluded that results of the calculations suggest good prospects for study of ocean waves on the basis of numerical integration of Eq. (1).

(Note: This is an expanded treatment of the same article reported earlier (Sov. Mat'l. on Int. W. Eff., no. 3, 1975, 61).

Davidan, I. N., and L. I. Lopatukhin.
Wind and wave distribution patterns in oceans and seas. Trudy GOIN, no. 122, 1974, 108-123.

A study was made of wind velocity and wave height distribution in the North Atlantic Ocean and its marginal seas, as well as of accuracy of visual observations on these parameters aboard commercial ships. The large volume of data used came from U. S., German and Soviet sources.

It was found that the parameter γ in the Weibull distribution, as well as median wind velocity evaluated from visual observations, are lower than corresponding values from instrumental data by 0.3 and 0.2-1.3 m/s respectively. The analysis of the relationship between visually and instrumentally estimated wave height was reduced to finding $f(h_{3\%})/h_{vis}$, where $h_{3\%}$ is the 3% - quartile of the measured wave height distribution and h_{vis} is visually observed height of a prevailing wave system. The results of the analysis are shown in Fig. 1. The best approximation of the regression line in Fig. 1 is in the form $y = ax^b$.

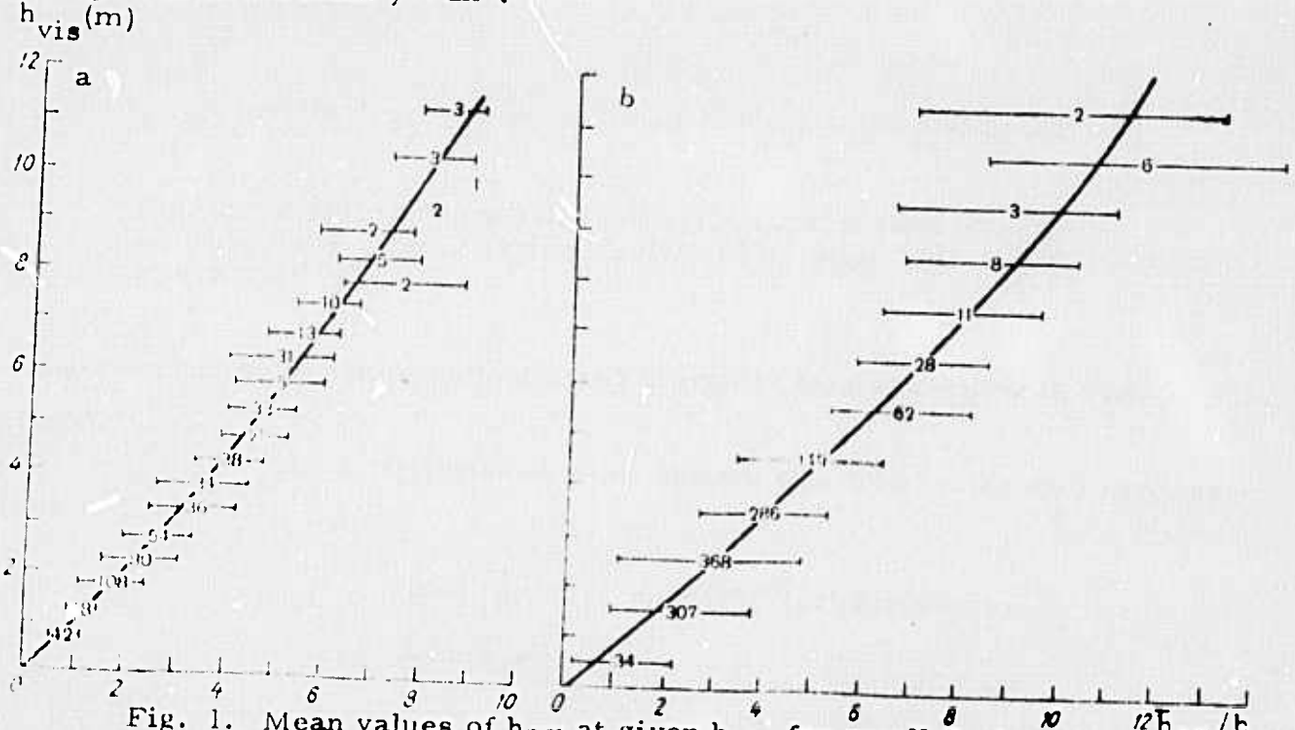

Fig. 1. Mean values of $h_{3\%}$ at given h_{vis} for small Soviet (a) and medium and large Soviet and foreign ships (b).

An analysis of wind velocity distribution revealed a close relationship between its deviation (in the ranges of very small and very high probabilities) from the Weibull distribution and parameter γ of the Weibull distribution, as shown in Fig. 2. The parameters of the Weibull

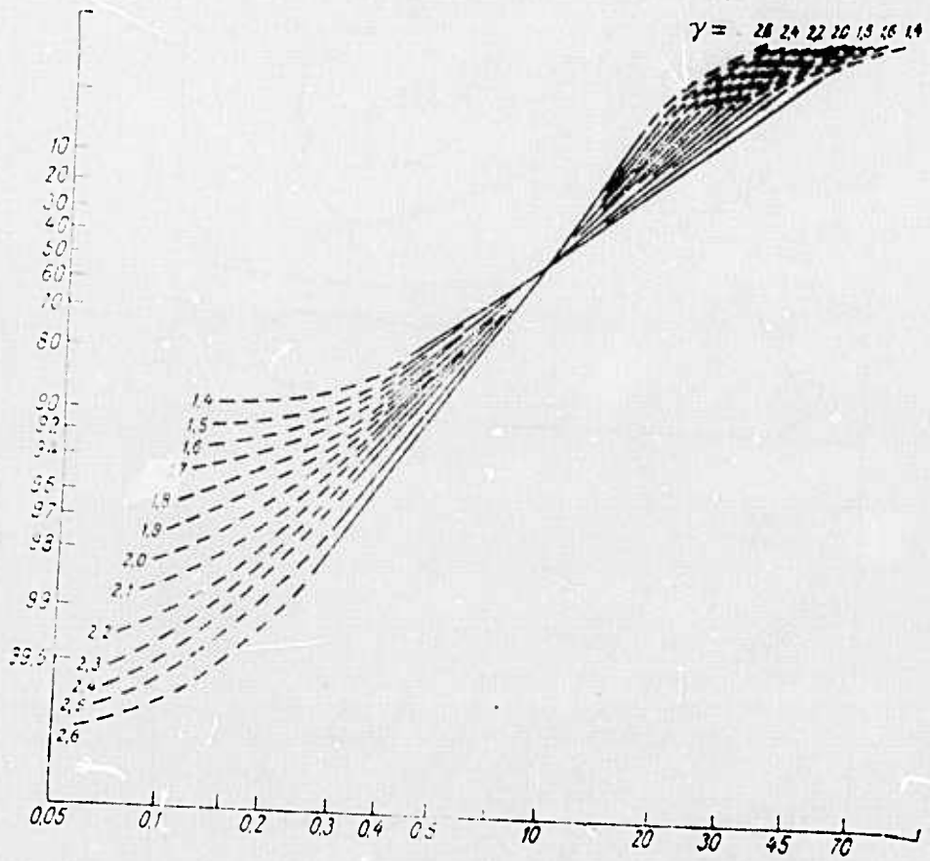

Fig. 2. Family of normalized distributions of wind velocity for various γ (linear segments defined by $F(v) = \exp\left[-\left(\frac{v}{\beta}\right)^{\gamma}\right]$, where $\alpha = 0.693$)

distribution for the North Atlantic and marginal seas are shown in Fig. 3.

The distribution of wave heights was found to be well expressed by

$$F(h^*) = \begin{cases} \frac{s}{\sqrt{2\pi}} \int_{\cdot}^{\infty} \frac{1}{h^*} \exp\left[-\frac{1}{2}\ln^2 (h^*)^{-s}\right] dh^* & \text{for } h^* \geq 1.0 \\ \exp\left[-a(h^*)^2\right] & \text{for } h^* \leq 1.0 \end{cases} \quad (1)$$

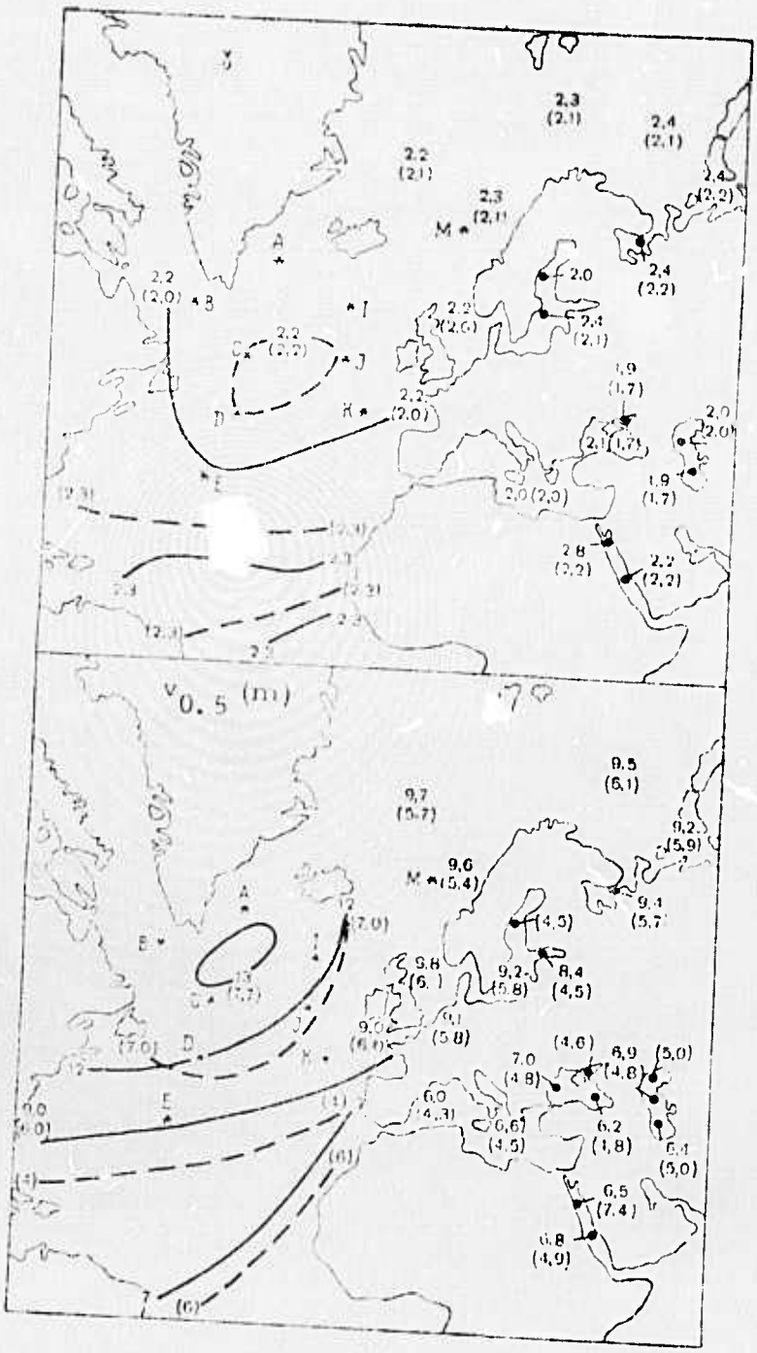

Fig. 3. Distribution of γ and $v_{0.5}$ for the North Atlantic and marginal seas.

solid lines - winter
dashed lines and bracketed figures - summer

where $s = 1/\sigma$, and $h^* = h/h_{0.5}$. The parameters of the log-normal distribution of wave heights for the North Atlantic and its marginal seas are shown in Fig. 4.

Reproduced from
best available copy.

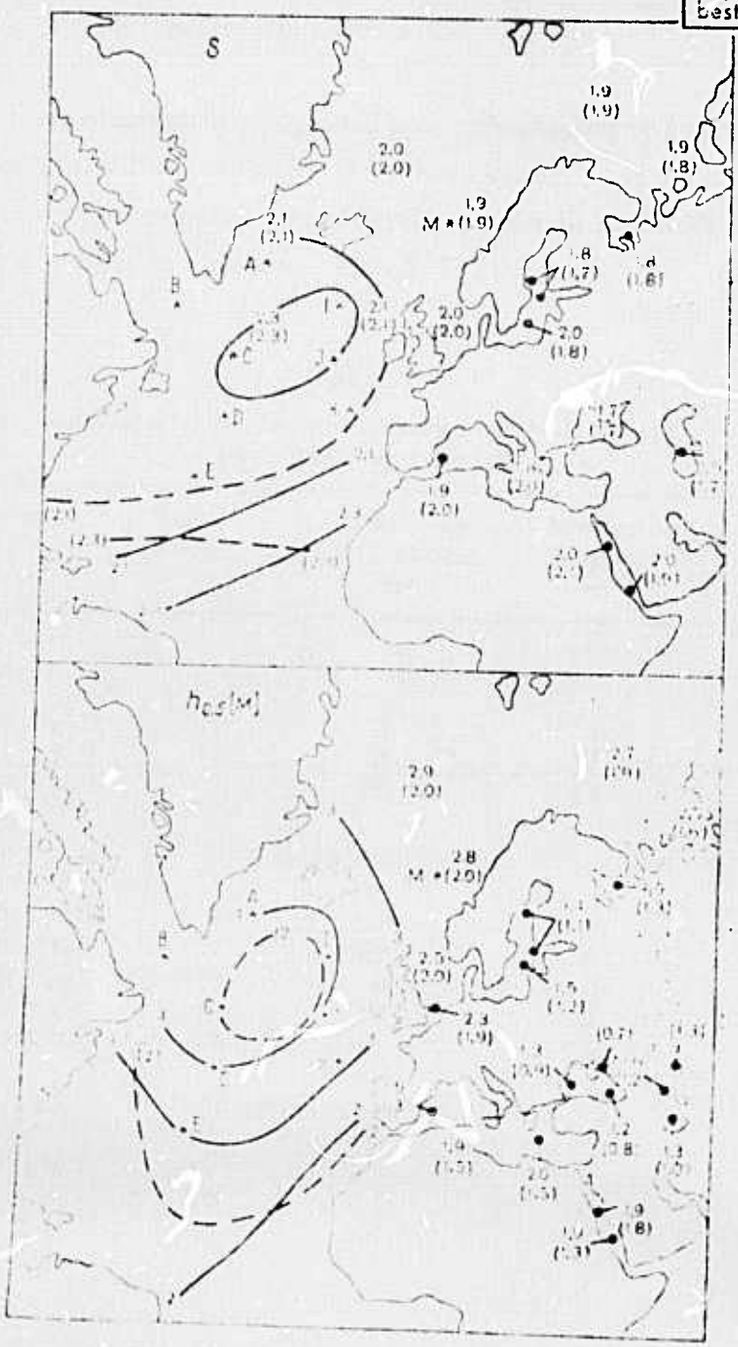

Fig. 4. Distribution of s and $h_{0.5}$ for the North Atlantic and marginal seas.

solid lines - winter; dashed lines and bracketed figures - summer.

Mikhaylov, Yu. D. Statistical characteristics of the turbulent field of flow velocity, and their evaluation in the coastal zone of the Baltic Sea. Trudy GOIN, no. 122, 1974, 90-107.

A method is proposed for calculating the parameters of turbulent flow from flow velocity field measured by the self-contained BPV-2 current meter. The results of calculations made for different regions of the Baltic Sea are shown in Tables 1-6 and Figs. 1-4.

Table 1

Change of turbulent energy with distance off shore and depth

Observation period	Sea depth, m	Distance off shore, km	Water depth, m	$\overline{u'^2} = \int_0^\infty S_u(\omega)d\omega$, $cm^2 s^{-2}$
		Narva Bay		
10/20 - 11/06 1968	10	2	5	49
10/23 - 11/21 1968	16	8	11	26
09/13 - 10/17 1968	40	20	14	24
		Northeastern Baltic		
10/09 - 10/26 1968	8	2	5	77
06/23 - 07/06 1963	17	12	6	47
06/23 - 07/05 1963	19	18	10	44
06/08 - 06/25 1969	42	24	14	41
10/10 - 10/30 1968	87	45	5	19
		Northeastern Baltic		
10/15 - 10/31 1967	87	65	14	27
"	87	65	60	41
"	87	65	80	55

Table 2

Region	ϵ, $cm^2\ s^{-3}$	$\bar{\epsilon}$, $cm^2\ sec^{-3}$
Northeastern Baltic	1.8×10^{-5} - 6.1×10^{-4}	2.0×10^{-4}
Southeastern Baltic	6.4×10^{-5} - 7.4×10^{-4}	2.7×10^{-4}
Gulf of Riga	1.2×10^{-4} - 9.2×10^{-4}	4.1×10^{-4}
Gulf of Finland (west)	4.4×10^{-4} - 2.2×10^{-3}	3.7×10^{-3}
Gulf of Finland (east)	6.1×10^{-4} - 1.8×10^{-3}	1.2×10^{-3}

Note: $\epsilon = \frac{|D(\bar{u}t_2) - D(\bar{u}t_1)|^3}{2^{3/2}|(\bar{u}t_2)^{3/2} - (\bar{u}t_1)^{3/2}|^2}$.

Table 3

Change of ϵ with distance off shore and depth

Observation period	Sea depth, m	Distance offshore, km	Water depth, m	ϵ, $cm^2 \cdot s^{-3}$
		Narva Bay		
10/20 - 11/06 1968	10	2	5	3×10^{-4}
10/23 - 11/21 1968	16	8	11	6.7×10^{-5}
09/23 - 10/17 1968	40	20	14	5.6×10^{-5}
		Northeastern Baltic		
10/05 - 10/31 1967	87	65	14	2.8×10^{-4}
"	87	65	60	4.2×10^{-4}
"	87	65	80	1.6×10^{-3}

Table 4

Region	K_ℓ, $cm^2\ s^{-1}$	$\bar{K}_\ell$, $cm^2\ s^{-1}$
Northeastern Baltic	2.4×10^6 - 1.5×10^7	6.0×10^6
Southeastern Baltic	1.1×10^6 - 3.5×10^6	2.0×10^6
Gulf of Riga	1.4×10^6 - 3.0×10^6	2.0×10^6
Gulf of Finland (west)	9.7×10^5 - 1.0×10^7	3.9×10^6
Gulf of Finland (east)	4.9×10^5 - 9.8×10^5	7.3×10^5

Note: $K_\ell = \frac{(\overline{u'})^2}{\varepsilon}$

Table 5

Region	τ_L, h	$\bar{\tau}_L$, h	S, km	$\bar{S}$, km
Northeastern Baltic	25.0 - 106.0	43.3	7.2 - 69.3	24.3
Southeastern Baltic	22.1 - 65.2	33.3	4.8 - 16.4	9.0
Gulf of Riga	13.3 - 44.0	23.8	1.1 - 8.0	5.5
Gulf of Finland (west)	8.3 - 44.4	29.1	1.2 - 24.5	10.8
Gulf of Finland (east)	7.9 - 9.7	8.8	0.8 - 0.9	0.8

Note: $\tau_L = \frac{\overline{u'^2}}{\varepsilon}$, $S = \bar{u}\frac{\overline{u'^2}}{\varepsilon}$,

Table 6

Change of τ_L with distance off shore and depth

Observation period	Sea depth, m	Distance offshore, km	Water depth, m	τ_L, h
		Narva Bay		
10/20 - 11/06 1968	10	2	5	44
10/23 - 11/21 1968	16	8	11	109
10/23 - 17/10 1968	40	20	14	117
		Northeastern Baltic		
10/05 - 10/31 1967	87	65	14	25
"	87	65	60	27
"	87	65	80	10

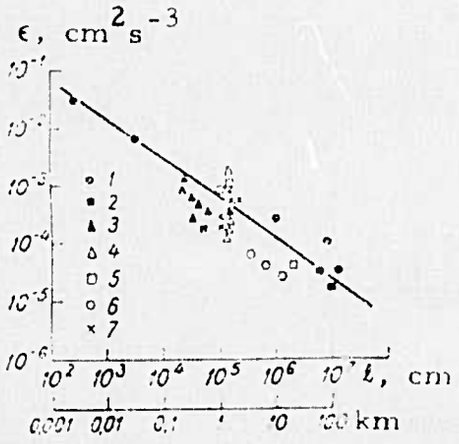

Fig. 1. Dependence of ϵ on turbulence scale.

1- Nan'niti; 2- Ozmidov and Okubo (5-14 m layer); 3- Gulf of Finland (east); 4- Southeastern Baltic; 5- Northeastern Baltic; 6- Gulf of Finland (west); 7- Gulf of Riga.

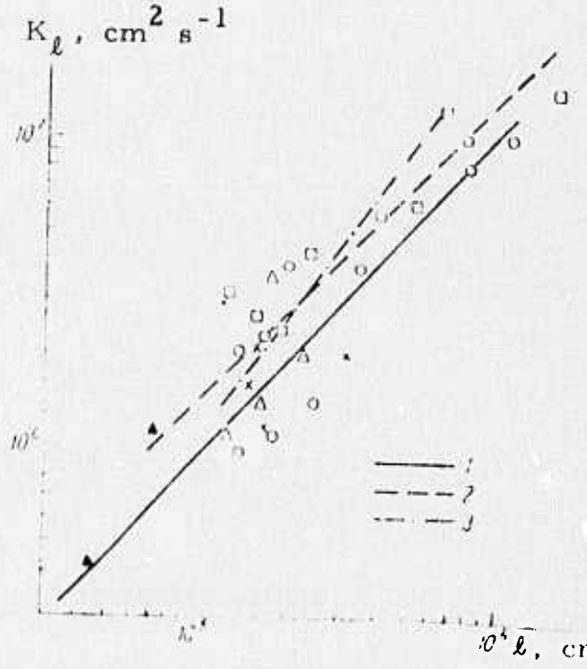

Fig. 2. Dependence of K_ℓ on turbulence scale.

1- offshore distance 1-10 km; 2- 10 to 20 km; 3- 20 to 65 km.

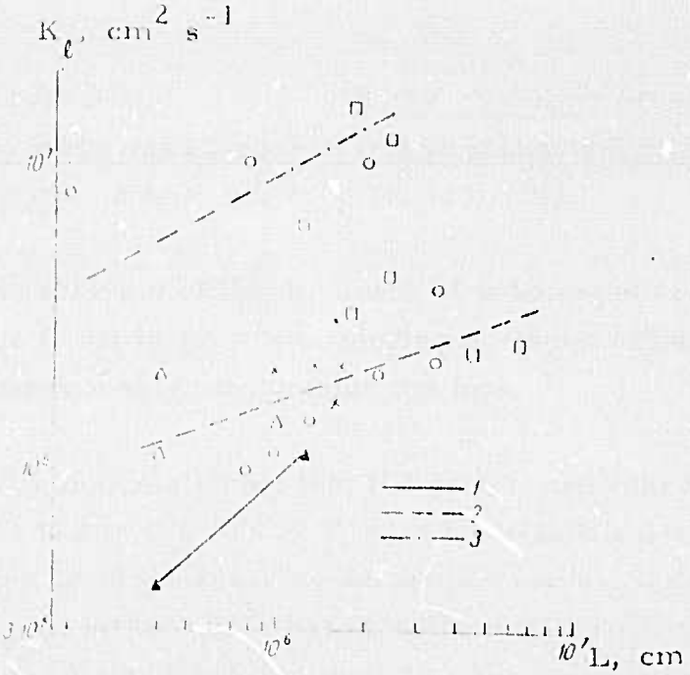

Fig. 3. Dependence of K_ℓ on offshore distance.

1 - turbulence scale 0.2 - 1 km; 2 - 1-4 km; 3 - 4-10 km. Designations as in Fig. 2.

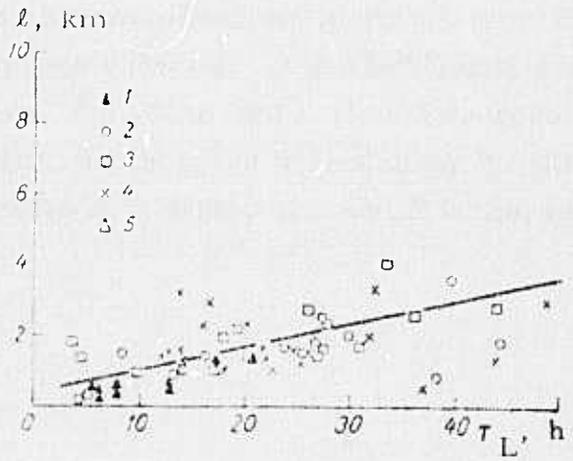

Fig. 4. Dependence of vortex life time τ_L on its size.

Designations as in Fig. 2.

Chashechkin, Yu. D. On the characteristics of submerged turbulent jets in inhomogeneous fluids. FAiO, no. 6, 1974, 1331-1333.

An analysis of the dynamics of submerged turbulent jets in inhomogeneous fluids is given, considering horizontal flows for the case of equal fluid density inside and outside the jets.

The analysis shows that if $Re \gg 1$, internal Froude number $F \gg 1$, and scale factor $C = \Lambda/d \gg 1$, then the stratification effect in the initial stage of the development of turbulent jets can be neglected. Estimates of $Re_c(x)$ and $F_c(x)$ at $Re > 10^5$, based on the self-similar solution of the equation of motion (Birkhof and Sarantonello) are given in the table.

The development of turbulent jets in stably stratified fluids is characterized by collapse - limited growth of their vertical dimension, which occurs before turbulence degeneration within the jets. Characteristics of geometrically similar turbulent jets in stably stratified fluids coincide if their F and C numbers coincide. If the similarity criterion with respect to C is to be satisfied, $\Lambda = (d\ell n\rho/dz)^{-1}$ should decrease with a decrease of jet size, which leads to an increase in frequency N. Similarity will occur if the jet size decreases by a factor of n and N increases by a factor of $\sqrt{n}$.

Reproduced from best available copy.

Table I

	Two-dimensional jet	Three-dimensional jet	Two-dimensional jet	Three-dimensional jet	Wake with zero excess pulse		Mixing zone
					Three-dimensional	Two-dimensional	
$L(x)$	x	x	$x^{1/2}$	$x^{1/3}$	$x^{1/5}$	$x^{1/4}$	x
$U(x)$	$x^{-1/2}$	x^{-1}	$x^{-1/2}$	$x^{-2/3}$	$x^{-4/5}$	$x^{-3/4}$	x^{o}
$Re_c(x)$	$x^{1/2}$	x^{o}	x^{o}	$x^{-1/3}$	$x^{-3/5}$	$x^{-1/2}$	x
$F_c(x)$	x	x^{4}	x^{-2}	x^{-2}	x^{-2}	x^{-2}	x^{-2}

Note: L(x) and U(x) after Birkhof and Sarantonello

2. Surface Effects

Zagorodnikov, A. A. Relationship between the parameters of the Doppler spectrum of a radar signal reflected from the sea surface and spatial characteristics of the sea waves. RiE, no. 2, 1975, 288-292.

A mathematical correlation is derived for measuring the three-dimensional spectrum $S_M(k, \theta, \varphi)$ of sea wave orbital velocity V_r (x, y, t) and wave height group distribution. The analysis assumes that the spatial fluctuation of the first and second moments of Doppler frequency f_D (x, y, t) of the reflected radar signal is known.

The S_M spectrum is given in polar coordinates k, θ, φ where k is wave number, cos θ is the wave propagation direction, and φ is the angle of transmitted beam direction to the x-axis (x and y are the Cartesian coordinates of the resolution area). The instantaneous distribution of V_r (x, y) components over a sea surface, and spatial characteristics of the sea waves, can be determined from Doppler characteristics of the signal, since the time Δt of radar return differs by 1 to 2 orders of magnitude from the correlation interval ΔT of sea wave profile fluctuations, i. e. during time Δt, the large-scale wave profile remains effectively unchanged (frozen).

The first moment $M[f_D (x, y, t)]$ is correlated with the radial velocity of a sea surface layer on the basis of the relation $f_D(x, y, t) = 2V_r (x, y, t)/\lambda$ using a procedure analogous to that described earlier by the author (RiE, no. 3, 1972, 477). In final integral form, the spatial correlation function R_m of a field of the $M[f_D (x, y)]$ random values is given as

$$R_m(r, \alpha) = \frac{4}{\lambda^2} \int_0^{\infty} \int_{-\pi}^{\pi} K g S_z(K, 0) S_\sigma(K, 0) (\cos^2\theta \cos^2\psi_0 + \sin^2\psi_0) \times$$
$$\times \cos[Kr\cos(\theta - \alpha)] dK d\theta; \qquad (1)$$
$$S_\sigma(K, \theta) = \exp(-h_x^2 K^2 \cos^2\theta - h_y^2 K^2 \sin^2\theta).$$

Here ρ and α are polar coordinates on the sea surface, r is the correlation coefficient, g is gravity acceleration, ψ_o is the glancing angle, $S_z(k, \theta)$ is the two-dimensional sea wave spectrum, and $S_G(k, \theta)$ is the frequency response of a two-dimensional filter represented by the resolution area. The function $R_m(r, \alpha)$ is the Fourier cosine transform of $S_Z(k, \theta)$ and $S_G(k, \theta)$. Hence the spectrum of the field of average f_D spatial fluctuations is determined by the relation

$$S_M(K, \theta, \varphi) = \frac{4}{\lambda^2} KgS_z(K, \theta) S_G(K, \theta - \varphi) [\cos^2(\theta - \varphi)\cos^2\psi_0 + \sin^2\psi_0]. \quad (2)$$

For high spatial resolution, when linear dimesnion of resolution area $D \leq (0.1\text{-}0.2)\Lambda$ (Λ is the average sea wave length), the spectrum $S_{V_z}(k, \theta)$ of the vertical component of V_r (1) and $S_Z(k, \theta)$ can be determined as the sum of two spectra of the average f_D field at mutually perpendicular irradiation directions:

$$S_{V_Z}(K, \theta) = KgS_Z(K, \theta) = \frac{\lambda^2}{4}\left[\frac{S_{V_P}(K, \theta, \varphi) + S_{V_P}\left(K, \theta, \varphi + \frac{\pi}{2}\right)}{1 + \sin^2\psi_0}\right]$$
$$S_z(K, \theta) = (Kg)^{-1} S_{V_Z}(K, \theta). \quad (3)$$

To simplify calculations, the one-dimensional spectrum $S_M(\nu, \varphi)$ of a radar return from the φ direction is substituted for the two-dimensional $S_M(k, \theta, \varphi)$ spectrum (2), by substituting the variables $\{\nu/|\cos(\theta - \varphi)|; \theta\}$ for $\{K, \theta\}$, and integrating over all θ directions.

Two practically important cases are analyzed for small glancing angles ($\cos\psi_o \cong 1$, $\sin\psi_o \cong 0$). In the case of a high spatial resolution of the radar in all directions,

$$S_G(K, \theta) \simeq 1; \quad S_M(\nu, \varphi) = \frac{4}{\lambda^2}\int_{\pi} \nu g S_z\left[\frac{\nu}{|\cos(\theta - \varphi)|}; \theta\right] d\theta. \quad (4)$$

In the case of high resolution in the longitudinal direction only,

$$D_{(\text{transv})} \gg \Lambda; \quad S_G(K, \theta - \varphi) \simeq \delta(\theta - \varphi);$$
$$S_M(\nu, \varphi) = \frac{4}{\lambda^2} \nu g S_z(\nu, \theta - \varphi). \quad (5)$$

In the latter case, $S_M(\nu, \varphi)$ which is proportional to $M[f_D(\rho, \varphi)]$ is equal, when corrected with a constant, to the cross-section of the two-dimensional spectrum of vertical component V_r in the direction of observation. The two-dimensional spectrum of V_r can be plotted from the cross-sections obtained from different φ directions; the two-dimensional spectrum of sea wave profile is then derived from the V_r spectrum.

Analogous but more complex correlations can be derived for spatial fluctuations of dispersion and spectral width of a signal. Evaluation of the group structure of sea waves is simpler, if the cited parameters are used. The 0.5-level width of the Doppler spectrum can be expressed through dispersion of the sea wave slope heights or through the average height $\bar{h}$ as

$$\Delta f_{0.5} = 0{,}415\sqrt{(gh)}\, B(D/\Lambda) F(m, \alpha, \psi_0); \quad \bar{h}^2 = 2\pi\sigma_z^2. \tag{6}$$

where m is a dimensionless factor.

Wave heights at the minimum of a group envelope may differ from h at the maximum by a factor of 3 to 7. The width $\Delta f_{0.5}$ is close to maximum, when dimensions of resolution area and average wave length are commensurate, e.g., $\Delta f_{0.5} = 0.97 f_{0.5\,max}$ at $\overline{D/\Lambda} = 1.2$.

It is recommended to average the visible wave heights because of the randomness of a wave profile. For example, given a sinusoidal wave profile, the ratio of visible height to the rms value of wave profile is equal to $2\sqrt{2}$, or nearly equal to $\sqrt{2\pi} = h/\sigma_z$ for a random profile with Rayleigh distribution of wave heights. Fluctuations of wave heights in a group of waves can be evaluated from spectral width fluctuations by shifting the resolution area along a cross-section of sea surface (Fig. 1).

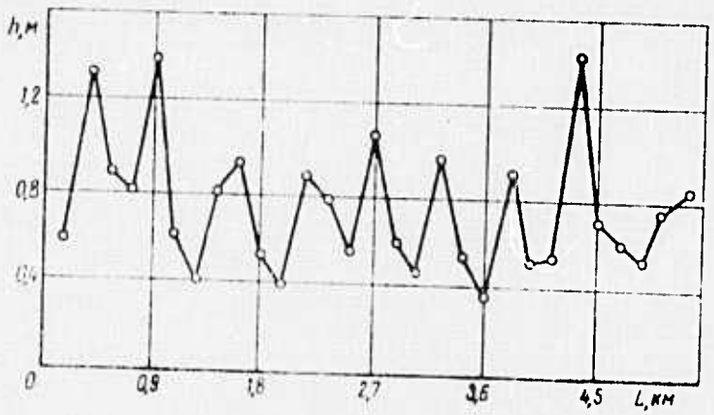

Fig. 1. Wave height envelope measured with an airborne Doppler radar wave recorder in sea waves with a group structure.

Similar data were obtained in parallel measurements with contact-type recorders. The author notes that the peak wave heights in a group also exhibit a group structure.

Zagorodnikov, A. A. Determining spectral characteristics of sea waves by analyzing the one-dimensional spatial spectrum of a radar signal. Morsk. gidrofiz. issled., no. 3(62), 1973, 140-154.

Mathematical proof is obtained that a radar must be considered as a two-dimensional filter of spatial frequencies in determining the spatial structure of a sea surface from its radar image.

The two-dimensional spatial spectrum of a radar image of a wavy sea surface is expressed as

$$S_Q(u_1; u_2) = S_F S_G S_H S_N = S_F S_N \quad (1)$$

where u_1, u_2 are the coordinates in the wave number plane, which are parallel to x_1, x_2 (y_1, y_2) axes, respectively; S_F and S_G are Fourier transforms of the echo pulse characteristic $F(x_1, x_2)$ and the pulse transient characteristic $G(x_1, x_2)$ of the resolution area; and $S_H(u_1, u_2)$, $S_N(u_1, u_2)$ and $S_W(u_1, u_2)$ are the space-frequency characteristics of the receiver-indicator circuitry, the beam spot, and the entire radar system respectively. The energy spectra S_Q and S_Q^P of the radar image for fundamental and cross-polarization signals are given by

$$\bar{S}_q : \bar{S}_q^n = S_q \cdot S_q^* = u_{1,2}^2 \bar{S}_z \bar{S}_W = u_{1,2}^2 \bar{S}_z \cdot \bar{S}_a \cdot \bar{S}_H \cdot \bar{S}_N . \tag{2}$$

where $\bar{S}_z = S_z \cdot S_z^*$, etc., (* denotes complex conjugate) in which S_z is the spectrum of the sea profile. Equations (1) and (2) show that $S_Q(u_1, u_2)$ depends on both $S_Z(u_1, u_2)$ and $S_W(u_1, u_2)$ of the entire radar circuit, the radar playing the role of a spatial two-dimensional filter.

To simplify the practical solution, various spectral characteristics of sea waves may be derived from statistical analysis of the one-dimensional spatial spectrum of the radar signal. The formulas

$$\begin{aligned}
&L_q(\xi);\ L_q^n(\xi) = \int_{-\infty}^{+\infty}\int u_{1,2}^2 S_z S_W \cos u_1 \xi \, du_1 du_2 ; \\
&S_q(u_1);\ S_q^n(u_1) = \int_{-\infty}^{+\infty} u_{1,2}^2 S_z S_W \, du_2 ; \\
&L_q(\eta);\ L_q^n(\eta) = \int_{-\infty}^{+\infty}\int u_{1,2}^2 S_z S_W \cos u_2 \eta \, du_1 du_2 ; \\
&S_q(u_2);\ S_q^n(u_2) = \int_{-\infty}^{+\infty} u_{1,2}^2 S_z S_W \, du_1 .
\end{aligned} \tag{3}$$

of one-dimensional correlation functions $L_Q(\xi)$, $L_Q^P(\xi)$, $L_Q(\eta)$, $L_Q^P(\eta)$ and spectra $S_Q(u_1)$, $S_Q^P(u_1)$, $S_Q(u_2)$, $S_Q^P(u_2)$ are derived from the corresponding formulas of the spatial temporal correlation functions $L_Q(\xi, \eta, \tau)$. The

latter take into account the increments ξ and η in radar signal level due to shifting of the observation point and wind wave components during time τ of image realization. Eqs. (3) indicate that filtering effects of the receiver-indicator circuit and the imaging system of the radar must be taken into account in evaluation of sea wave characteristics. The possibility is shown of deriving from (3) such characteristics as one-dimensional sea wave spectra in a random direction, and cross-sections of two-dimensional sea wave spectra, in three particular cases. Furthermore, the coefficient m of sea wave three-dimensionality can be determined by analyzing one-dimensional spectra of the radar signal. For simplicity, the one-dimensional spectrum of wave profile slope in polar coordinates is used to formulate m, which is then defined as

$$m = \left(\bar{\Lambda}_r / \bar{\Lambda}_0\right)^2 - 1. \tag{4}$$

where $\bar{\Lambda}_r$ and $\bar{\Lambda}_0$ are the average crest length and wave length, respectively. By using (4) and the approximation of $S_Z(K, \theta) = S_{ZK}(K) \cdot S_{Z\theta}(\theta)$, m is expressed as

$$m = 3\left\{\left[\frac{\bar{\Lambda}_y(\pi/2)}{\bar{\Lambda}_y(0)}\right]^2 - 1\right\}. \tag{5}$$

The formula (5) can be used for calculating m, given an adequate selection of radar filter parameters.

Leykin, I. A., I. Ye. Ostrovskiy, A. D. Rozenberg, V. G. Ruskevich, and I. M. Fuks. The effect of long waves on energy spectra of radar signals scattered from a sea surface. IVUZ Radiofiz, no. 3, 1975, 346-357.

An experimental study on the fine structure of radar signals backscattered from a sea surface at small glancing angles is described. Results of the study are interpreted in the framework of a suggested model of the scattering surface. An increase in magnitude of radar signal frequency shift with respect to emitted signal, and signal polarization-dependence of the shift, which were observed earlier by other authors to be in disagreement with the theory of resonance scattering, are explained on the basis of the proposed model.

A coherent-pulse radar transmitting at $\lambda = 3.2$ cm and providing for change in radiation polarization was used, together with a parabolic antenna, to measure the return signal $E(t) = A(t) \exp [i\Phi(t)]$, where A is the amplitude and Φ is the "slow" phase. During E(t) measurements carried out in the summer and fall of 1972 at Point Kodor in the Black Sea, the antenna was placed on a 12m elevation at 50 m. from the water's edge. At a 150 to 750 m radar range, the transverse dimension of the irradiated surface area varied from 4 to 20 m. and the glancing angle ψ from 1 to 5 degrees. Both horizontally and vertically polarized E(t) were recorded on magnetic tape for 3sec to 2 min. intervals, with irradiation directed counter to sea waves. A wire-type recording wave gauge was simultaneously placed on a taut mooring in 25m of water and 400m offshore.

The results of computer processing of recorded data are shown in Fig. 1.

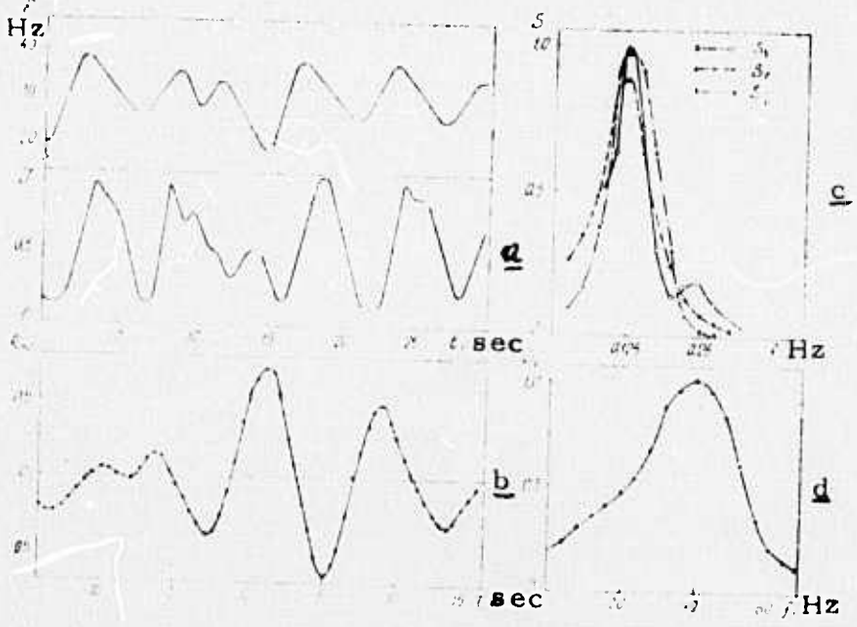

Fig. 1. Typical results of processed experimental data (20 Sept 72, no. 3, vertical polarization: a- F(t) and J(t) are distribution functions of instant frequency and intensity of the signal; b- $R_{JF}(\tau)$ is the cross correlation function of F(t) and J(t); c- $S_S(f)$ is the sea roughness energy spectrum, $S_J(f)$ and $S_F(f)$ are frequency fluctuation spectra of J(t) and F(t); d- $S_E(f)$ is the signal energy spectrum. All spectra and J values are plotted in relative units.

The J(t) and F(t) values for each E(t) recording were determined as the integral of the "instant" energy spectra s(f,t) of sequential E(t) segments, each of 0.25 sec duration, and as the mean frequency (at half power point) of the energy-carrying spectral component, respectively. The maximum rms error of $S_E(f)$ evaluation (30 to 40%) is sufficiently small to determine the mean frequency shift ΔF which is defined as the center-of-gravity position of $S_E(f)$.

The foregoing process was applied to data of over ten experiments carried out in moderate seas at wind velocities to 6 m/sec. Analysis of the F(t) data from each experiment, such as in Fig. 1a, shows that the mean $\overline{F}$ value and the mean square deviation $(F-\overline{F})^2$ are identical at both polarizations. This finding is illustrated by the linear approximation of the $\overline{F}_V$(VP) plot versus $\overline{F}_h$ (HP) values of several experiments. In contrast, J(t) distribution depends on polarization, with $\overline{J}_h$ values as a rule lower than J_v values. It is shown that the maximum values R_m of the $R_{JF}(\tau)$ function (Fig. 1b) are high (0.4 to 0.8) and the calculated phase shift φ_m between F(t) and J(t) at τ_m maximum of $R_{JF}(t)$ is zero. Both R_m and φ_m are independent of polarization and glancing angle. The absence of phase shift between F and J at both polarizations indicates that differently polarized signals are backscattered from the same elementary sea surface. Hence, polarization dependence of $S_E(f)$ can be correlated only with difference in signal amplitude modulation. The fact that the peaks of $S_F(f)$ and $S_J(f)$ coincide with the peak of $S_s(f)$ at $f = f_s$ of the energy-carrying spectral component (Fig. 1c) confirms that long waves are the main factor in controlling frequency and amplitude modulation of the signal. As the signal reaches peak amplitude at F_{max}, the peak of $S_E(f)$ (Fig. 1d) is expected to shift toward higher frequencies in relation to $\overline{F}$. Thus, ΔF is increased on account of modulation by long waves.

The geometrical optics model of radar signal scattering from a sea surface (Fig. 2) is used to formulate $S_E(f)$ and calculate ΔF at

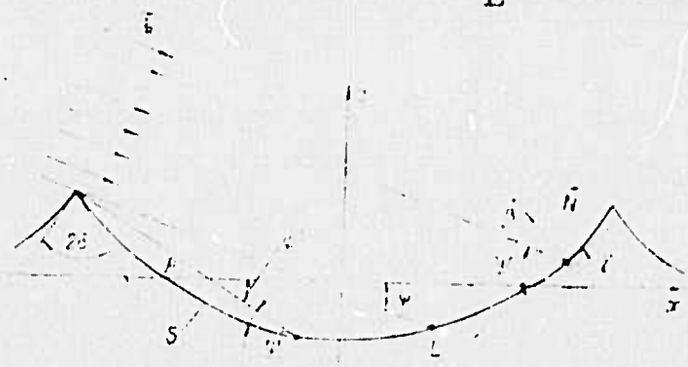

Fig. 2. Model of radar signal backscatter: S= sea surface, N= normal to S in a point $r \in s$; $\vec{k}$= incident wave vector, $\beta = k'/k$, k'- backscattered wave vector, ψ = local angle of incidence, ρ = distance from wave crest to r, 2δ= crest vertex angle, γ = slope of d^2r = arctg (dz/dx).

at different polarizations. Using concepts of resonance scattering theory, the authors simulate the sea surface by superposition of small ripples on long waves. Scattering of a linearly polarized plane monochromatic wave from such a surface is analyzed, with allowance for surface shading $\eta(r)$. In the first quasistatic approximation of S shape, $\eta(r) = 1$ for the irradiated S segment (to the right of point L in Fig. 2) and $\eta(r) = 0$ for the shaded S area (left of L). Under certain assumptions, the formula

$$S_E(f) \sim \int_S d^2r\, |\eta(r)\, B(r)|^2 \delta[\omega - \omega_0 - 2k\beta V(r)] \qquad (\omega = 2\pi f). \tag{1}$$

is derived, where d^2r is an element of S, B(r) is the amplitude factor, ω_o is the wave carrier frequency, and V is the Lagrangian (orbital) velocity of d^2r. It is shown that B(r) versus ψ plots, hence $\eta(r)$- and γ-dependences of intensity of a signal scattered from a long wave element, are different for vertically and horizontally polarized radiation. In contrast, $F = k\beta V(r)/\pi$ is independent of polarization. The spectrum $S_E(f)$ can be calculated from (1), if the long wave profile and V at any point of S are given. In the first approximation of a real sea surface, the wave profile is represented by a smooth cusped trochoidal curve which is described during time T in the x-z plane by a surface element along the major axis $\underline{a}$ of an ellipse. For this profile and sufficiently small ψ, ΔF depends only on the horizontal V component,

$$V_x = -\frac{2\pi a}{T} \cos\left(\frac{2\pi}{\Lambda} x\right). \tag{2}$$

where Λ is the wave length. A significant phase shift between F(x) as calculated from the cited F and Eq. (2) formulas, and backscatter intensity $J(x) \sim \eta(x)B(x)^2$, contradicts the cited experimental data, even for the extremely cusped profile a = 1.5H where H is the wave amplitude. This discrepancy led to adoption of the simplest profile, which features a discontinuity at the crest and which is described by the parametric equation

$$z = 16H|x|^3/\Lambda^3 - H \quad (|x| < \Lambda/2), \tag{3}$$

The shading function $\eta(r)$ was calculated as the result of plane wave diffraction by a wedge with $2\delta = \pi - 2 \operatorname{arctg}(12.h/\Lambda)$. The angle $\psi = \psi' + \gamma$ in the shaded area and $\psi = \psi + \gamma$ in the irradiated area (Fig. 2).

An example of numerical calculation of $S_E(f)$ and other characteristics of the signal and the scattering surface are illustrated in Fig. 3 for the parameters λ = 3cm., ψ = 7 deg., $H/\Lambda = 0.03$, and T = 2.3 sec. The $S_E(f)$ plots show that ΔF for horizontal polarization is significantly greater

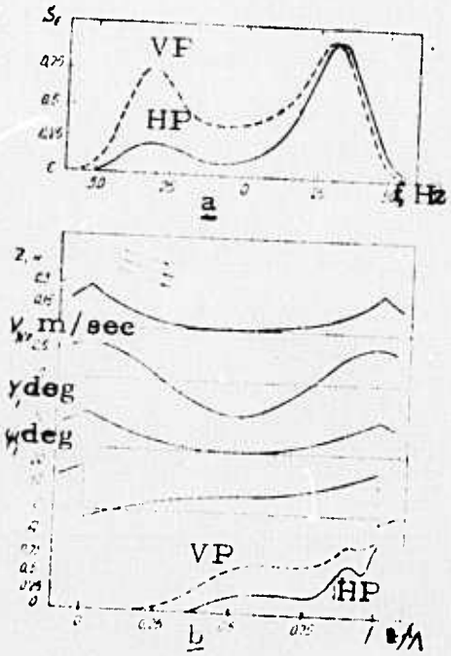

Fig. 3. a- Signal energy spectrum $S_E(f)$ (in relative units), period averaged for two polarizations; b- plots of surface profile Z, V_x, surface slope γ, ψ, and backscatter amplitude $A = J^{1/2}$ (in relative units).

than for vertical, because in the former case the area around a crest with $V_x > 0$ is the major contributor to backscattered signal intensity as shown by long wave profile-distribution of A(Fig. 3b). With a vertical signal, it is a wave trough with $V_x < 0$ which contributes significantly to backscatter, as shown by high $S_E(f)$ values at negative f (Fig. 3a). The theoretical plots of the relative frequency shift $\delta F = \Delta F/F_m$, where $F_m = 2V/\lambda$ is the maximum Doppler shift, versus ψ (Fig. 4a), show that at the limit

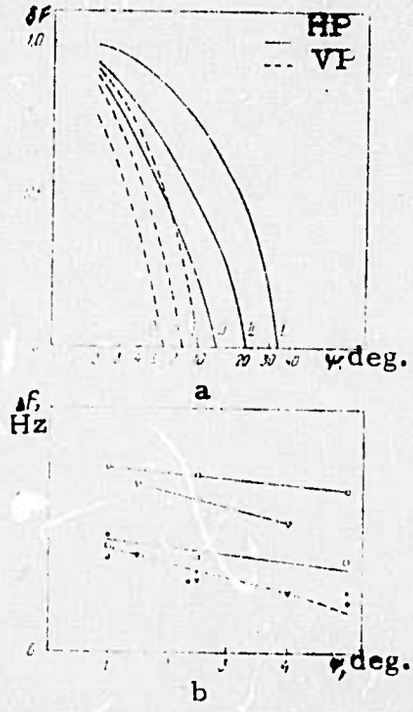

Fig. 4. a- Relative F shift versus glancing angle ψ. Curves I, II, III correspond to H/ = 0.008; 0.015, and 0.03, respectively, at a = 1.5 H; b- shift ΔF versus ψ: dashed and continuous lines are theoretical curves for VP and HP points represent experimental data for sea states with H = 0.2 m, wind velocity W = 3.5 m/sec, H = 1 m, W = 1.5 m/sec, and H = 0.4 m, W = 3.5 m/sec, respectively (black points correspond to vertical, clear points to horizontal polarization).

$\Delta F \rightarrow F_m (\psi = 0)$ only wave crests, where $V_x = V$, are irradiated. At increasing ψ, ΔF decreases because of power amplification of backscatter from a wave trough. The steepest waves with the highest slope H/Λ exhibit the strongest polarization dependence of ΔF. Comparison of the theoretical $\Delta F (\psi)$ curves with experimental data (Fig. 4b) shows that the proposed surface model adequately describes the experimental data only in the case of a gentle breeze (W = 1.5 m/sec). In two other experiments, ΔF values for vertical polarization differ significantly from those for horizontal, in contrast with the corresponding theoretical values.

In discussing the cited theoretical $S_E(f)$ data in the framework of resonance scattering theory, the authors offer a fairly simple physical interpretation. The basic causes of polarization dependence of ΔF are a strong decrease in backscatter intensity for a horizontally polarized signal, when ψ is decreased, and a difference in shading function $\eta(r)$, with vertical polarized radiation penetrating the shaded region more than a horizontally-polarized signal. As a result of the cited factors, horizontally-polarized radiation is backscattered mainly from near-crest areas moving at a high speed toward the radar site. These effects are clearly evident even with the simplest surface model, provided the crests of trochoidal waves are cusped. Even better agreement between theoretical and experimental ΔF values can be expected by simultaneously adjusting the orbital velocity field V (r). Evidently, smoothing of the double-humped spectra (Fig. 3a) to approach the shape observed in nature can be achieved by assuming that the ripple spectral density, hence backscatter intensity, is higher at a wave crest than in a trough, and by taking into account the randomness of the long wave profile. Also, signals reflected from breaking wave crests may contribute significantly, especially with horizontal polarization, to backscatter intensity by increasing ΔF and altering the radar return pulse with powerful spikes, as observed by A. I. Kalmykov, et al. (Preprint IRE, AS UkSSR, Khar'kov, 1975).

Polovinko, V. V. Study of the sea surface by a photographic method. IVUZ Geod, no. 4, 1974, 91-95.

An analysis is given of the relationship between slope angles of sea waves and transmission coefficients of a photograph of the sea surface, and the accuracy was evaluated of calculations based on this relationship.

The expression obtained for the illumination intensity at a point on a photograph of the sea surface allows one to calculate slope angles of sea waves. Errors in determination of wave slope angles are shown to be due to nonlinearity of the transfer function of the optical system. The degree of nonlinear distortion is defined by the coefficient of nonlinear distortion, γ. An empirical expression for the dependence of γ on image angle is obtained in the form

$$\gamma(2\omega') = m + n(2\omega') \quad [\%], \tag{1}$$

where m = 22, n = 0.713, $2\omega' \leq 30^\circ$.

Other errors caused by variation in salinity or temperature of the seawater are shown to be negligible in comparison to the nonlinearity error.

Lyapin, K. K., and I. F. Shishkin. On the problem of radio wave scattering by a sea surface. Radiotekhnika, no. 12, 1974, 34-39.

The calculation is given of effective r-f scattering area using the Kur'yanov model of a sea surface with normal height distribution. The sea surface in this model is considered as a superposition of large-scale and small-scale gently-sloping elements defined by their statistical characteristics. A large-scale element of the sea surface satisfies the conditions for application of the Kirchhoff formula, and the problem is reduced to determination of the diffraction field of the sources on that element.

The results of calculations by the developed formulas, illustrated in Figs. 1 and 2, agree well with experimental data. Here the effective scattering area is given by

$$\sigma_0 \approx \frac{1}{4\alpha_x\alpha_y} e^{-\frac{\operatorname{tg}^2\theta_0}{4\alpha_x^2}}, \tag{1}$$

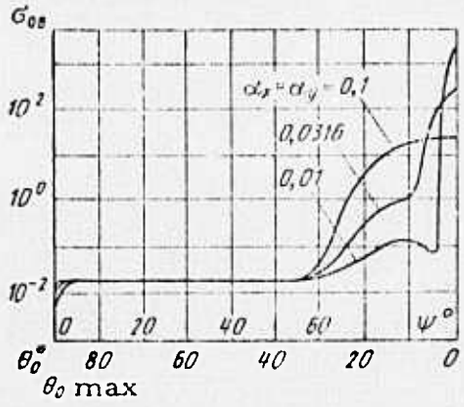

Fig. 1. Effective scattering area vs. incidence angle for the case of vertical polarization.

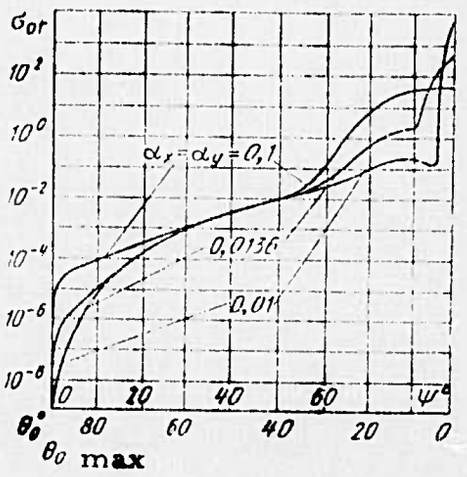

Fig. 2. Effective scattering area in the case of horizontal polarization.

At incidence angles $\theta_o > \theta_{omin}$ the effective scattering area of the sea surface is seen to depend on polarization and r-f wavelength; reflection of radio waves is determined mainly by scattering on small-scale elements which satisfy the condition $\lambda \approx 4,4 l_c \sin\theta_o$. It was further noted that shading of scattering elements is appreciable only at large incidence angles. The authors hence suggest that the "resonance" mechanism observed in acoustics can be extended to back-scattering of radio waves by a disturbed sea surface, when irradiated at certain angles.

Trokhan, A. M., and S. R. Stefanov.
Optical-acoustic method for measurements of turbulence characteristics. Tr. VNII fiz.-tech. i radiotekhn. izmereniy, no. 14(44), 1974, 40-46. (RZhMekh, 12/74, #12 B1338). (Translation)

The principle in the use of the proposed method is described. Various characteristics of measuring circuitry and basic metrological parameters are considered.

Stefanov, S. R., G. S. Trubetskaya, V. M. Sysak, and A. S. Salomatin. Contact measuring devices for turbulence characteristics. IN: Tr. VNII fiz.-tekhn. i radiotekhn. izmereniy, no. 14(44), 1974, 98-102. (RZhMekh, 12/74, #12B1339). (Translation)

Contact measuring devices are described for turbulence characteristics (pulsations in temperature, electrical conductivity, velocity), with grouped sensing elements using various types of transducers.

3. SOURCE ABBREVIATIONS

AiT	-	Avtomatika i telemekhanika
APP	-	Acta physica polonica
DAN ArmSSR	-	Akademiya nauk Armyanskoy SSR. Doklady
DAN AzSSR	-	Akademiya nauk Azerbaydzhanskoy SSR. Doklady
DAN BSSR	-	Akademiya nauk Belorusskoy SSR. Doklady
DAN SSSR	-	Akademiya nauk SSSR. Doklady
DAN TadSSR	-	Akademiya nauk Tadzhikskoy SSR. Doklady
DAN UkrSSR	-	Akademiya nauk Ukrainskoy SSR. Dopovidi
DAN UzbSSR	-	Akademiya nauk Uzbekskoy SSR. Doklady
DBAN	-	Bulgarska akademiya na naukite. Doklady
EOM	-	Elektronnaya obrabotka materialov
FAiO	-	Akademiya nauk SSSR. Izvestiya. Fizika atmosfery i okeana
FGiV	-	Fizika goreniya i vzryva
FiKhOM	-	Fizika i khimiya obrabotka materialov
F-KhMM	-	Fiziko-khimicheskaya mekhanika materialov
FMiM	-	Fizika metallov i metallovedeniye
FTP	-	Fizika i tekhnika poluprovodnikov
FTT	-	Fizika tverdogo tela
FZh	-	Fiziologicheskiy zhurnal
GiA	-	Geomagnetizm i aeronomiya
GiK	-	Geodeziya i kartografiya
IAN Arm	-	Akademiya nauk Armyanskoy SSR. Izvestiya. Fizika
IAN Az	-	Akademiya nauk Azerbaydzhanskoy SSR. Izvestiya. Seriya fiziko-tekhnicheskikh i matematicheskikh nauk

IAN B	-	Akademiya nauk Belorusskoy SSR. Izvestiya. Seriya fiziko-matematicheskikh nauk
IAN Biol	-	Akademiya nauk SSSR. Izvestiya. Seriya biologicheskaya
IAN Energ	-	Akademiya nauk SSSR. Izvestiya. Energetika i transport
IAN Est	-	Akademiya nauk Estonskoy SSR. Izvestiya. Fizika matematika
IAN Fiz	-	Akademiya nauk SSSR. Izvestiya. Seriya fizicheskaya
IAN Fizika zemli	-	Akademiya nauk SSSR. Izvestiya. Fizika zemli
IAN Kh	-	Akademiya nauk SSSR. Izvestiya. Seriya khimicheskaya
IAN Lat	-	Akademiya nauk Latviyskoy SSR. Izvestiya
IAN Met	-	Akademiya nauk SSSR. Izvestiya. Metally
IAN Mold	-	Akademiya nauk Moldavskoy SSR. Izvestiya. Seriya fiziko-tekhnicheskikh i matematicheskiki nauk
IAN SO SSSR	-	Akademiya nauk SSSR. Sibirskoye otdeleniye. Izvestiya
IAN Tadzh	-	Akademiya nauk Tadzhiksoy SSR. Izvestiya. Otdeleniye fiziko-matematicheskikh i geologo-khimicheskikh nauk
IAN TK	-	Akademiya nauk SSSR. Izvestiya. Tekhnicheskaya kibernetika
IAN Turk	-	Akademiya nauk Turkmenskoy SSR. Izvestiya. Seriya fiziko-tekhnicheskikh, khimicheskikh, i geologicheskikh nauk
IAN Uzb	-	Akademiya nauk Uzbekskoy SSR. Izvestiya. Seriya fiziko-matematicheskikh nauk
IBAN	-	Bulgarska akademiya na naukite. Fizicheski institut. Izvestiya na fizicheskaya institut s ANEB
I-FZh	-	Inzhenerno-fizicheskiy zhurnal

IiR	-	Izobretatel' i ratsionalizator
ILEI	-	Leningradskiy elektrotekhnicheskiy institut. Izvestiya
IT	-	Izmeritel'naya tekhnika
IVUZ Avia	-	Izvestiya vysshikh uchebnykh zavedeniy. Aviatsionnaya tekhnika
IVUZ Cher	-	Izvestiya vysshikh uchebnykh zavedeniy. Chernaya metallurgiya
IVUZ Energ	-	Izvestiya vysshikh uchebnykh zavedeniy. Energetika
IVUZ Fiz	-	Izvestiya vysshikh uchebnykh zavedeniy. Fizika
IVUZ Geod	-	Izvestiya vysshikh uchebnykh zavedeniy. Geodeziya i aerofotos"yemka
IVUZ Geol	-	Izvestiya vysshikh uchebnykh zavedeniy. Geologiya i razvedka
IVUZ Gorn	-	Izvestiya vysshikh uchebnykh zavedeniy. Gornyy zhurnal
IVUZ Mash	-	Izvestiya vysshikh uchebnykh zavedeniy. Mashinostroyeniye
IVUZ Priboro	-	Izvestiya vysshikh uchebnykh zavedeniy. Priborostroyeniye
IVUZ Radioelektr	-	Izvestiya vysshikh uchebnykh zavedeniy. Radioelektronika
IVUZ Radiofiz	-	Izvestiya vysshikh uchebnykh zavedeniy. Radiofizika
IVUZ Stroi	-	Izvestiya vysshikh uchebnykh zavedeniy. Stroitel'stvo i arkhitektura
KhVE	-	Khimiya vysokikh energiy
KiK	-	Kinetika i kataliz
KL	-	Knizhnaya letopis'
Kristall	-	Kristallografiya
KSpF	-	Kratkiye soobshcheniya po fizike

LZhS	-	Letopis' zhurnal'nykh statey
MiTOM	-	Metallovedeniye i termicheskaya obrabotka materialov
MP	-	Mekhanika polimerov
MTT	-	Akademiya nauk SSSR. Izvestiya. Mekhanika tverdogo tela
MZhiG	-	Akademiya nauk SSSR. Izvestiya. Mekhanika zhidkosti i gaza
NK	-	Novyye knigi
NM	-	Akademiya nauk SSSR. Izvestiya. Neorganicheskiye materialy
NTO SSSR	-	Nauchno-tekhnicheskiye obshchestva SSSR
OiS	-	Optika i spektroskopiya
OMP	-	Optiko-mekhanicheskaya promyshlennost'
Otkr izobr	-	Otkrytiya, izobreteniya, promyshlennyye obraztsy, tovarnyye znaki
PF	-	Postepy fizyki
Phys abs	-	Physics abstracts
PM	-	Prikladnaya mekhanika
PMM	-	Prikladnaya matematika i mekhanika
PSS	-	Physica status solidi
PSU	-	Pribory i sistemy upravleniya
PTE	-	Pribory i tekhnika eksperimenta
Radiotekh	-	Radiotekhnika
RiE	-	Radiotekhnika i elektronika
RZhAvtom	-	Referativnyy zhurnal. Avtomatika, telemekhanika i vychislitel'naya tekhnika
RZhElektr	-	Referativnyy zhurnal. Elektronika i yeye primeneniye

RZhF	-	Referativnyy zhurnal. Fizika
RZhFoto	-	Referativnyy zhurnal. Fotokinotekhnika
RZhGeod	-	Referativnyy zhurnal. Geodeziya i aeros"-yemka
RZhGeofiz	-	Referativnyy zhurnal. Geofizika
RZhInf	-	Referativnyy zhurnal. Informatics
RZhKh	-	Referativnyy zhurnal. Khimiya
RZhMekh	-	Referativnyy zhurnal. Mekhanika
RZhMetrolog	-	Referativnyy zhurnal. Metrologiya i izmeritel'naya tekhnika
RZhRadiot	-	Referativnyy zhurnal. Radiotekhnika
SovSciRev	-	Soviet science review
TiEKh	-	Teoreticheskaya i eksperimental'naya khimiya
TKiT	-	Tekhnika kino i televideniya
TMF	-	Teoreticheskaya i matematicheskaya fizika
TVT	-	Teplofizika vysokikh temperatur
UFN	-	Uspekhi fizicheskikh nauk
UFZh	-	Ukrainskiy fizicheskiy zhurnal
UMS	-	Ustalost' metallov i splavov
UNF	-	Uspekhi nauchnoy fotografii
VAN	-	Akademiya nauk SSSR. Vestnik
VAN BSSR	-	Akademiya nauk Belorusskoy SSR. Vestnik
VAN KazSSR	-	Akademiya nauk Kazakhskoy SSR. Vestnik
VBU	-	Belorusskiy universitet. Vestnik
VNDKh SSSR	-	VNDKh SSSR. Informatsionnyy byulleten'
VLU	-	Leningradskiy universitet. Vestnik. Fizika, khimiya
VMU	-	Moskovskiy universitet. Vestnik. Seriya fizika, astronomiya

ZhETF	-	Zhurnal eksperimental'noy i teoreticheskoy fiziki
ZhETF P	-	Pis'ma v Zhurnal eksperimental'noy i teoreticheskoy fiziki
ZhFKh	-	Zhurnal fizicheskoy khimii
ZhNiPFiK	-	Zhurnal nauchnoy i prikladnoy fotografii i kinematografii
ZhNKh	-	Zhurnal neorganicheskoy khimii
ZhPK	-	Zhurnal prikladnoy khimii
ZhPMTF	-	Zhurnal prikladnoy mekhaniki i tekhnicheskoy fiziki
ZhPS	-	Zhurnal prikladnoy spektroskopii
ZhTF	-	Zhurnal tekhnicheskoy fiziki
ZhVMMF	-	Zhurnal vychislitel'noy matematiki i matematicheskoy fiziki
ZL	-	Zavodskaya laboratoriya

4. AUTHOR INDEX